The Dissertation Committee for Courtney Lawrence Sherman

certifies that this is the approved version of the following dissertation:

Electrospray Ionization Mass Spectrometric Techniques for the Study of Molecular Recognition

Committee:

Jennifer S. Brodbelt, Supervisor

Jonathan L. Sessler

Jason B. Shear

Greg. O. Sitz

Keith J. Stevenson

Electrospray Ionization Mass Spectrometric Techniques for the Study of Molecular Recognition

by

Courtney Lawrence Sherman, B.S.

Dissertation

Presented to the Faculty of the Graduate School of

the University of Texas at Austin

in Partial Fulfillment

of the Requirements

for the Degree of

Doctor of Philosophy

The University of Texas at Austin

May 2005

To my wife Karen, for her love, support, encouragement, and inspiration.

Acknowledgements

Through the many trials of graduate school, I have had the guidance and support of many wonderful people. First of all, I must offer my deepest thanks to Jennifer Brodbelt who has consistently given me the freedom to succeed on my own merits while helping me to grow and develop as a scientist. Her knowledge and wisdom have been the guiding force behind my studies. I could never have hoped for a better advisor, and I am honored to have had the opportunity to work with her.

Next, the members of the Brodbelt research group with whom I have worked these past few years have made this research group one to which I am proud to claim membership. The work done in this laboratory is first-rate, but even more valuable is the ability of my fellows to teach and learn from each other. Our friendly and helpful atmosphere helps each of us thrive and has greatly contributed to my success.

Much of my work in graduate school has been collaborative, and I thank my collaborators whose knowledge has picked up where mine has left off. Our interactions have allowed me to pursue many areas of research that extended far beyond my own areas of expertise, and I have learned greatly from the experience.

Lastly, I could never have made it to this point without my wife Karen. Together, we have celebrated my successes and overcome my failures, we have fought the many battles of graduate school, and in the process we have only grown in our love for each other. Karen has loved me, supported me, encouraged me, and inspired me more than words can describe. This accomplishment I share with her.

Electrospray Ionization Mass Spectrometric Techniques for the Study of Molecular Recognition

Publication No._____

Courtney Lawrence Sherman, Ph.D.

the University of Texas at Austin, 2005

Supervisor: Jennifer S. Brodbelt

The ability of electrospray ionization mass spectrometry (ESI-MS) to quantitatively analyze the distribution of complexes resulting from molecular recognition in solution was modeled, and ESI-MS techniques were developed to analyze complexes involving several different types of novel compounds in different areas of molecular recognition and supramolecular chemistry.

To better understand the relationship between ion abundances observed by ESI-MS and concentrations of host-guest complexes in solution, mathematical models based on equilibrium partitioning theory were developed to relate ESI-MS ion abundances to relative solution concentrations of complexes resulting from host-guest binding. The predictions of these new models were evaluated and experimentally confirmed through the analysis of complexes of crown ethers with alkali metal cations in an ESI quadrupole

ion trap mass spectrometer, yielding a greater understanding of the behavior of host-guest complexes in ESI-MS, allowing for more accurate measurements of solution binding interactions.

The self-assembly of ligand-metal-ligand sandwich complexes involving a novel quinoxaline-containing crown ether was studied to evaluate the contribution of pi-stacking interactions between the ligands towards the overall stability of the complexes. Donor-acceptor pi-stacking interactions between the electron-poor quinoxaline group and electron-rich benzene groups from benzo- or dibenzo-18-crown-6 were found to significantly enhance the formation of mixed-ligand sandwich complexes.

A synthetic pyrrole-inosine nucleoside, capable of forming an extended three-point Hoogsteen-type hydrogen-bonding interaction with guanine, was shown to bind guanosine selectively over other individual nucleosides, and ESI-MS results indicated the formation of specific complexes between the pyrrole-inosine nucleoside and two different quadruplex DNA structures. The specificity of the pyrrole-inosine nucleoside for quadruplex DNA suggests that it or similar structures based on this binding modality may ultimately demonstrate utility as anti-tumor agents.

The interactions between a novel enediyne drug and various cytidine-containing oligonucleotides were studied, and the structures of the DNA-enediyne adducts known to lead to cytidine-specific DNA cleavage were examined. Collisionally activated dissociation of the adducts confirmed their strength and suggest a direct linkage between the enediyne and the cytidine nucleobase, likely the result of a nucleophilic attack by the cytidine amine.

Table of Contents

CHAPTER 1

Introduction: Electrospray Ionization Mass Spectrometry as a Tool for Studying Molecular Recognition in Solution

1.1 Introduction

In recent years, a significant portion of chemical research has centered on developing and characterizing molecules capable of interacting specifically with some target. The interactions of these molecules define a process generally known as molecular recognition. The specific types of molecular recognition that have been studied take countless forms and have exceptionally wide-ranging applications. As examples, metal chelation by macrocyclic ligands has applications to development of metal sensors (1-3) and the removal of toxic metals from waste water streams (4-6), and the attachment of compounds to different DNA structures has profound implications for the design of drugs to fight cancer (7-9). Although molecular recognition is studied in many different ways, electrospray ionization-mass spectrometry (ESI-MS) is emerging as a new tool which is amenable to a wide range of chemical and biological systems (10-13). Because of the great potential impact of ESI-MS across the field of molecular recognition, the studies presented in this dissertation aim to further develop ESI-MS through its application to new and interesting chemical systems and by explaining some

of the quantitative aspects of the ESI process when used to probe the specific interactions between molecules in solution.

1.2 Importance of Electrospray Ionization

1.2.1 The Electrospray Ion Source

Following the initial development by Dole, et al. of an electrospray source for producing ion beams from solution (14), electrosprays were used for various types of sample deposition, including preparation of samples for subsequent analysis by Californium-252 plasma desorption (15), laser ionization (16), field desorption (17), and chemical ionization (17) mass spectrometry. Not until fifteen years later, however, did Fenn, in the work for which he earned a Nobel prize, couple an electrospray ionization (ESI) source directly to a mass spectrometer (18). In the time since, the ESI source has been successfully mated to a range of mass analyzers, including the quadrupole ion traps (19) used in the studies presented in this dissertation. Owing to the many advantages of the ESI source described in detail below, ESI-MS has in recent years become a widespread technique for analyzing countless types of molecules and chemical interactions.

Part of the appeal of the ESI source is the simplicity of its design. Producing an electrospray merely requires pumping a solution through a conductive needle held at a potential of several kilovolts. The electric field between this needle and a counter-electrode causes the formation of small, multiply-charged droplets of solvent that migrate towards the counter-electrode. As the solvent evaporates from these droplets and the droplets undergo fission due to electrostatic repulsions, individual gas-phase ions are

ultimately produced (14). Since this process occurs at atmospheric pressure, interfacing the ion beam produced by ESI to a mass spectrometer typically requires the use of one or more skimmers to sample the ion beam and bridge the pressure differential between the source and the vacuum chamber housing the mass spectrometer (18-19). Although various enhancements and modifications to the ESI source have been made (20), the fundamental design remains strikingly similar to the source developed by Fenn and the original electrosprays produced by Dole and coworkers (14, 18).

1.2.2 Characteristics of Electrospray Ionization

Despite the simplicity of the basic ESI source design, the mechanisms of ion production have proven to be particularly complex. Two competing theories have emerged to explain the ionization mechanism of ESI. The first, termed the charged-residue mechanism, was originally described by Dole, et al. in their report of the first electrosprays (14). According to this mechanism, free gas-phase ions result from the complete evaporation of solvent from droplets containing a single analyte molecule resulting from successive fissions of the initially formed charged droplets. The charged-residue mechanism appears to be particularly applicable to the ionization of large molecules (21-22). Iribarne and Thomson subsequently proposed an alternative, the ion evaporation mechanism (23). They contended that ions produced by ESI evaporate directly from the surface of the multiply-charged droplets, assisted by the electrostatic repulsions enhanced from the evaporative loss of neutral solvent. Evidence suggests that ion evaporation dominates for the production of smaller ions which would be expected to have higher rates of evaporation (22).

Regardless of the ionization mechanism dominant for a given analyte, one of the primary benefits of ESI is its ability to produce ions directly from solution, effectively avoiding the mass-range limitations of other techniques which result from the high decomposition and low desorption rates of larger molecules from solid samples. Furthermore, only a very limited amount of excess energy is imparted to the ions produced from an electrospray (24-25), allowing intact ions to be observed in most cases. In fact, ESI is typically gentle enough to preserve not only the covalent structure of a molecule but also a wide range of much weaker non-covalent interactions (26-30). Beyond these primary advantages, qualities such as the multiple charging which allows very large molecules to be detected at significantly lower mass/charge ratios (31-32) and the ease of interfacing ESI to solvent-based separations such as high-performance liquid chromatography (33) and capillary electrophoresis (34-35) account for the widespread use ESI mass spectrometry now enjoys.

1.3 Using ESI to Probe Molecular Recognition

The ability of ESI-MS to examine weakly bound species formed in solution makes it particularly useful for studying many types of molecular recognition processes. Examples of the molecular recognition systems that have been successfully studied with ESI-MS include the interactions between macrocyclic crown ether ligands and metal cations and the targeting of drugs to DNA, both of which are discussed in greater detail below, and the binding of a protein to small-molecule substrates (10, 36-37) or drugs (10, 38), other proteins (37), DNA (12, 36, 39-40), or RNA (10, 40). While just a sampling of

the many studies that have been presented using ESI-MS to probe molecular recognition, the crown ether-metal and DNA-drug complexes provide an illustrative sample of the work that has been done in the field and the work presented in this dissertation.

1.3.1 Studies of Interactions between Metal Cations and Crown Ether Ligands

Crown ethers were initially developed by Pedersen in the late 1960's, and their ability to strongly chelate metal cations was immediately recognized (41-43). Since then, extensive work has been done developing a wide range of crown ether macrocycles and measuring their binding affinities towards the different metal cations (44-45). With the development of ESI-MS and the recognition of its ability to detect non-covalent complexes formed in solution, interest quickly focused on analyzing the crown ether-metal complexes, particularly once a correlation between ESI-MS abundances and solution concentrations for them was established (46). The utility of ESI-MS to identify the binding stoichiometry of these crown ether-metal complexes is immediately apparent, but more detailed information about the molecular recognition interactions can also be obtained. Some studies have used ESI-MS to gauge the ability of crown ethers and metal cations to form stable complexes in solution (47-48), and methods have been developed for directly measuring the selectivity of crown ethers for different metals (49-51).

The ease with which ESI-MS can detect the recognition of metal cations by crown ethers has also been leveraged to allow simplified mass measurements of systems not particularly amenable to ESI. The attachment of a crown ether macrocycle to another compound can create a tag to greatly enhance the ionization efficiency of that compound through metal complexation as has been demonstrated for fullerenes (52-54), vitamin D

and its metabolites (55), organic dyes (56-57), and even self-assembled supramolecular assemblies (58). A related technique used crown ether complexation to enhance the detection of the metal cations themselves in an elemental analysis application (59).

Beyond the analysis of these relatively straightforward crown ether systems, ESI-MS has become an invaluable tool for characterizing novel crown ether macrocycles as they are developed. A common method for modifying the binding properties of a crown ether has been through the incorporation of additional functional groups on the macrocycle. Among the crown ethers with added functional groups that have been studied with ESI-MS are various aromatic-substituted crowns (60-64), crown ether acetals (65), lariat ethers (66-67), crowns with photoionizable side chains (68-69), caged crowns (70-72), and thymine-substituted crowns (73). As a variation on the theme, ESI-MS has also been used to characterize the behavior of a range of tethered crown compounds, each of which contains two or more crown ether macrocycles connected via a covalent linker either to complex multiple metal cations or to form particularly strong interactions with a single metal (74-80). Various crown ether analogs such as thiacrown (81-82) and metallacrown (83-84) ethers have also been successfully analyzed.

1.3.2 Evaluation of DNA-Interactive Compounds

Stepping up from the relatively small crown ether-metal complexes, ESI-MS has also proven useful in analyzing the formation of molecular recognition complexes involving very large biological molecules. Complexes formed between drug molecules and DNA were first detected by ESI-MS in the early 1990's (85). Since then, ESI-MS has been used to probe many of the characteristics DNA-drug interactions, demonstrating

success in areas such as screening drug candidates for DNA activity (86-89), measuring binding strengths of DNA-drug complexes (86, 88, 90-95), evaluating the extent of DNA sequence selectivity of drugs (86, 91-92, 94, 96-101), and determining the specificity of interactions between a particular drug and DNA (89-90, 98). Techniques have also been developed for deeper analyses of the DNA-drug complexes. In experiments analogous to melting curves measured in solution, ESI-MS can yield gas-phase "melting" curves through energy-variable collisionally-activated dissociation (CAD) experiments (92, 102-104). CAD has also demonstrated the ability do distinguish between different modes of binding of drugs to DNA, resulting in differences in the observed fragmentation based on whether a drug intercalates or binds in one of the grooves of a duplex (86, 89-90, 102, 104-105). Lastly, the ability to mass analyze the fragment ions produced by ESI and subsequent CAD can provide clues about the specific structure of a DNA-drug complex (106-108).

These types of analyses of DNA-drug complexes via ESI-MS have been applied to a range of DNA structures. At the most basic level, the interactions of some drugs can be probed at the single nucleoside level (109). More typical analyses focus on attachment of a drug to a single strand oligonucleotide (91-92, 97, 101, 107, 110) or a DNA duplex (85-86, 89-96, 98, 100-105, 110-115). As more exotic DNA structures have become the focus of much research, the applicability of ESI-MS to their complexes with drugs has been established as well. A few reports have been presented illustrating the interactions between drugs and triplex DNA (101, 108). With its relevance to the functioning of tumor cells (88, 113, 116-119), quadruplex DNA has the subject of

numerous studies as researchers seek drugs that specifically bind and stabilize the quadruplex (88, 100-101, 105, 108, 113, 118). The ability of ESI-MS to provide such a breadth of information about complexes involving many types of DNA structures has far-reaching applications to the areas of drug discovery and biological research.

1.4 Quantitatively Measuring Solution Binding with ESI-MS

Beyond simply evaluating the presence of binding or the relative strengths of a molecular recognition interaction in solution, much recent effort has been directed towards quantitatively measuring the strength of these interactions using ESI-MS. When using ESI-MS to measure solution equilibria, however, several potential pitfalls must be considered. First, although an ESI mass spectrum reflects the species present in solution, not all species are ionized with the same efficiency (120-122). Second, since ESI is a competitive process in the sense that the different species compete for the limited number of charges available in an ESI droplet (123), variations in the concentrations of matrix elements can impact mass spectral abundances (123-126). Lastly, there is some valid concern that changes in the chemical environment as solvent evaporates from the ESI droplets could cause shifts in the equilibrium, although the magnitude of these shifts has been shown to be small (127). If care is taken in experimental design, the impact of all of these factors can be minimized or the appropriate corrections can be made.

A variety of techniques have been presented for using ESI-MS to measure binding constants of complexes formed via molecular recognition in solution. One group of techniques relies on using ESI-MS as a detector for changes resulting from solution

manipulations performed outside the mass spectrometer. For example, the research groups of Smith and Robinson have each presented methods for monitoring melting curves for the temperature-dependent dissociation of biological complexes (128-129). There have also been many reports of using ESI-MS to monitor various titration experiments in solution (75, 130-149). The majority of these make the justifiable assumption that a large biomolecule and its complex with a small molecule have similar ionization efficiencies, although a few studies are notable in that they apply some sort of efficiency correction in the pursuit of more accurate binding data (134, 147-148). Another, somewhat simpler technique merely requires comparing the abundances for a molecule and its complex from a single mass spectrum, using these to calculate the binding constant directly by assuming that the relative abundances directly relate to the relative concentrations of each species in solution (150-153).

The method above for calculating solution equilibrium constants from ESI mass spectral data work well for analyzing complexes where the attachment of the smaller compound does not greatly affect the size, shape, and chemical behavior of the larger compound. For this reason, these techniques have been successfully applied to a range of biological complexes. This assumption that the ionization efficiencies are unaffected by complexation is not valid, however, for many of the complexes resulting from a molecular recognition event. To make quantitative measurements of solution binding in these cases, several other analysis schemes have been reported. Liu and coworkers used the abundance of a competitive complex with similar binding strength to the complex of interest as a means of normalizing ionization efficiencies (154). Kempen developed an

analysis where the decrease in the abundance of a competitive reference complex was monitored after the addition of the second component of the complex of interest (155). Although successful, the two methods were limited in their applicability due to the requirement for a well-characterized reference complex that was not always available. Clark and Konermann presented a technique that avoids both the issues of ionization efficiency and the need for a reference complex by monitoring the different rates of movement of a macromolecule alone and bound to a smaller molecule in a laminar flow tube due to differences in their rates of diffusion (156-157). This method, however, is limited to species that undergo a significant change in their diffusion coefficient on complexation.

While some methods have clearly been successful at quantitatively measuring solution binding with ESI-MS, the techniques are not in widespread use largely due to their limited applicability and often unexplained problems. The many unresolved questions about the behavior of host-guest complexes in the electrospray source provided the impetus for the studies presented herein which probe more deeply some of the fundamental issues surrounding the ionization of weakly-bound species.

1.5 Overview of Chapters

The work in this dissertation concerns several different aspects of the use of ESI-MS for studying molecular recognition. A general overview of the experimental methods and instrumentation used in the studies is given in Chapter 2. In particular, the operation

of the electrospray ionization source and the quadrupole ion trap mass analyzer is described as is the general approach for the computational methods employed.

To better explain how an electrospray source perturbs the distribution of host-guest complexes in solution as they are transferred to the gas phase, Chapters 3 and 4 explore the development of a mathematical model to account for the processes which enhance the abundance of some complexes at the expense of others. Based on the understanding that an electrospray source is limited in the amount of charge it can impart to solution and that species in electrospray droplets partition between the surface and interior of these droplets based on their relative affinities for the chemically different phases, the various equilibria were considered to calculate the concentration of each analyte on the droplet surfaces which directly relates to the observed ion abundances. Comprehensive evaluation of the resulting mathematical models yielded a series of conclusions about the behavior of different types of host-guest complexes in ESI-MS which were supported through experimental testing with some model crown ether-metal complexes.

Chapter 5 presents the characterization of the complexation of a novel quinoxaline-substituted crown ether. This crown and crowns with aromatic substituents were shown to readily form 2:1 crown ether-metal-crown ether "sandwich" complexes when mixed with appropriate metal cations. The electron-poor pi-electron system of the quinoxaline proved able to direct the formation of mixed-ligand sandwich complexes with crowns containing electron-rich benzene substituents, presumably through donor-acceptor interactions which would strengthen the pi-stacking.

Beginning with Chapter 6, the focus shifts from the analysis of molecular recognition by crown ether ligands to the analogous interaction between drugs and DNA. Chapter 6 probes the interactions of some novel pyrrole-inosine nucleosides with guanosine and guanosine-rich DNA structures. The optimal pyrrole-inosine formed specific interactions with guanosine preferentially over the other natural nucleosides and displayed activity in disrupting the guanine tetrads which form spontaneously in solution. This affinity of the pyrrole-inosine for guanine tetrads led to the discovery that this novel nucleoside exhibits a remarkable specific affinity for quadruplex DNA.

In Chapter 7, the adduction of DNA by an acyclic analog to the natural enediyne anti-tumor drugs was studied. In addition to the non-specific DNA cleavage common to this class of drugs, ESI-MS enabled the detection and structural characterization of an adduct between the drug and DNA that effects a cytidine-specific cleavage of the DNA sequence. The binding site of the enediyne drug was determined through multiple tandem mass spectrometry experiments, and further information about the efficiency of this specific cleavage was obtained.

1.6 References

(1) Memon, S.; Roundhill, D. M.; Yilmaz, M. *Collect. Czech. Chem. Commun.* **2004**, *69*, 1231-1250.

(2) Mohapatra, P. K.; Pathak, P. N.; Kelkar, A.; Manchanda, V. K. *New J. Chem.* **2004**, *28*, 1004-1009.

(3) Cipurkovic, A.; Kibicek, R.; Petrovski, P. *J. Env. Prot. Eco.* **2004**, *5*, 673-686.

(4) Lewis, J. D.; Moore, J. N. *Dalton Trans.* **2004**, 1376-1385.

(5) Pinalli, R.; Suman, M.; Dalcanale, E. *Eur. J. Org. Chem.* **2004**, 451-462.

(6) Pratt, M. D.; Beer, P. D. *Tetrahedron* **2004**, *60*, 11227-11238.

(7) Wheate, N. J.; Collins, J. G. *Coord. Chem. Rev.* **2003**, *241*, 133-145.

(8) Gniazdoeski, M.; Denny, W. A.; Nelson, S. M.; Czyz, M. *Curr. Med. Chem.* **2003**, *10*, 909-924.

(9) Tse, W. C.; Boger, D. L. *Chem. Biol.* **2004**, *11*, 1607-1617.

(10) Brodbelt, J. S. *Int. J. Mass Spectrom.* **2000**, *200*, 57-69.

(11) Loo, J. A. *Int. J. Mass Spectrom*. **2000**, *200*, 175-186.

(12) Beck, J. L.; Colgrave, M. L.; Ralph, S. F.; Sheil, M. M. *Mass Spectrom. Rev.* **2001**, *20*, 61-87.

(13) Ganem, B.; Henion, J. D. *Bioorg. Med. Chem.* **2003**, *11*, 311-314.

(14) Dole, M.; Mack, L. L.; Hines, R. L.; Mobley, R. C.; Ferguson, L. D.; Alice, M. B. *J. Chem. Phys.* **1968**, *49*, 2240-2249.

(15) McNeal, C. J.; Macfarlane, R. D.; Thurston, E. L. *Anal. Chem.* **1979**, *51*, 2036-2039.

(16) Hardin, E. D.; Vestal, M. L. *Anal. Chem.* **1492**, *53*, 1492-1497.

(17) Murphy, R. C.; Clay, K. L.; Matthews, W. R. *Anal. Chem.* **1982**, *54*, 336-338.

(18) Yamashita, M.; Fenn, J. B. *J. Phys. Chem.* **1984**, *88*, 4451-4459.

(19) Van Berkel, G. J.; Glish, G. L.; McLuckey, S. A. *Anal. Chem.* **1990**, *62*, 1284-1285.

(20) Cody, R. B. In *Applied Electrospray Mass Spectrometry*. Pramanik, B. N.; Ganguly, A. K.; Gross, M. L., Eds. Marcel Dekker, Inc.: New York, **2002**; Chap. 1, pp. 1-104.

(21) Cole, R. B. *J. Mass Spectrom.* **2000**, *35*, 763-772.

(22) Kebarle, P.; Peschke, M. *Anal. Chim. Acta.* **2000**, *406*, 11-35.

(23) Iribarne, J. V.; Thomson, B. A. *J. Chem. Phys.* **1976**, *64*, 2287-2294.

(24) Yamashita, M.; Fenn, J. B. *J. Phys. Chem.* **1984**, *88*, 4671-4675.

(25) Jones, J. L.; Dongré, A. R.; Somogyi, Á.; Wysocki, V. H. *J. Am. Chem. Soc.* **1994**, *116*, 8368-8369.

(26) Ganem, B.; Li, Y.-T.; Henion, J. D. *J. Am. Chem. Soc.* **1991**, *113*, 6294-6296.

(27) Katta, V.; Chait, B. T. *J. Am. Chem. Soc.* **1991**, *113*, 8534-8535.

(28) Jaquinod, M.; Leiza, E.; Potier, N.; Albrecht, A.-M.; Shanzer, A.; Van Dorsselaer, A. *Tetrahedron Lett.* **1993**, *34*, 2771-2774.

(29) Smith, R. D.; Light-Wahl, K. J.; Winger, B. E.; Loo, J. A. *Org. Mass Spectrom.* **1992**, *27*, 811-821.

(30) Smith, R. D.; Light-Wahl, K. J. *Biol. Mass Spectrom.* **1993**, *22*, 493-501.

(31) Wong, S. F.; Meng, C. K.; Fenn, J. B. *J. Phys. Chem.* **1988**, *92*, 546-550.

(32) Meng, C. K.; Mann, M.; Fenn, J. B. *Z. Phys. D* **1988**, *10*, 361-368.

(33) Whitehouse, C. M.; Dreyer, R. N.; Yamashita, M.; Fenn, J. B. *Anal. Chem.* **1985**, *57*, 675-679.

(34) Olivares, J. A.; Nguyen, N. T.; Yonker, C. R.; Smith, R. D. *Anal. Chem.* **1987**, *59*, 1230-1232.

(35) Smith, R. D.; Olivares, J. A.; Nguyen, N. T.; Udseth, H. R. *Anal. Chem.* **1988**, *60*, 436-441.

(36) Loo, J. A. *Mass Spectrom. Rev.* **1997**, *16*, 1-23.

(37) Heck, A. J. R.; Van den Heuvel, R. H. H. *Mass Spectrom. Rev.* **2004**, *23*, 368-389.

(38) Siegel, M. M. *Curr. Top. Med. Chem.* **2002**, *2*, 13-33.

(39) Veenstra, T. D. *Biochem. Biophys. Res. Commun.* **1999**, *257*, 1-5.

(40) Hofstadler, S. A.; Griffey, R. H. *Chem. Rev.* **2001**, *101*, 377-390.

(41) Pedersen, C. J. *J. Am. Chem. Soc.* **1967**, *89*, 7017-7036.

(42) Pedersen, C. J. *J. Am. Chem. Soc.* **1970**, *92*, 386-391.

(43) Pedersen, C. J. *J. Am. Chem. Soc.* **1970**, *92*, 391-394.

(44) Izatt, R. M.; Bradshaw, J. S.; Nielsen, S. A.; Lamb, J. D.; Christensen, J. J.; Sen, D. *Chem. Rev*. **1985**, *85*, 271-339.

(45) Izatt, R. M.; Pawlak, K.; Bradshaw, J. S. *Chem. Rev.* **1991**, *91*, 1721-2085.

(46) Wang, K.; Gokel, G. W. *J. Org. Chem.* **1996**, *61*, 4693-4697.

(47) Henderson, W.; Taylor, M. J. *Inorg. Chim. Acta* **1998**, *277*, 26-30.

(48) Abdoul-Carime, H. *J. Chem. Soc., Faraday Trans.* **1998**, *94*, 2407-2410.

(49) Blair, S. M.; Kempen, E. C.; Brodbelt, J. S. *J. Am. Soc. Mass Spectrom.* **1998**, *9*, 1049-1059.

(50) Brodbelt, J. S.; Kempen, E. C.; Reyzer, M. *Struct. Chem.* **1999**, *10*, 213-219.

(51) Shen, J.; Brodbelt, J. *J. Mass Spectrom.* **1999**, *34*, 137-146.

(52) Wilson, S. R.; Wu, Y. *J. Chem. Soc., Chem. Commun.* **1993**, 784-786.

(53) Wilson, S. R.; Wu, Y. *J. Am. Soc. Mass Spectrom.* **1993**, *4*, 596-603.

(54) Wilson, S. R.; Wu, Y. *J. Am. Chem. Soc.* **1993**, *115*, 10334-10337.

(55) Wilson, S. R.; Lu, Q.; Tulchinsky, M. L.; Wu, Y. *J. Chem. Soc., Chem. Commun.* **1993**, 664-665.

(56) Kimura, K.; Mizutani, R.; Yokoyama, M.; Arakawa, R. *Anal. Chem.* **1999**, *71*, 2922-2928.

(57) Kimura, K.; Mizutani, R.; Yokoyama, M.; Arakawa, R.; Sakurai, Y. *J. Am. Chem. Soc.* **2000**, *122*, 5448-5454.

(58) Russell, K. C.; Leize, E.; Van Dorsselaer, A.; Lehn, J.-M. *Angew. Chem. Int. Ed.* **1995**, *34*, 209-213.

(59) Shou, W. Z.; Brower, R. F. *Anal. Chem.* **1999**, *71*, 3365-3373.

(60) Colton, R.; Mitchell, S.; Traeger, J. C. *Inorg. Chim. Acta* **1995**, *231*, 87-93.

(61) Yam, V. W.-W.; Lee, V. W.-M.; Ke, F.; Siu, K.-W. M. *Inorg. Chem.* **1997**, *36*, 2124-2129.

(62) Rahman, M. A.; Doe, H.; Okamoto, M.; Arakawa, R. *Electrochim. Acta* **1998**, *44*, 39-46.

(63) Bryant, W. S.; Guzei, I. A.; Rheingold, A. L.; Merola, J. S.; Gibson, H. W. *J. Org. Chem.* **1998**, *63*, 7634-7639.

(64) Tsuda, A.; Moriwaki, H.; Oshima, T. *J. Chem. Soc., Perkin Trans. 2* **1999**, 1235-1240.

(65) Oshima, T.; Matsuda, F.; Fukushima, K.; Tamura, H.; Matsubayashi, G.; Arakawa, R. *J. Chem. Soc., Perkin Trans. 2* **1998**, 145-148.

(66) Kempen, E. C.; Brodbelt, J. S.; Bartsch, R. A.; Jang, Y.; Kim, J. S. *Anal. Chem.* **1999**, *71*, 5493-5500.

(67) Williams, S.; Blair, S. M.; Brodbelt, J. S.; Huang, X.; Bartsch, R. A. *Int. J. Mass Spectrom.* **2001**, *212*, 389-401.

(68) Kimura, K.; Sakamoto, H.; Kado, S.; Arakawa, R.; Yokoyama, M. *Analyst*, **2000**, *125*, 1091-1095.

(69) Nakamura, M.; Fujioka, T.; Sakamoto, H.; Kimura, K. *New. J. Chem.* **2002**, *26*, 554-559.

(70) Blair, S. M.; Brodbelt, J. S.; Marchand, A. P.; Kumar, K. A.; Chong, H.-S. *Anal. Chem.* **2000**, *72*, 2433-2445.

(71) Reyzer, M. L.; Brodbelt, J. S.; Marchand, A. P.; Chen, Z.; Huang, Z.; Namboothiri, I. N. N. *Int. J. Mass Spectrom.* **2001**, *204*, 133-142.

(72) Williams, S. M.; Brodbelt, J. B.; Huang, Z.; Lai, H.; Marchand, A. P. *Analyst* **2003**, *128*, 1352-1359.

(73) De Wall, S. L.; Barbour, L. J.; Schall, O. F.; Gokel, G. W. *J. Chem. Crystallog.* **2000**, *30*, 227-231.

(74) Wilson, S. R.; Tulchinsky, M. L. *J. Org. Chem.* **1993**, *58*, 1407-1408.

(75) Wang, K.; Han, X.; Gross, R. W.; Gokel, G. W. *J. Chem. Soc., Chem. Commun.* **1995**, 641-642.

(76) Blair, S. M.; Brodbelt, J. B.; Reddy, G. M.; Marchand, A. P. *J. Mass Spectrom.* **1998**, *33*, 721-728.

(77) Kemmer, M.; Ghys, L.; Gielden, M.; Biesemans, M.; Tiekink, E. R. T.; Willem, R. *J. Organomet. Chem.* **1999**, *582*, 195-203.

(78) Yam, V. W.-W.; Lam, C.-H.; Cheung, K.-K. *Inorg. Chim. Acta* **2001**, *316*, 19-24.

(79) Wu, H.-F.; Huan, S.-M.; Wu, C.-F. *Eur. J. Mass Spectrom.* **2002**, *8*, 375-380.

(80) Sherman, C. L.; Brodbelt, J. S.; Srinivas, G.; Sivappa, R.; Marchand, A. P. *ARKIVOC*, **2005**, Part (iii), 1-7.

(81) Santana-Marques, M. G. O.; Amado, F. M. L.; Correia, A. J. F.; Lucena, M.; Madureira, J.; Goodfellow, B. J.; Félix, V.; Santos, T. M. *J. Mass Spectrom.* **2001**, *36*, 529-537.

(82) Williams, S. M.; Brodbelt, J. S.; Marchand, A. P.; Cal, D.; Mlinaric-Makerski, K. *Anal. Chem.* **2002**, *74*, 4423-4433.

(83) Gibney, B. R.; Kessissoglou, D. P.; Kampf, J. W.; Pecoraro, V. L. *Inorg. Chem.* **1994**, *33*, 4840-4849.

(84) Stang, P. J.; Cao, D. H.; Chen, K.; Gray, G. M.; Muddiman, D. C.; Smith, R. D. *J. Am. Chem. Soc.* **1997**, *119*, 5163-5168.

(85) Gale, D. C.; Goodlett, D. R.; Light-Wahl, K. J.; Smith, R. D. *J. Am. Chem. Soc.* **1994**, *116*, 6027-6028.

(86) Wan, K. X.; Shibue, T.; Gross, M. L. *J. Am. Chem. Soc.* **2000**, *122*, 300-307.

(87) Greig, M. J.; Robinson, J. M. *J. Biomol. Screening* **2000**, *5*, 441-454.

(88) Rosu, F.; De Pauw, E.; Guittat, L.; Alberti, P.; Lacroix, L.; Mailliet, P.; Riou, J.-F.; Mergny, J.-L. *Biochemistry* **2003**, *42*, 10361-10371.

(89) Oehlers, L.; Mazzitelli, C. L.; Brodbelt, J. S.; Rodriguez, M.; Kerwin, S. *J. Am. Soc. Mass Spectrom.* **2004**, *15*, 1593-1603.

(90) Gabelica, V.; De Pauw, E.; Rosu, F. *J. Mass Spectrom.* **1999**, *34*, 1328-1337.

(91) Carte, N.; Legendre, F.; Leize, E.; Potier, N.; Reeder, F.; Chottard, J.-C.; Van Dorsselaer, A. *Anal. Biochem.* **2000**, *284*, 77-86.

(92) Reyzer, M. L.; Brodbelt, J. S.; Kerwin, S. M.; Kumar, D. *Nucleic Acids Res.* **2001**, *29*, e103.

(93) Rosu, F.; Gabelica, V.; Houssier, C.; De Pauw, E. *Adv. Mass Spectrom.* **2001**, *15*, 795-796.

(94) Rosu, F.; Gabelica, V.; Houssier, C.; De Pauw, E. *Nucleic Acids Res.* **2002**, *30*, e82.

(95) Furlan, R. L. A.; Watt, S. J.; Garrido, L. M.; Amarante-Mendes, G. P.; Nur-e-Alam, M.; Rohr, J.; Brana, A.; Mendez, C.; Salas, J. A.; Sheil, M. M.; Beck, J. L.; Padilla, G. *J. Antibiot.* **2004**, *57*, 647-654.

(96) Gao, Q.; Cheng, X.; Smith, R. D.; Yang, C. F.; Goldberg, I. H. *J. Mass Spectrom.* **1996**, *31*, 31-36.

(97) Iannitti, P.; Sheil, M. M.; Wickham, G. *J. Am. Chem. Soc.* **1997**, *119*, 1490-1491.

(98) Kapur, A.; Beck, J. L.; Sheil, M. M. *Rapid Commun. Mass Spectrom.* **1999**, *13*, 2489-2497.

(99) Paz, M. M.; Das, A.; Palom, Y.; He, Q.-Y.; Tomasz, M. *J. Med. Chem.* **2001**, *44*, 2834-2842.

(100) Carrasco, C.; Rosu, F.; Gabelica, V.; Houssier, C.; De Pauw, E.; Garbay-Jaureguiberry, C.; Roques, B.; Wilson, W. D.; Chaires, J. B.; Waring, M. J.; Bailly, C. *ChemBioChem*. **2002**, *3*, 1235-1241.

(101) Guittat, L.; Alberti, P.; Rosu, F.; Van Miert, S.; Thetiot, E.; Pieters, L.; Gabelica, V.; De Pauw, E.; Ottaviani, A.; Riou, J.-F.; Mergny, J.-L. *Biochimie*. **2003**, *85*, 535-547.

(102) Wan, K. X.; Gross, M. L.; Shibue, T. *J. Am. Soc. Mass Spectrom.* **2000**, *11*, 450-457.

(103) Gabelica, V.; Rosu, F.; Houssier, C.; De Pauw, E. *Rapid Commun. Mass Spectrom.* **2000**, *14*, 464-467.

(104) Gupta, R.; Kapur, A.; Beck, J. L.; Sheil, M. M. *Rapid Commun. Mass Spectrom.* **2001**, *15*, 2472-2480.

(105) David, W. M.; Brodbelt, J.; Kerwin, S. M.; Thomas, P. W. *Anal. Chem.* **2002**, *74*, 2029-2033.

(106) Doerge, D. R.; Yi, P.; Churchwell, M. I.; Preece, S. W.; Langridge, J.; Fu, P. P. *Rapid Commun. Mass Spectrom.* **1998**, *12*, 1665-1672.

(107) Iannitti-Tito, P.; Weimann, A.; Wickham, G.; Sheil, M. M. *Analyst* **2000**, *125*, 627-634.

(108) Rosu, F.; Gabelica, V.; Houssier, C.; Colson, P.; De Pauw, E. *Rapid Commun. Mass Spectrom.* **2002**, *16*, 1729-1736.

(109) Shen, L.; Qiu, S.; Chen, Y.; Zhang, F.; Van Breemen, R. B.; Nikolic, D.; Bolton, J. L. *Chem. Res. Toxicol.* **1998**, *11*, 94-101.

(110) Kloster, M. B. G.; Hannis, J. C.; Muddiman, D. C.; Farrell, N. *Biochemistry* **1999**, *38*, 14731-14737.

(111) Taatjes, D. J.; Gaudiano, G.; Resing, K.; Koch, T. H. *J. Med. Chem.* **1996**, *39*, 4135-4138.

(112) Taatjes, D. J.; Gaudiano, G.; Resing, K.; Koch, T. H. *J. Med. Chem.* **1997**, *40*, 1276-1286.

(113) Nakatani, K.; Hagihara, S.; Sando, S.; Sakamoto, S.; Yamaguchi, K.; Maesawa, C.; Saito, I. *J. Am. Chem. Soc.* **2003**, *125*, 662-666.

(114) Gupta, R.; Beck, J. L.; Ralph, S. F.; Sheil, M. M.; Aldrich-Wright, J. R. *J. Am. Soc. Mass Spectrom.* **2004**, *15*, 1382-1391.

(115) Qu, Y.; Scarsdale, N. J.; Tran, M.-C.; Farrell, N. *J. Inorg. Biochem.* **2004**, *98*, 1585-1590.

(116) Kerwin, S. M. *Curr. Pharm. Des.* **2000**, *6*, 441-471.

(117) Zahler, A. M.; Williamson, J. R.; Cech, T. R.; Prescott, D. M. *Nature.* **1991**, *350*, 718-720.

(118) Rosu, F.; Gabelica, V.; Shin-ya, K.; De Pauw, E. *Chem. Commun.* **2003**, 2702-2703.

(119) Han, H.; Bennett, R. J.; Hurley, L. H. *Biochemistry* **2000**, *39*, 9311-9316.

(120) Tang, L.; Kebarle, P. *Anal. Chem.* **1993**, *65*, 3654-3668.

(121) Lieze, E.; Jaffrezic, A.; Van Dorsselaer, A. *J. Mass Spectrom.* **1996**, *31*, 537-544.

(122) Young, D.-S.; Hung, H.-Y.; Liu, L. K. *J. Mass Spectrom.* **1997**, *32*, 432-437.

(123) Enke, C. G. *Anal. Chem.* **1997**, *69*, 4885-4893.

(124) Tang, L.; Kebarle, P. *Anal. Chem.* **1991**, *63*, 2709-2715.

(125) Wang, G.; Cole, R. B. *Anal. Chem.* **1994**, *66*, 3702-3708.

(126) King, R.; Bonfiglio, R.; Fernandez-Metzler, C.; Miller-Stein, C.; Olah, T. *J. Am. Soc. Mass Spectrom.* **2000**, *11*, 942-950.

(127) Wang, H.; Agnes, G. R. *Anal. Chem.* **1999**, *71*, 3785-3792.

(128) Cheng, X.; Gao, Q.; Smith, R. D.; Jung, K.-E.; Switzer, C. *Chem. Commun.* **1996**, 747-748.

(129) Fändrich, M.; Tito, M. A.; Leroux, M. R.; Rostom, A. A.; Hartl, F. U.; Dobson, C. M.; Robinson, C. V. *Proc. Natl. Acad. Sci. USA* **2000**, *97*, 14151-14155.

(130) Lin, H.-K.; Hsieh, Y. L.; Ganem, B.; Henion, J. *J. Mass Spectrom.* **1995**, *30*, 708-714.

(131) Greig, M. J,; Gaus, H.; Cummins, L. L.; Sasmor, H.; Griffey, R. H. *J. Am. Chem. Soc.* **1995**, *117*, 10765-10766.

(132) Eckart, K.; Spiess, J. *J. Am. Soc. Mass Spectrom.* **1995**, *6*, 912-919.

(133) Loo, J. A.; Hu, P.; McConnell, P.; Mueller, W. T.; Sawyer, T. K.; Thanabal, V. *J. Am. Soc. Mass Spectrom.* **1997**, *8*, 234-243.

(134) Ayed, A.; Krutchinsky, A. N.; Ens, W.; Standing, K. G.; Duckworth, H. W. *Rapid. Commun. Mass Spectrom.* **1998**, *12*, 339-344.

(135) Griffey, R. H.; Hofstadler, S. A.; Sannes-Lowery, K. A.; Ecker, D. J.; Crooke, S. T. *Proc. Natl. Acad. Sci. USA* **1999**, *96*, 10129-10133.

(136) Sannes-Lowery, K. A.; Griffey, R. H.; Hofstadler, S. A. *Anal. Biochem.* **2000**, *280*, 264-271.

(137) Kapur, A.; Beck, J. L.; Brown, S. E.; Dixon, N. E.; Sheil, M. M. *Protein Sci.* **2002**, *11*, 147-157.

(138) Gabelica, V.; Galic, N.; Rosu, F.; Houssier, C.; De Pauw, E. *J. Mass Spectrom.* **2003**, *38*, 491-501.

(139) Bligh, S. W. A.; Haley, T.; Lowe, P. N. *J. Mol. Recognit.* **2003**, *16*, 139-147.

(140) Daniel, J. M.; McCombie, G.; Wendt, S.; Zenobi, R. *J. Am. Soc. Mass Spectrom.* **2003**, *14*, 442-448.

(141) Zhu, M. M.; Rempel, D. L.; Du, Z.; Gross, M. L. *J. Am. Chem. Soc.* **2003**, *125*, 5252-5253.

(142) Zhang, S.; Van Pelt, C. K.; Wilson, D. B. *Anal. Chem.* **2003**, *75*, 3010-3018.

(143) Hagan, N.; Fabris, D. *Biochemistry* **2003**, *42*, 10736-10745.

(144) Dotsikas, Y.; Loukas, Y. L. *J. Am. Soc. Mass Spectrom.* **2003**, *14*, 1123-1129.

(145) Wendt, S.; McCombie, G.; Daniel, J.; Kienhöfer, A.; Hilvert, D.; Zenobi, R. *J. Am. Soc. Mass Spectrom.* **2003**, *14*, 1470-1476.

(146) Zhu, M. M.; Rempel, D. L.; Gross, M. L. *J. Am. Soc. Mass Spectrom.* **2004**, *15*, 388-397.

(147) Tjernberg, A.; Carnö, S.; Oliv, F.; Benkestock, K.; Edlund, P.-O.; Griffiths, W. J.; Hallén, D. *Anal. Chem.* **2004**, *76*, 4325-4331.

(148) Peschke, M.; Verkerk, U. H.; Kebarle, P. *J. Am. Soc. Mass Spectrom.* **2004**, *15*, 1424-1434.

(149) De Vriendt, K.; Sandra, K.; Desmet, T.; Nerinckx, W.; Van Beeumen, J.; Devreese, B. *Rapid Commun. Mass Spectrom.* **2004**, *18*, 3061-3067.

(150) Jørgensen, T. J. D.; Roepstorff, P.; Heck, A. J. R. *Anal. Chem.* **1998**, *70*, 4427-4432.

(151) Jørgensen, T. J. D.; Staroske, T.; Roepstorff, P.; Williams, D. H.; Heck, A. J. R. *J. Chem. Soc., Perkin Trans. 2* **1999**, 1859-1863.

(152) Henroutte, V.; Laurent, S.; Gabelica, V.; Vander Elst, L.; Depauw, E.; Muller, R. N. *Rapid Commun. Mass Spectrom.* **2004**, *18*, 1919-1924.

(153) Zampronio, C. G.; Giannakopulos, A. E.; Zellér, M.; Bitziou, E.; Macpherson, J. V.; Derrick, P. J. *Anal. Chem.* **2004**, *76*, 5172-5179.

(154) Young, D.-S.; Hung, H.-Y.; Liu, L. K. *Rapid Commun. Mass Spectrom.* **1997**, *11*, 769-773.

(155) Kempen, E. C.; Brodbelt, J. S. *Anal. Chem.* **2000**, *72*, 5411-5416.

(156) Clark, S. M.; Konermann, L. *Anal. Chem.* **2004**, *76*, 1257-1263.

(157) Clark, S. M.; Konermann, L. *Anal. Chem.* **2004**, *76*, 7077-7083.

CHAPTER 2

Experimental Methods

2.1 Introduction

The mass spectral analyses presented in subsequent chapters were all obtained on a LCQ Duo quadrupole ion trap mass spectrometer (ThermoFinnigan, San Jose, CA) that was equipped with an electrospray ionization (ESI) source. The characteristics of both the ESI source and the quadrupole ion trap are described in detail below. Equilibrium calculations were performed on a personal computer using procedures written for the Waterloo Maple computer algebra software package (Waterloo, ON, Canada).

2.2 Electrospray Ionization

2.2.1 Ion Production

To produce the ions analyzed in these studies from their native solutions, an electrospray ionization source was used. The mating of Dole's electrospray source (1) directly to a mass spectrometer was accomplished by Fenn in the early 1980's (2). Unlike most other ionization sources, ESI produces gas-phase ions directly from solution without any intermediate steps. Its simple design requires only a flowing analyte solution, a needle with a conductive tip, and a counter electrode (Figure 2-1).

For these experiments, the solution was pumped through a stainless steel needle at 5-10 μL/min with either a syringe pump or an HPLC pump. The needle was held at a potential of +4 to +6 kV to generate positive ions or -4 to -6 kV to generate negative ions.

This high voltage applied to the ESI needle induces electrochemical oxidation reactions in the solution (or reduction if operating in negative ion mode) resulting in an excess of charge at the tip of the needle. The electric field between the needle and the counter-electrode held at ground forces the charged solution out of the tip of the needle where the electrostatic repulsions between the like charges leads to the formation of what is termed a Taylor cone (3). From the tip of the Taylor cone, charged droplets are ejected which then migrate through the air towards the counter electrode.

As the charged droplets travel towards the counter electrode, solvent evaporates from the droplets causing them to shrink. At some point, the size of a droplet approaches what is known as the Rayleigh limit, the point at which the electrostatic repulsions between the charges in the droplet overcome the surface tension holding the droplet together (4-5). When a droplet approaches the Rayleigh limit, the droplet can undergo a fission process where smaller offspring droplets are produced in a manner analogous to the droplet formation from the initial Taylor cone (5-6). The offspring droplets then can

Figure 2-1. Simplified diagram of an electrospray ionization source.

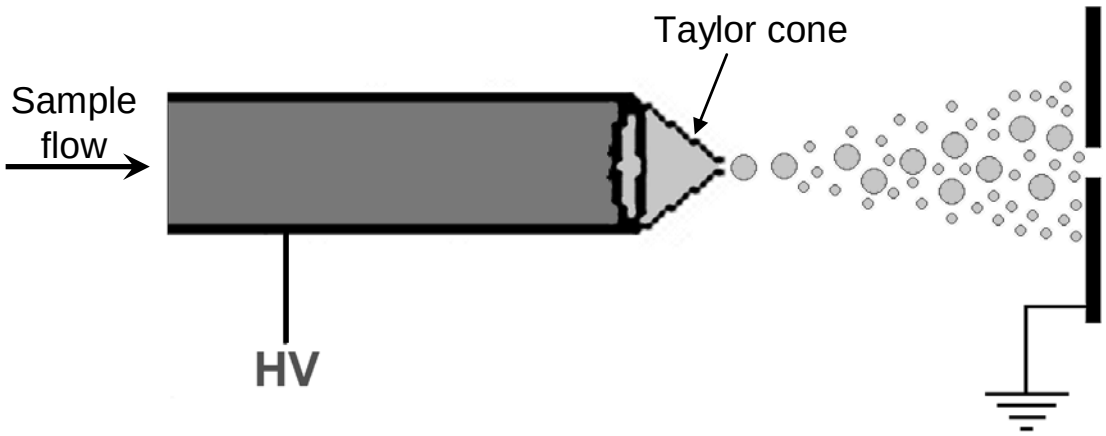

repeat the process, and on again reaching the Rayleigh limit the droplets can either produce ions via evaporation directly from the droplet into the gas phase (7), or they can undergo further fissions until all solvent is gone leaving a charged residue (8). Many of the ions produced are neutralized by the counter electrode, completing the electric circuit, but an aperture in the counter electrode through which the ions can travel allows it to serve as the first stage of an interface between the atmospheric pressure ESI source and the vacuum chamber of the mass spectrometer.

2.2.2 Atmospheric Pressure Interface

While an ESI source produces ions at atmospheric pressure, mass spectrometers must be operated under vacuum. Although the pressures required for successful mass analysis vary depending on the particular mass analyzer used, all analyzers require pressures many orders of magnitude lower than atmosphere. The quadrupole ion trap mass analyzers used herein typically operate in the microTorr pressure regime. (The pressure in these analyzers is often raised through the introduction of a background gas, but this does not significantly alter the vacuum requirements of the atmospheric pressure interface.) To bridge these extreme pressure differentials without overloading the vacuum system, one or more differentially pumped regions separated by skimming apertures allow the ions to be transferred to sequentially lower pressure regions. A variety of electrostatic lenses and other types of ion guides have been employed to enhance ion transmission through these regions, but a discussion of them is beyond the scope of this dissertation since their differences typically have little impact on the experimental results obtained.

2.3 Quadrupole Ion Trap Mass Spectrometry

Paul and Steinwedel developed the quadrupole ion trap in the early 1950's (9). Not until the 1980's, however, were advances developed that enhanced the performance of the quadrupole ion trap and made them competitive as a mass analyzers such as the mass selective instability scan and the use of higher background gas pressures (10). The shape of a quadrupole ion trap results from rotating a hyperbola in three dimensions about one of its axes, forming a toroidal ring electrode and two end-cap electrodes (Figure 2-2). Application of a radio frequency (rf) potential to the ring electrode creates a quadrupolar field between it and the grounded end-cap electrodes that can trap ions in the central cavity. Ions can be generated inside the trap, but most modern instruments, including the one used in these studies, utilize external ionization and injection of the ions into the trap through holes in one of the end-cap electrodes (11). Once in the trap, ions are kinetically cooled through collisions with a bath gas as they are confined by the rf trapping field. The frequency of the rf waveform and its voltage define the lowest mass-to-charge ratio (m/z) of ions that can be trapped; the trajectories of the lower m/z ions in the trap are unstable, causing them to be rapidly ejected. For practical reasons, the frequency of the rf waveform is fixed in a given experiment. To mass analyze the trapped ions, the voltage of the rf waveform is scanned upward, causing the m/z-dependent ejection of ions from the trap, starting at the lowest masses and progressing upwards until the limits of the rf power supply are reached (10). Many of the ejected ions pass through holes in the end-cap electrodes where they are detected with an electron multiplier or other ion-sensitive detector.

Figure 2-2. A cutaway view of a quadrupole ion trap mass analyzer.

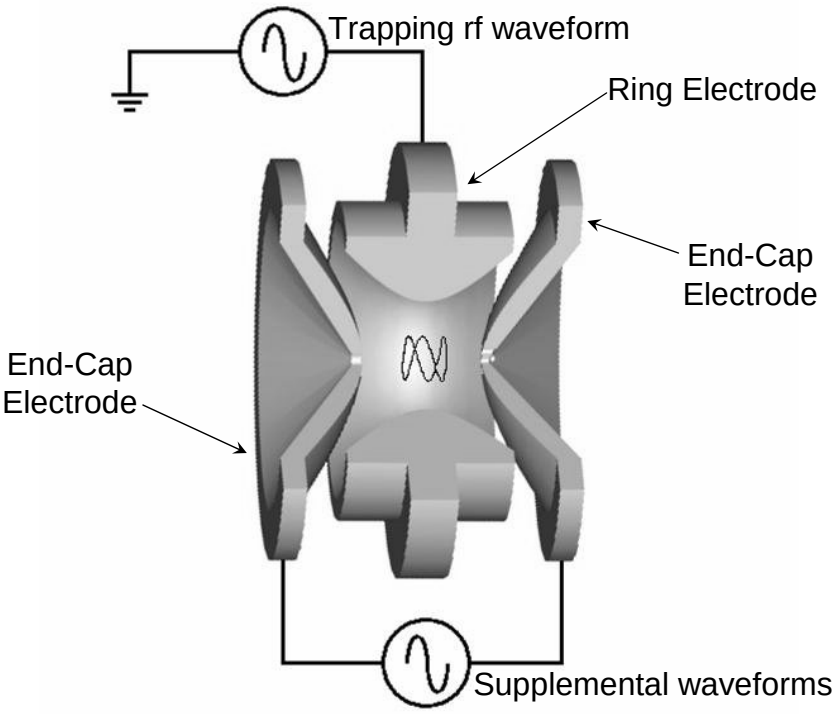

Further manipulations of ions trapped in a quadrupole ion trap can be done through the application of supplementary waveforms to the end-cap electrodes. For a given set of trapping conditions, each m/z has a characteristic frequency of oscillation in the trap. Applying a waveform across the end-cap electrodes with the same frequency of a particular ion increases the kinetic energy of that ion. If the added kinetic energy of the ion is low enough that the ion remains trapped, the collisions it undergoes with gas molecules in the trap become more energetic resulting in an increase in the internal energy of the ion which can after many collisions ultimately lead to fragmentation of the ion in a process known as collisionally activated dissociation (CAD). If the added kinetic energy is too great, the ion overcomes the trapping fields and is ejected from the trap.

Through the judicious selection of supplementary waveform frequencies and voltages, particular ions can be isolated in the trap and made to fragment via CAD (12). Supplemental waveforms applied in this manner also are commonly used to manipulate the ejection of ions during the mass selective instability scan to increase ejection efficiency and increase the upper mass range of the mass spectrometer (13).

2.4 Computational Methods

To evaluate the distributions of host-guest complexes in solution and to model their behavior in the ESI source, different types of equilibrium calculations were performed. In the traditional equilibrium analyses used to determine concentrations in solution, equations fulfilling the required mass balances, charge balances, and equilibrium reactions define sets of n equations with n unknown concentrations. For the mathematical modeling of the ESI source, additional equations reflecting the partitioning of the various species between the interior and surface of the ESI droplets were included yielding somewhat larger sets of equations and unknown concentrations. In both cases, rather than solve the sets of equations analytically, procedures were written using the Waterloo Maple computer algebra software package (Waterloo, ON, Canada) to solve the systems of equations numerically. Since a set of n equations and n unknown variables will have up to n solutions, procedures were also written to select the physically meaningful solutions. In particular, solutions with imaginary components or values which would lead to negative concentrations cannot have physical relevance. In no case did the calculations fail to produce a single relevant solution. The results of these

calculations were compared with equilibrium concentrations calculated by hand for some simple systems to validate the method.

2.5 References

(1) Dole, M.; Mack, L. L.; Hines, R. L.; Mobley, R. C.; Ferguson, L. D.; Alice, M. B. *J. Chem. Phys.* **1968**, *49*, 2240-2249.

(2) Yamashita, M.; Fenn, J. B. *J. Phys. Chem.* **1984**, *88*, 4451-4459.

(3) Taylor, G. I. *Proc. R. Soc. London A* **1964**, *280*, 383.

(4) Rayleigh, Lord *Philos. Mag.* **1882**, *14*, 184.

(5) Taflin, D. C.; Ward, T. L.; Davis, E. J. *Langmuir*. **1989**, *5*, 376-384.

(6) Gomez, A.; Tang, K. *Phys. Fluids.* **1994**, *6*, 404-414.

(7) Iribarne, J. V.; Thomson, B. A. *J. Chem. Phys.* **1976**, *64*, 2287-2294.

(8) Dole, M.; Mack, L. L.; Hines, R. L.; Mobley, R. C.; Ferguson, L. D.; Alice, M. B. *J. Chem. Phys.* **1968**, *49*, 2240-2249.

(9) Paul, W.; Steinwedel, H. Z. *Z. Naturforsch*. **1953**, *8a*, 448-450.

(10) Stafford, G. C.; Kelley, P. E.; Syka, J. E. P.; Reynolds, W. E.; Todd, J. F. J. *Int. J. Mass Spectrom. Ion Proc.* **1984**, *60*, 85-98.

(11) Kaiser, R. E., Jr.; Cooks, R. G.; Stafford, G. C., Jr.; Syka, J. E. P.; Hemberger, P. H. *Int. J. Mass Spectrom. Ion Proc.* **1991**, *106*, 79-115.

(12) Louris, J. N.; Cooks, R. G.; Syka, J. E. P.; Kelley, P. E.; Stafford, G. C., Jr.; Todd, J. F. J. *Anal. Chem.* **1987**, *59*, 1677-1685.

(13) Kaiser, R. E.. Jr.; Cooks, R. G.; Moss, J.; Hemberger, P. H. *Rapid Commun. Mass Spectrom.* **1989**, *3*, 50-53.

CHAPTER 3

An Equilibrium Partitioning Model for Predicting Response to Host-Guest Complexation in ESI-MS

3.1 Introduction

Electrospray ionization (ESI) has revolutionized the study of host-guest chemistry by allowing the analysis of solution-phase non-covalent complexes by mass spectrometry. In recent years, a wide variety of types of interactions have been studied by ESI-MS, including such diverse areas as protein-substrate interactions (1-4), DNA-drug binding (2, 5-7), and metal chelation (2, 8-16). While much of the research in this area has centered on more qualitative types of analyses of the complexation reaction (2, 7, 9-17), some methods have been developed for quantitative study of host-guest interactions by exploiting different aspects of the electrospray process (1-2, 8, 18-20).

Typically, these types of quantitative analyses have relied on the assumption that the ESI response to a particular compound is dependant only on its concentration in solution and is not affected significantly by the presence of other species or any other factors. In many cases, especially when experimental conditions are carefully controlled, this assumption holds true, but more thorough studies of the electrospray process itself have revealed behavior that may challenge its validity in some situations. For instance, it has been unambiguously demonstrated that ESI signal response is not only nonlinear at moderate concentrations but also static at relatively high concentrations (21-24). Also,

experimental parameters often not considered can cause dramatic shifts in signal intensity (23, 25-26). Particularly, the presence of additional species such as salts and other ionic species in surprisingly low concentrations has been shown to cause rather large decreases in the observed signal intensity (21-24, 27-31). Compounding the problems faced when designing quantitative ESI-MS experiments is the fact that different analytes often have greatly differing electrospray "efficiencies" (2, 11). To overcome this issue, various schemes for making corrections have been developed (2, 8, 11, 16-17), but these corrections often have depended on the same assumption of linear ESI response independent of other species that makes quantitation difficult in the first place.

Making measurements that allow more accurate conclusions about the solution-phase equilibrium processes being studied requires a greater understanding of the processes taking place in ESI that effect the transferal of charged complexes from solution into the gas-phase. Enke laid the foundations for such a study when he presented a mathematical model explaining quantitatively the relationship between solution-phase concentration and the ion abundances generated through ESI for permanently charged analytes (32). Named the equilibrium partitioning model, it applied an equilibrium treatment to the ESI droplets to calculate the expected ESI-MS signal intensity for these simple analytes for a particular set of experimental conditions.

The theoretical basis for the equilibrium partitioning model lies in several key observations about the chemistry and physics of the ESI droplets. As Gomez and Tang elegantly demonstrated with their photographs of droplets undergoing fission (33), smaller offspring droplets are "pinched" from the edges of the large parent droplets

formed initially in ESI. As a result, these offspring droplets are highly enriched in the species which were on the surface of the parent droplet (24, 34-36). Since most of the ion current generated by an ESI source originates from the smaller droplets formed from the fissions early in the electrospray process (21, 35-36), it has been concluded that the gas-phase ions generated in ESI were typically present on the surface of the initial droplets formed (32).

Next, to understand the flow of charged species in ESI, the source must be considered from an electrical and electrochemical perspective. Due to its extremely high resistance, the ESI source is essentially a controlled current device (30, 37-40). This small current (on the order of microamps) drives the electrochemical oxidation (or reduction) at the ESI emitter in positive (or negative) ion mode. It is this process that creates the excess charge generated in ESI. By considering the volume flow rate of solution into the ESI source, the concentration of the excess charge on the initial droplets can be calculated:

$$[Q] = I / \Gamma F \qquad (3\text{-}1)$$

where [Q] is the concentration of excess charge, I is the current through the ESI source, Γ is the volume flow rate, and F is Faraday's constant (32). Furthermore, through electrostatic repulsions, all of the excess charge resides on the droplet surface, while the droplet interior maintains electro-neutrality (32). Together with the fact that molecules on the droplet surface are necessarily less well solvated, this charge separation creates chemically different states on the surface and interior of the ESI droplets (2, 21). As a

result, the molecules and ions in the droplets partition between the two states according to an equilibrium relationship.

This partitioning equilibrium lies at the heart of the model and has serious implications for the behavior of different analytes in ESI. Using an equation for the partitioning of species in the ESI droplets, as well as equations for mass and charge balance, concentration of the analyte on the surface of the initial ESI droplets was calculated by solving the system of equilibrium. Since the gas-phase ions originate on this surface, the ion abundance detected by the mass spectrometer is proportional to this concentration according to the following relationship:

$$A = P\, f\, [A^+]_s \qquad (3\text{-}2)$$

where A is the abundance of ions introduced into the mass spectrometer, $[A^+]_s$ is the surface concentration of the analyte, and P and f are the sampling efficiency of the ESI-MS interface and the efficiency of the ESI process in transferring surface ions into the gas phase respectively. P and f are specific to a particular instrumental configuration but would be the same for all molecular species in a given experiment (32).

While others have studied various aspects of the equilibrium partitioning model (25-26, 29, 34, 41-43), most research to date has been limited to nearly ideal analytes – simple, permanently charged molecules. While useful for studying the ESI source itself, these analytes are of limited chemical significance. To apply the lessons learned about ESI to the many types of host-guest chemistry that are currently being intensely studied, the research presented herein focuses on developing an equilibrium partitioning model to

explain the relationships between the host-guest complexes observed in ESI-MS and the solution-phase host-guest equilibria of interest.

3.2 Experimental

3.2.1 Mathematical Modeling.

The simultaneous equilibrium equations were solved and appropriate solutions selected by a program written using the Waterloo Maple 7 (Waterloo, Ontario, Canada) computer algebra software running on a Windows-based personal computer. Response curves were fit to experimental data by manually varying partitioning constants to minimize deviation.

3.2.2 Reagents.

Host compound 18-crown-6, rubidium chloride (RbCl), tetramethylammonium iodide (Me_4NI), tetraethylammonium iodide (Et_4NI), tetrapropylammonium iodide (Pr_4NI), and tetrapentylammonium bromide (Pe_4NBr) were obtained from the Aldrich Chemical Company (Milwaukee, WI). Sodium chloride (NaCl) and potassium chloride (KCl) were obtained from EM Science (Gibbstown, NJ). Tetrabutylammonium chloride (Bu_4NCl) was obtained from Fluka Chemie AG (Buchs, Switzerland), and tetrabutylammonium iodide (Bu_4NI) and ammonium chloride (NH_4Cl) were obtained from the Sigma Chemical Company (St. Louis, MO). All reagents were of at least 98% purity and were used without further purification. Stock solutions of the compounds at 10 mM in spectroscopic grade OmniSolv methanol (EM Science) were mixed and diluted

again with methanol to prepare the analyzed solutions. Concentrations ranged from 100 nM to 3 mM.

3.2.3 Instrumentation.

Mass spectrometric measurements were made on an LCQ Duo quadrupole ion trap mass spectrometer equipped with an ESI source (ThermoFinnigan, San Jose, CA). Peak widths were monitored and the ionization time was adjusted as necessary to prevent space charging effects in the ion trap. A three resistor network was added between the high voltage supply and the ESI source to facilitate accurate measurement of the electrospray current and to guard against arcing. Data was collected using the Xcalibur acquisition software (ThermoFinnigan), and one hundred scans were averaged to minimize the effects of instrumental fluctuations. Instrumental parameters were optimized for detection of the (18-crown-6 + $K)^+$ ion. Direct infusion analyses were performed at 5 μL/min using a Harvard Apparatus PHD 2000 syringe pump (South Natick, MA).

3.3 Discussion

As with Enke's model (32), the equilibrium partitioning model for host-guest complexation relies on three key assumptions. First, ESI is a current controlled source, limiting the total amount of excess charge that can reside on the droplets. Second, through electrostatic repulsions the excess charge will reside completely on the surface of the droplets. Third, the various chemical species in the droplets can partition between the surface and interior of the droplets. With these premises in hand, the distribution of

species in the droplets at the beginning of the ESI process was modeled through an analysis of the various simultaneous equilibrium processes occurring.

Throughout the analysis, the following naming conventions are used for the various terms: H, G^+, E^+, and HG^+ represent the different chemical species: the neutral host compound, the charged guest ion, the background electrolyte, and the charged host-guest complex, respectively. For simplicity, ions are assumed to be positively charged, and counter-ions are not included in the analysis. As defined above, [Q] is the concentration of excess charge in the droplets. C_x represents the formal concentration of a species in the original solution where x is the symbol for one of the chemical species. Likewise, K_x represents the partitioning constant for species x. K_b represents the binding

Figure 3-1. Diagram of the various equilibria present in an ESI droplet with host-guest complexation.

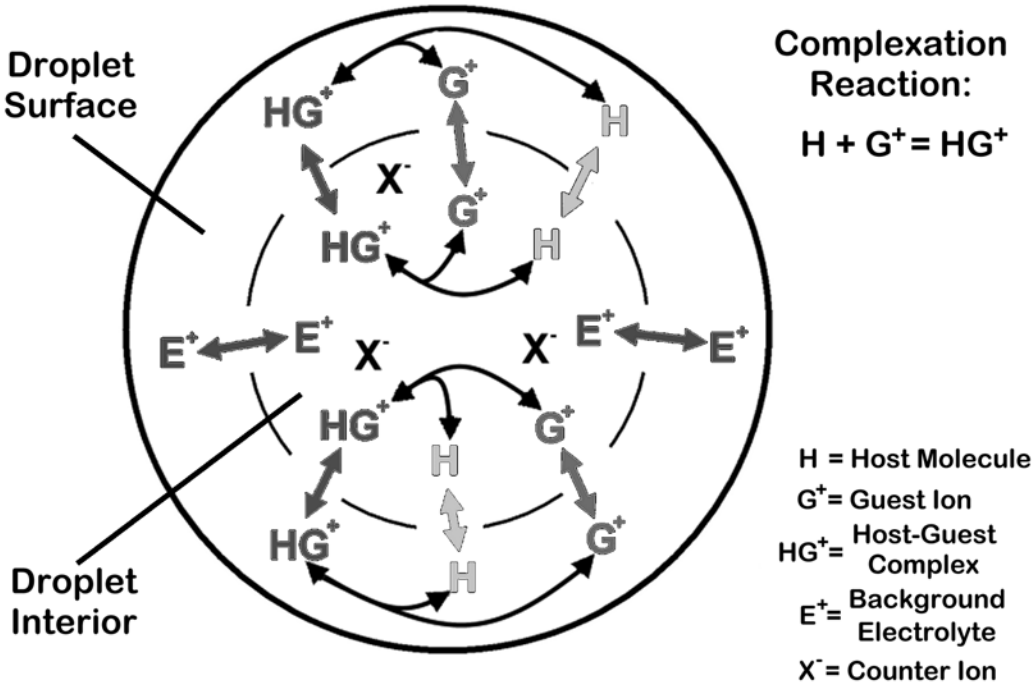

constant for complexation equilibria. Finally, the subscripts s and i denote the surface and interior of the ESI droplets respectively. The various binding and partitioning equilibria that are possible in the ESI droplet are depicted in Figure 3-1.

In any system, charge and mass must be conserved. This tenet led to the introduction of charge and mass balance equations in equilibrium based analyses. In ESI, the excess charge generated by the electrochemical reactions at the ESI emitter is of particular import and is represented by the concentration of excess charge on the droplets, [Q]. Equation 3-1 demonstrated that [Q] is an experimental parameter that can be calculated from the measured ESI current and the set volume flow rate of solution. The value of [Q] must always be equal to the sum of the concentrations of the ions comprising the excess charge. Since the excess charge must reside on the droplet surface, [Q] is the sum of the surface concentrations of the different ions:

$$[Q] = [HG^+]_s + [G^+]_s + [E^+]_s \quad (3\text{-}3)$$

While the excess charge resides on the droplet surfaces, the droplet interiors retain electro-neutrality and essentially reflect the properties of the bulk solution. As a result, no separate charge balance equation is required for the droplet interior.

Since the solutions analyzed contain three primary components, H, G^+, and E^+, three mass balance equations were required. These equations simply summed the concentrations of all species that contained a particular component:

$$C_H = [H]_s + [H]_i + [HG^+]_s + [HG^+]_i \quad (3\text{-}4)$$

$$C_G = [G^+]_s + [G^+]_i + [HG^+]_s + [HG^+]_i \quad (3\text{-}5)$$

$$C_E = [E^+]_s + [E^+]_i \quad (3\text{-}6)$$

In most experiments, C_H and C_G would be the prepared concentrations of H and G^+. C_E would typically be the concentration of the unavoidable ionic contaminants, although it can be raised by including additional electrolyte in the solution.

Next, the partitioning of species between the droplet surface and interior had to be considered. This phenomenon is analogous to the partitioning in a chemical separation and is the result of differences in the chemical environments between the droplet interior and droplet surface. Since analytes which have lower solvation energies in polar solvents like water or methanol tend to have greater affinities for the droplet surface (2, 21), the chemical environment on the droplet surface must be less polar than the droplet interior, implying that the lesser degree of solvation of analytes on the surface accounts for the difference in the surface affinities of different analytes.

Regardless of the actual chemical interactions occurring, the partitioning can be represented as the ratio of the surface concentrations to the interior concentrations for the different species:

$$K_H = [H]_s / [H]_i \quad (3\text{-}7)$$

$$K_C = [HG^+]_s / [HG^+]_i \quad (3\text{-}8)$$

$$K_G = [G^+]_s / [G^+]_i \quad (3\text{-}9)$$

$$K_E = [E^+]_s / [E^+]_i \quad (3\text{-}10)$$

For a particular experiment, however, since the different species are all competing for the same surface positions, the relative values of these partitioning constants are important instead of their absolute values. As such, the constants were redefined as relative partitioning constants by taking the ratio of an analyte's partitioning constant to that of

the background electrolyte. For example, equation 3-7 divided by equation 3-10 yielded equation 3-11 (below):

$$K_{HE} = ([H]_s \times [E^+]_i) / ([H]_i \times [E^+]_s) \quad (3\text{-}11)$$

$$K_{HGE} = ([HG^+]_s \times [E^+]_i) / ([HG^+]_i \times [E^+]_s) \quad (3\text{-}12)$$

$$K_{GE} = ([G^+]_s \times [E^+]_i) / ([G^+]_i \times [E^+]_s) \quad (3\text{-}13)$$

Finally, the host-guest complexation reactions at the heart of this analysis had to be considered. With all species present both on the surface and in the interior of the droplets, complexation and dissociation can occur in both places. These reactions were represented by traditional association equilibria:

$$K_{bi} = [HG^+]_i / ([H]_i \times [G^+]_i) \quad (3\text{-}14)$$

$$K_{bs} = [HG^+]_s / ([H]_s \times [G^+]_s) \quad (3\text{-}15)$$

Equations 3-7 to 3-9 were then rearranged and substituted into equation 3-15:

$$K_{bs} = (K_H \times K_G / K_C) ([HG^+]_i / ([H]_i \times [G^+]_i) \quad (3\text{-}16)$$

Substituting equation 3-14 into the result revealed that the equations for complexation on the surface and interior are not independent:

$$K_{bs} = (K_H \times K_G / K_C) K_{bi} \quad (3\text{-}17)$$

Since equation 3-14 is equivalent to the binding constant for the complex in the bulk solution, it was kept and equation 3-15 discarded.

The final result of this analysis was a system of eight equations (equations 3-3 through 3-6 and 3-11 through 3-14) with eight unknown concentrations ($[H]_s$, $[H]_i$, $[G^+]_s$, $[G^+]_i$, $[HG^+]_s$, $[HG^+]_i$, $[E^+]_s$, and $[E^+]_i$) that could then be solved. Ideally, the system could be solved analytically, allowing for a detailed analysis of the effects of the different

parameters. Unfortunately, the symbolic solution was too complex to allow meaningful analysis. The system of equations, however, could be solved numerically quite easily with mathematical software. These numerical solutions were then used to plot concentration-dependant response curves so that the effect of the different parameters could be evaluated.

In general, the response curves ($[HG^+]_s$ vs. C_H) predicted by this model behaved similarly to those for permanently charged analytes. When C_H (and as a result, $[HG^+]_s$) were at concentrations much below [Q], the curves were nicely linear. In this range, where the background electrolyte was the dominant ion on the droplet surface and accounted for nearly all of the ESI current, changes in the surface concentration of the host-guest complex barely affected conditions in the droplet. As C_H was increased to a level near that of [Q], the ESI current was distributed among the various ions in solution, causing a direct competition for the limited number of surface positions. This caused the response curve to begin exhibiting saturation behavior. Finally, when C_H was much greater than [Q], $[HG^+]_s$ carried most of the ESI current, and response was flat since no additional ions could reach the droplet surface.

It should be noted that [Q] cannot be greater than the sum of the concentrations of the ionic components in the solution since these ions are themselves the charge carriers across the ESI interface. As a result, if the concentrations of analytes in the solution are very low, [Q] cannot be greater than C_E. This fact is what limits the current in an ESI source and also explains somewhat the increase in current often observed when spraying solutions with a high salt content (21, 23, 27, 31, 39).

To evaluate the effects of the different parameters on the ESI response to the HG^+ ion, different series of response curves were generated varying one parameter while holding the others constant. These curves are shown in Figures 3-2 through 3-4. For these calculations, C_H and C_G were kept in a 1:1 ratio with their values varying from 3 nM to 3 mM. Except when varied, [Q] was 10 μM, C_E was 100 μM, partitioning constants were 1, and K_b was 10^6.

First, the effects of varying [Q] on the ESI response to the host-guest complex was evaluated. Since [Q] determines the number of ions that can be present on the droplet surface, any change in its value led to a corresponding change in the overall ion signal. As [Q] was increased, the concentrations of all ions on the surface increased, including that of the host-guest complex of interest as shown in Figure 3-2a. Unlike most other parameters which affected only the response at lower concentrations, a change in [Q] affected the response over the entire concentration range since [Q] also determines the limiting response at high concentrations.

One of the more common issues faced in ESI experiments is the presence of additional electrolytes in the sample. As such, the effect of C_E on the response was evaluated. Consistent with both conventional wisdom concerning salt suppression in ESI and the results of Enke's original partitioning model (32), as the electrolyte concentration was increased, response to the host-guest complex decreased as shown in Figure 3-2b. The decrease in response was due to a competitive effect. With a greater proportion of background electrolyte in the droplets, other ions were less able to displace the electrolyte from the droplet surface, particularly at low concentrations where the background

Figure 3-2. ESI-MS response to a host-guest complex, HG^+, predicted by the equilibrium partitioning model when [Q] (a) or C_E (b) is varied.

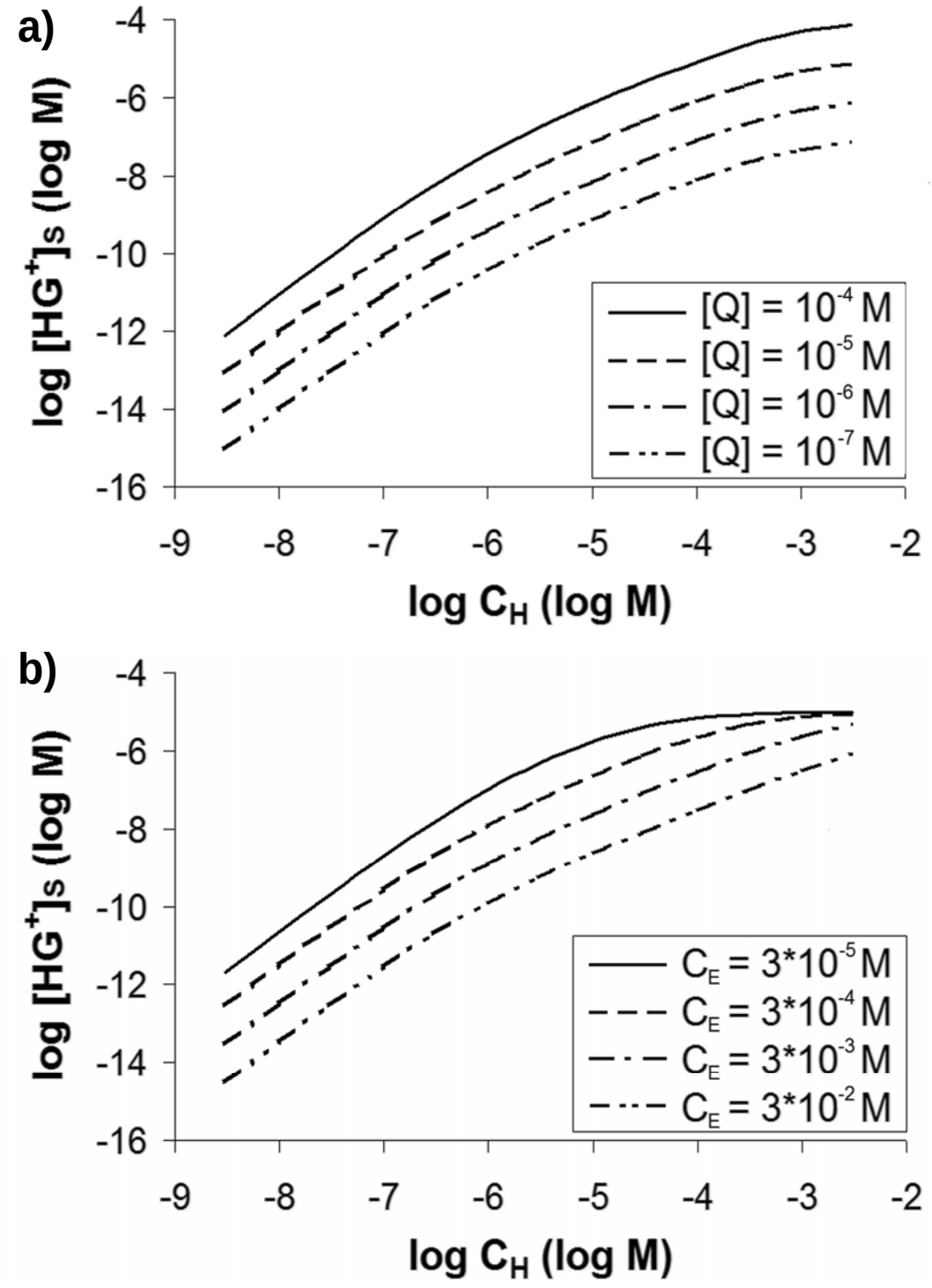

electrolyte comprised essentially all the ions on the droplet surface. As with all the curves, as $[HG^+]_s$ reached C_E the response saturated at a level determined by [Q]. That the saturation occured at higher analyte concentrations and that the response remained more linear over a wider range for higher concentrations of background electrolyte created an interesting trade-off. Essentially, by varying the concentration of the background electrolyte, signal can be traded for a greater dynamic range.

The strength of the binding interaction is one of the most important parameters in host-guest complexation. As expected, an increase in K_b increased the ESI response to the complex, albeit with somewhat unusual behavior at higher binding strengths as shown in Figure 3-3. As K_b was increased, the relative concentration of HG^+ also increased, increasing both its presence on the droplet surface and its ESI response. At lower binding

Figure 3-3. ESI-MS response to a host-guest complex, HG^+, predicted by the equilibrium partitioning model when K_b is varied.

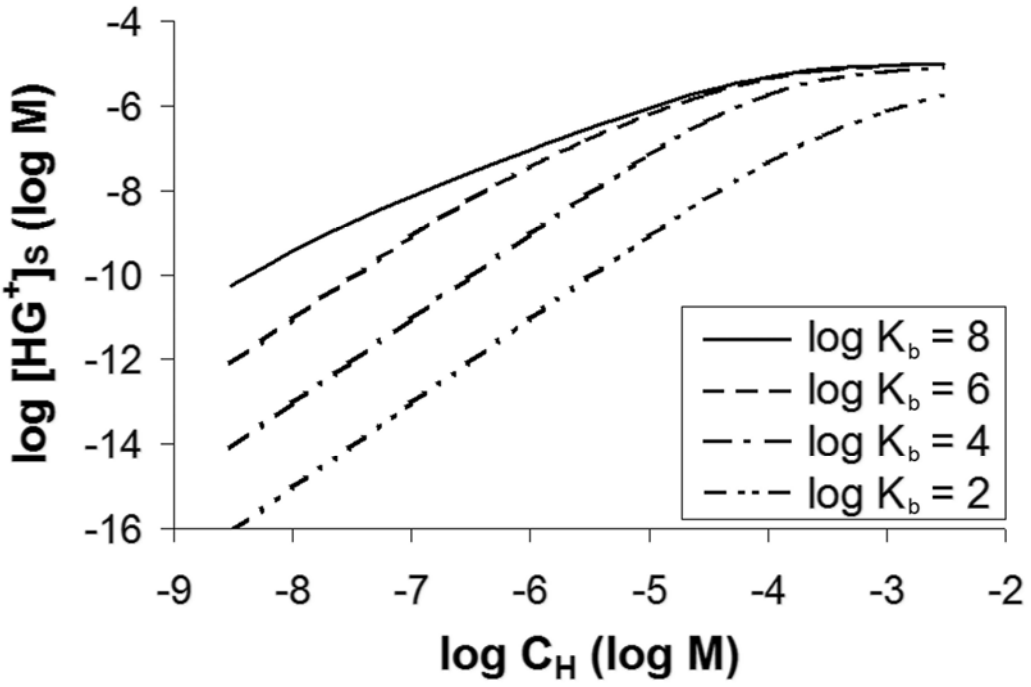

strengths ($K_b \leq 10^6$ for the conditions modeled), a change in K_b altered the concentration of HG^+ at all except the very highest concentrations of the host, resulting in the change in ESI response observed over the entire concentration range below the point of saturation. With higher K_b's, however, essentially all of the host was complexed starting at much lower concentrations. As a result, increasing K_b only increased the ESI response to the host-guest complex at concentrations below that where the host is completely bound. This effect caused the unusual shape and non-linearity of the response curves for complexes with high K_b.

To probe the effects of the partitioning equilibria on the ESI response, these partitioning constants were varied as well. In general, as the partitioning constant of one species was increased, its presence on the droplet surface increased, displacing some amount of the other species. This effect was demonstrated quite clearly as K_{HGE} was varied in Figure 3-4a. As K_{HGE} was increased, HG^+ displaced more species from the droplet surface, causing an increase in its ESI response. Likewise, as K_{HGE} was decreased below the partitioning constants of the other species, the ESI response to HG^+ was suppressed since the complex was largely unable to compete for the limited surface positions.

While the effect of the partitioning equilibria on the ESI response to HG^+ was fairly straightforward, for some species the interaction between the partitioning and complexation equilibria caused more complicated behavior. For instance, as shown in Figure 3-4b, at some values of K_{GE} a change affected $[HG^+]_s$ while at others it did not. Increasing K_{GE} to a level greater than K_{HGE} decreased the ESI response due to the

Figure 3-4. ESI-MS response to a host-guest complex, HG^+, predicted by the equilibrium partitioning model when the relative partitioning constants are varied: (a) K_{HGE}; (b) K_{GE}; (c) K_{HE}.

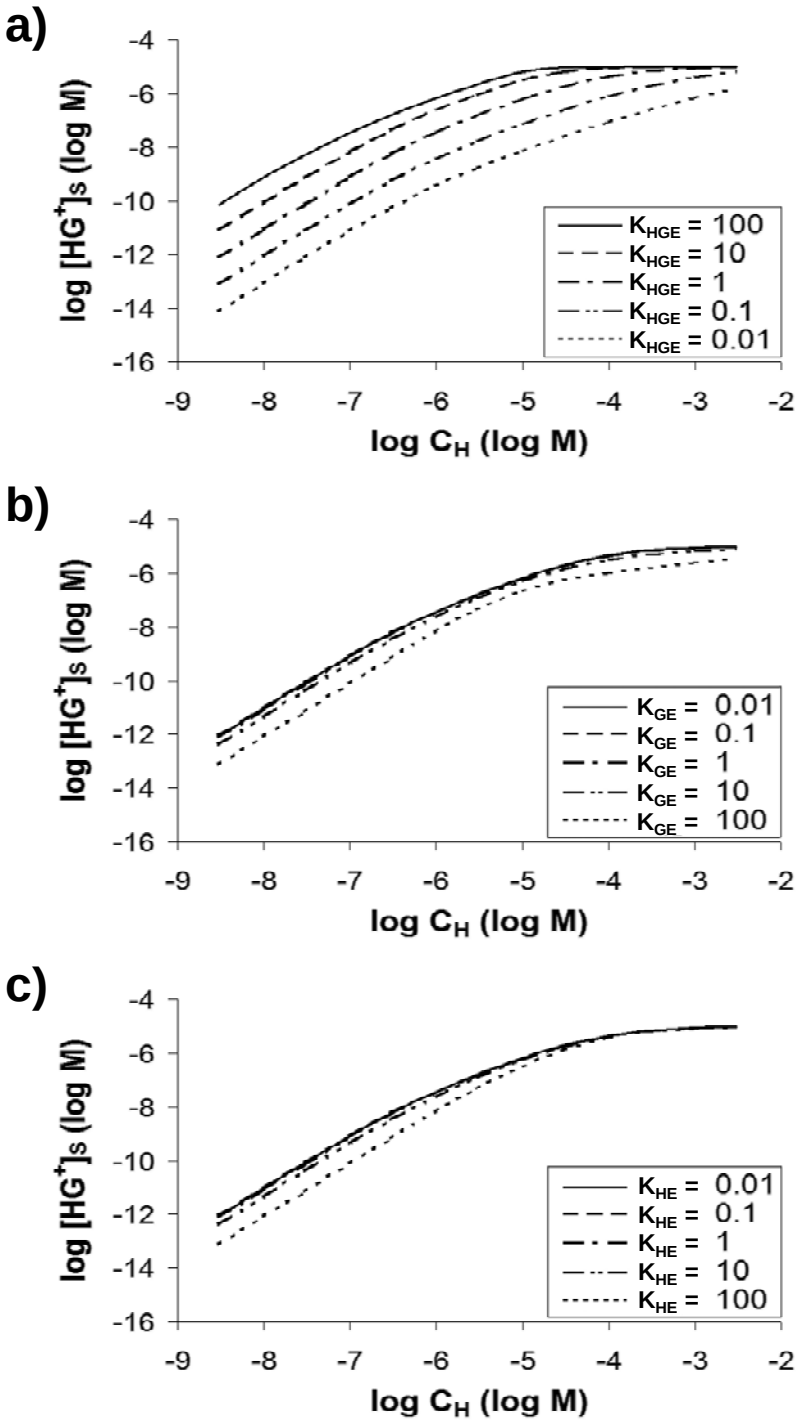

increased competition for the limited number of positions for ions on the droplet surface. The competition not only decreased signal intensity at lower concentrations, but at high concentrations, when C_G was set to increase with C_H, the host-guest complex, and the guest ion had to share the limited number surface positions. The result was lower response at the saturation point and an unusual dip that appeared in the response curve at very high levels of K_{GE}. When K_{GE} was lower than K_{HGE}, however, a change in K_{GE} had no effect on the response to the complex. In this case, the complexation equilibrium became the dominant force driving the partitioning of the guest. Recall that complexation can occur both on the surface of the droplet and in the interior. As a result, the stronger partitioning of the host-guest complex drove changes in the guest ion concentrations through the complexation equilibrium as explained by Le Châtlier's principle. The weaker partitioning of the guest, therefore, had essentially no effect on the system as a whole.

The similar behavior observed when K_{HE} was varied in Figure 3-4c can also be explained as an interaction between the complexation and partitioning equilibria. As with K_{GE}, as K_{HE} was increased beyond K_{HGE}, a decrease in the ESI response to the complex was observed. This would not be surprising in light of the previous discussion concerning K_{GE} except for the fact that H is a *neutral* molecule and would not be expected to impact the partitioning of ions. The effect predicted by the model must, therefore, be the result of interactions through the complexation equilibria. When K_{HE} was larger than K_{HGE}, the host molecules in the ESI droplets tended to partition to the surface, depleting the host concentration in the droplet interior. Through Le Châtlier's

principle this forced some of the host-guest complex in the droplet interior to dissociate, causing more of the complex to partition back into the droplet interior. The net effect was to drive the complex into the interior of the droplet decreasing its ESI response. Also of interest was the absence of the "dip" in the response curve seen when K_{GE} is varied. Since H is neutral, it would not affect the charge balance and, as a result, would not alter the signal response when the surface ion concentrations were saturated with analyte. When K_{HE} was lower than K_{HGE}, as with K_{GE}, the complexation drove the system and H's partitioning had little effect.

3.4 Results

While a theoretical model can independently analyze the effects of many different parameters, reality seldom retains such simplicity. Recognizing that most experimental changes affect multiple parameters, several experiments were devised to test and validate the different predictions of the equilibrium partitioning model for host-guest complexation.

In the first experiment, five series of solutions were analyzed with each series containing a different concentration of Bu_4NCl as the background electrolyte. The results are shown in Figure 3-5. In the ideal case where C_E was varied independently, a family of curves were observed that was very similar to those in Figure 3-2b where the decrease in response to HG^+ was proportional to the increase in C_E. However, a couple of deviations from this behavior were observed. For the two lowest values of C_E, the experimental results showed practically no change in the ESI response. This was due to

Figure 3-5. ESI-MS response to the $(18\text{-crown-6} + K)^+$ ion for solutions containing 1:1 18-crown-6 and KCl as the concentration of the added background electrolyte, Bu_4NCl, was varied.

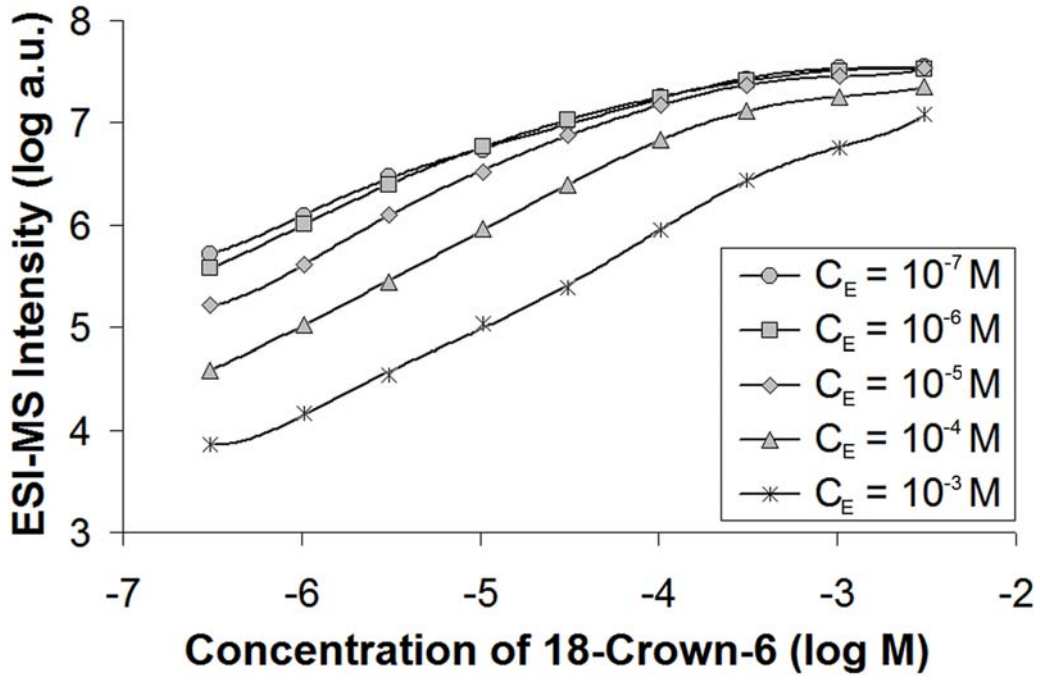

the unavoidable presence of additional ionic contaminants in the solvents used. Others have demonstrated that even at the highest purity levels of methanol available, NaCl is present at around 1 to 10 μM concentrations (25, 30). As a result, C_E can never be less than the concentration of these ionic contaminants. From the experimental results, based on when an added electrolyte affects the ESI response it was estimated that the contaminant concentration in the solvent used is between 1 and 10 μM, consistent with prior estimates.

In addition to the behavior at low Bu_4N^+ concentrations, as C_E was increased, the decrease in response increased as opposed to the proportional decrease predicted by the model. The predictions assume, though, that the identity of the background electrolyte

remains unchanged. In the experiment, at the lowest values of C_E the background electrolyte was predominantly Na^+, and as C_E increased the background electrolyte contained greater and greater amounts of Bu_4N^+. This caused a shift in all the relative partitioning constants in addition to the change in C_E. Since Bu_4N^+ is known to have an extremely high ESI efficiency due to its greater non-polar character (21), it was assumed that it has a greater partitioning constant that Na^+. This assumption was further confirmed below. Since the partitioning constants were defined relative to that of the background electrolyte, as K_E shifted to higher values with the shift from Na^+ to Bu_4N^+, the relative partitioning constants for the other species decreased. By creating an additional reason for the ESI response to decrease, the shift in K_E caused the response to the host-guest complex to be suppressed more greatly than if the C_E alone were increased.

To measure the effect of a change in the partitioning constants of the analytes, a similar experiment was performed where the identity of the background electrolyte was varied rather than its concentration. Five different series of solutions were analyzed, each with a different tetraalkylammonium salt as the background electrolyte. The resulting response curves are presented in Figure 3-6. Since the tetraalkylammonium salts have nearly identical chemical behavior and nothing else differed among the five series, K_E was the only parameter that changes. So as K_E was increased, all other species became less able to compete for positions on the droplet surface. From the model's predictions, a decrease in ESI response would be expected at host and guest concentrations below C_E. At higher concentrations, HG^+ becomes the dominant ion in the droplets, and the effect of K_E would diminish. The experimental results nicely demonstrated this trend, with the

Figure 3-6. ESI-MS response to the (18-crown-6 + K)$^+$ ion for solutions containing 1:1 18-crown-6 and KCl as the identity of the background electrolyte was varied among several tetraalkylammonium salts with different length alkyl groups. C_E was 100 μM.

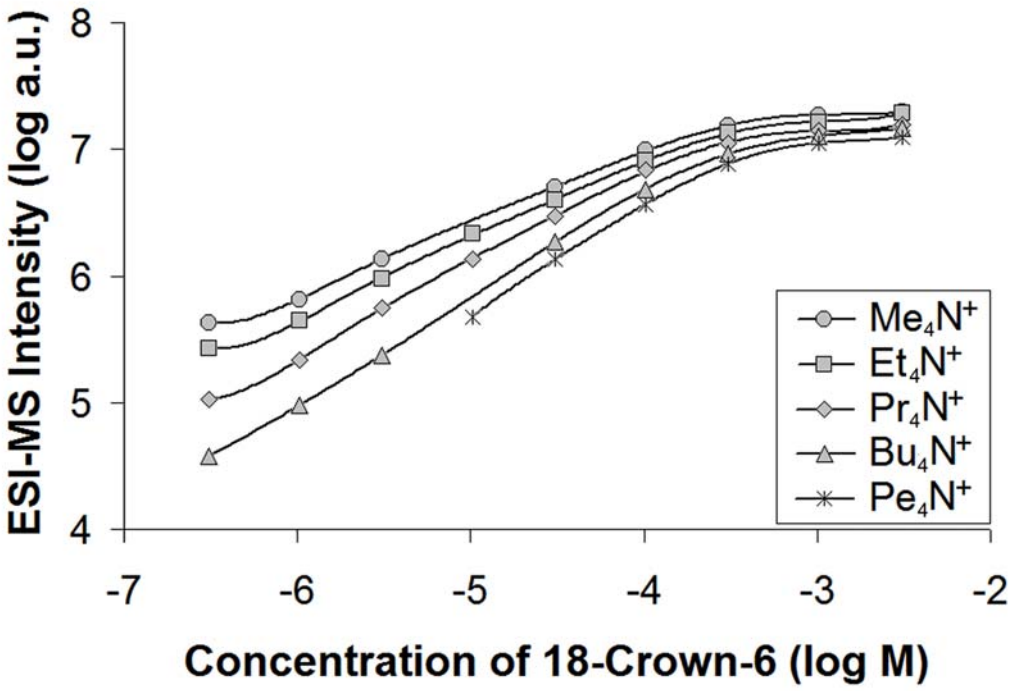

ESI response to the complex decreasing at lower concentrations of the host and guest as the length of the alkane chains on the ammonium ions increased, and at higher concentrations the response curves converged to an ESI response of around 10^7 (a.u.).

The trend observed also supports the idea that a molecule's partitioning constant is related to its energy of solvation. In this case, since the tetraalkylammonium ions are so similar, the solvation energy is determined primarily by the degree of non-polarity of the alkyl groups. With longer alkyl groups, Pe_4N^+ and Bu_4N^+ are relatively non-polar ions that are not well solvated in methanol. As a result, these ions partitioned to the droplet surface extremely easily, accounting for their extremely high signal response in ESI-MS. Ions with shorter alkyl groups like Me_4N^+ and Et_4N^+ have a lesser non-polar

character allowing them to be better solvated by methanol. The stronger solvation created a higher energy barrier the ions had to overcome when partitioning to the droplet surface where many of the solvation interactions were lost. These ions, therefore, had lower partitioning constants and tended to suppress other species less in ESI.

In the experiments described above, the effects of *extra* species in solution on the ESI response to host-guest complexes were probed, but in many situations, the primary changes are in the analytes themselves and not the contaminants. One common experiment is to evaluate the binding of a host compound to various guests. To evaluate such a case, the binding of 18-crown-6 to Na^+, K^+, and Rb^+ was evaluated experimentally and in the context of the model. Three series of solutions were analyzed, each containing the host 18-crown-6 and one of the three guest ions. When the identity of a guest was altered, three different parameters relevant to the equilibria in an ESI droplet could be altered. First, the binding strength, K_b, of the host-guest complexation could change. Second, the partitioning constant of the guest itself, K_{GE}, could be different. Third, changes in the conformation of the host-guest complex due to the different guest could alter its partitioning constant, K_{HGE}. By considering all three of these effects simultaneously, the effect of changing the guest ion on ESI response can be understood.

When the three series of solutions were analyzed, the response curves as seen in Figure 3-7 each had fairly different shapes as a result of the variations in the parameters discussed above. First of all, the log K_b's of the complexes with Na^+, K^+, and Rb^+ are 4.37, 6.05, and 5.56, respectively (44), giving the following relationship:

$$K_b(\text{18-crown-6} + K^+) > K_b(\text{18-crown-6} + Rb^+) > K_b(\text{18-crown-6} + Na^+)$$

Figure 3-7. ESI-MS response to the (18-crown-6 + G)$^+$ ion for solutions containing 1:1 18-crown-6 and GCl where the guest ion G was either Na^+, K^+, or Rb^+. The concentration of the added background electrolyte, Bu_4NCl, was 100 μM.

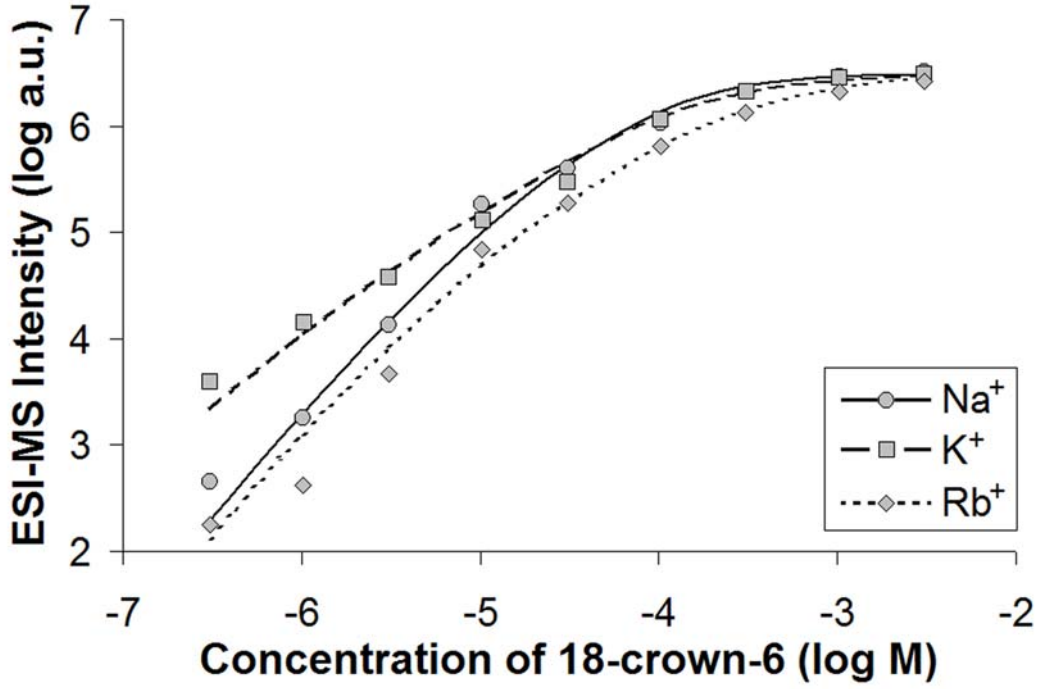

The variation of K_{GE}, however, related to the size of the guest ions. With ionic radii of 1.24, 1.51, and 1.61 for Na^+, K^+, and Rb^+, respectively (45), the larger Rb^+ ion is much more diffuse that the smaller K^+ and Na^+ ions. This caused Na^+ to be the most strongly solvated of the three, followed by K^+ and Rb^+ giving the following relationship for the partitioning constants:

$$K_{GE}(Rb^+) > K_{GE}(K^+) > K_{GE}(Na^+)$$

Similarly, the overall shape and size of the host-guest complexes affected their partitioning constants. From thermodynamic calculations, smaller ions such as Na^+ and K^+ have an energy minimum at the center of the crown ether host (46), allowing their charge to be more thoroughly shielded by the host. Larger ions like Rb^+, however,

cannot reach the center of the crown ether (46), forcing them to perch on top of the ring structure. Since the larger ions were more exposed to the environment, they must be better solvated, causing them to have lower partitioning constants:

$$K_{HGE}(\text{18-crown-6} + Na^+) > K_{HGE}(\text{18-crown-6} + K^+) > K_{HGE}(\text{18-crown-6} + Rb^+)$$

Considering these three relationships, response curves predicted from the model were fit to the experimental data. The parameters used are listed in Table 3-1. Although the fairly rough manual fitting would not be sufficient for a quantitative analysis, the qualitative results clearly demonstrated the same variations in the shapes of the response curves as in the experimental data. Of particular interest was the fact that the binding strength alone was *not* enough to rank the signal intensities. Based on K_b's alone, the ESI-MS response to (18-crown-6 + Rb)$^+$ should be greater than the response to (18-crown-6 + Na)$^+$. Such an assumption has often been made when the host-guest complexes were very similar, but the assumption was clearly demonstrated to be incorrect in this case both by the predictions of the equilibrium partitioning model and by the experimental results.

Table 3-1. Parameters used to fit response curves from the model to experimental data.

Guest Ion:	**Na^+**	**K^+**	**Rb^+**
Complex Binding Strength, log K_b[a]	4.37	6.05	5.56
Host Partitioning Constant, K_{HE}	5	5	5
Guest Partitioning Constant, K_{GE}	0.05	0.1	0.3
Complex Partitioning Constant, K_{HGE}	20	2	0.3

[a] From reference 44.

3.5 Conclusions

ESI-MS response to host-guest complexation interactions were accurately modeled by treating the ESI droplets as a system at equilibrium in which ions partition between the surface and interior of the droplets. The ion abundance observed in a mass spectrometer is then proportional to the concentration of the host-guest complex on the surface of the initial ESI droplets. Through a theoretical evaluation of the effect of various experimental parameters, the ESI response to a host-guest complex was limited by the electric current through the ESI source as with any other analyte. The response was suppressed by the presence of additional ionic species in solution, and the overall shape of the signal response was determined by a combination of the various equilibrium processes including both the strength of the binding interaction and the partitioning equilibria of the various species. Response to a host-guest complex was generally linear at host and guest concentrations lower that the concentration of any background ionic species and exhibits saturation behavior at higher concentrations.

Through varying the identity and concentration of the background electrolyte as well as the identity of the guest in the host-guest interaction, the predictions of the equilibrium partitioning model were confirmed experimentally. In polar solvents such as methanol, it was also confirmed that the magnitude of an ion's partitioning constant was related to its solvation energy with better solvated ions having lower partitioning constants and ESI response. Finally, the strength of a host-guest binding interaction alone was not sufficient for predicting relative intensities of host-guest complexes without an accounting of the partitioning of the various species in solution.

3.6 References

(1) Jorgensen, T. J. D.; Roepstorff, P.; Heck, A. J. R. *Anal. Chem.* **1998**, *70*, 4427-4432.

(2) Brodbelt, J. S. *Int. J. Mass Spectrom.* **2000**, *200*, 57-69.

(3) Beck, J. L.; Colgrave, M. L.; Ralph, S. F.; Sheil, M. M. *Mass Spectrom. Rev.* **2001**, *20*, 61-87.

(4) Loo, J. A. *Mass Spectrom. Rev.* **1997**, *16*, 1-23.

(5) Wan, K. X.; Shibue, T.; Gross, M. L. *J. Am. Chem. Soc.* **2000**, *122*, 300-307.

(6) Gabelica, V.; De Pauw, E.; Rosu, F. *J. Mass Spectrom.* **1999**, *34*, 1328-1337.

(7) David, W. M.; Brodbelt, J.; Kerwin, S. M.; Thomas, P. W. *Anal. Chem.* **2002**, *74*, 2029-2033.

(8) Young, D. S.; Hung, H. Y.; Liu, L. K. *Rapid Commun. Mass Spectrom.* **1997**, *11*, 769-773.

(9) Williams, S.; Blair, S. M.; Brodbelt, J. S.; Huang, X.; Bartsch, R. A. *Int. J. Mass Spectrom.* **2001**, *212*, 389-401.

(10) Williams, S. M.; Brodbelt, J. S.; Marchand, A. P.; Cal, D.; Mlinaric-Majerski, K. *Anal. Chem.* **2002**, *74*, 4423-4433.

(11) Blair, S. M.; Kempen, E. C.; Brodblet, J. S. *J. Am. Soc. Mass Spectrom.* **1998**, *9*, 1049-1059.

(12) Brodbelt, J. S.; Kempen, E.; Reyzer, M. *Struc. Chem.* **1999**, *10*, 213-220.

(13) Blair, S. M.; Brodbelt, J. S.; Marchand, A. P.; Kumar, K. A.; Chong, H. S. *Anal. Chem.* **2000**, *72*, 2433-2445.

(14) Kempen, E. C.; Brodbelt, J. S.; Bartsch, R. A.; Jang, Y.; Kim, J. S. *Anal. Chem.* **1999**, *71*, 5493-5500.

(15) Blair, S. M.; Brodbelt, J. S.; Reddy, G. M.; Marchand, A. P. *J. Mass Spectrom.* **1998**, *33*, 721-728.

(16) Goolsby, B. J.; Brodbelt, J. S.; Adou, E.; Blanda, M. *Int. J. Mass Spectrom.* **1999**, *193*, 197-204.

(17) Young, D. S.; Hung, H. Y.; Liu, L. K. *J. Mass Spectrom.* **1997**, *32*, 432-437.

(18) Sannes-Lowery, K. A.; Griffey, R. H.; Hofstadler, S. A. *Anal. Biochem.* **2000**, *280*, 264-271.

(19) Kempen, E. C.; Brodbelt, J. S. *Anal. Chem.* **2000**, *72*, 5411-5416.

(20) Griffey. R. H.; Hofstadler, S. A.; Sannes-Lowery, K. A.; Ecker, D. J.; Crooke, S. T. *Proc. Natl. Acad. Sci. USA* **1999**, *96*, 10129-10133.

(21) Tang, L.; Kebarle, P. *Anal. Chem.* **1993**, *65*, 3654.

(22) Zook, D. R.; Bruins, A. P. *Int. J. Mass Spectrom. Ion Processes* **1997**, *162*, 129-147.

(23) Ikonomou, M. G.; Blades, A. T.; Kebarle, P. *Anal. Chem.* **1990**, *62*, 957-967.

(24) Cech, N. B.; Enke, C. G. *Mass Spectrom. Rev.* **2001**, *20*, 362-387.

(25) Constantopoulos, T. L.; Jackson, G. S.; Enke, C. G. *Anal. Chem. Acta* **2000**, *406*, 37-52.

(26) Sjöberg, P. J. R.; Bökman, C. F.; Bylund, D.; Markides, K. E. *J. Am. Soc. Mass Spectrom.* **2001**, *12*, 1002-1010.

(27) Wang, G.; Cole, R. B. *Anal. Chem.* **1994**, *66*, 3702-3708.

(28) King, R.; Bonfiglio, R.; Fernandez-Metzler, C.; Miller-Stein, C.; Olah, T. *J. Am. Soc. Mass Spectrom.* **2000**, *11*, 942-950.

(29) Constantopoulos, T. L.; Jackson, G. S.; Enke, C. G. *J. Am. Soc. Mass Spectrom.* **1999**, *10*, 625-634.

(30) Cole, R. B. *J. Mass Spectrom.* **2000**, *35*, 763-772.

(31) Tang, L.; Kebarle, P. *Anal. Chem.* **1991**, *63*, 2709-2715.

(32) Enke, C. G. *Anal. Chem.* **1997**, *69*, 4885-4893.

(33) Gomez, A.; Tang, K. *Phys. Fluids.* **1994**, *6*, 404-414.

(34) Cech, N. B.; Enke, C. G. *Anal. Chem.* **2001**, *73*, 4632-4639.

(35) Tang, K.; Smith, R. D. *J. Am. Soc. Mass Spectrom.* **2001**, *12*, 343-347.

(36) Tang, K.; Smith, R. D. *Int. J. Mass Spectrom.* **1999**, *185/186/187*, 97-105.

(37) Van Berkel, G. J. In *Electrospray Ionization Mass Spectrometry*. Cole, R. B, Ed. Wiley: New York, **1997**; Chap. 1, pp. 65-105.

(38) Jackson, G. S.; Enke, C. G. *Anal. Chem.* **1999**, *71*, 3777-3784.

(39) Blades, A. T.; Ikonomou, M. G.; Kebarle, P. *Anal. Chem.* **1991**, *63*, 2109-2114.

(40) Van Berkel, G. J.; Zhou, F. *Anal. Chem.* **1995**, *67*, 2916-2923.

(41) Cech, N. B.; Enke, C. G. *Anal. Chem.* **2000**, *72*, 2717-2723.

(42) Sjöberg, P. J. R.; Bökman, C. F.; Bylund, D.; Markides, K. E. *Anal. Chem.* **2001**, *73*, 23-28.

(43) Sjöberg, P. J. R.; Bökman, C. F.; Bylund, D.; Markides, K. E. *Anal. Chem.* **2001**, *73*, 23-28.

(44) Izatt, R. M.; Pawlak, K.; Bradshaw, J. S. *Chem. Rev.* **1991**, *91*, 1721-2085.

(45) Lide, D. R., Ed. *CRC Handbook of Chemistry and Physics*, 75th ed., CRC Press: Ann Arbor, MI, **1994**.

(46) Schmidt, K. F.; Kast, S. M. *J. Phys. Chem.* **2002**, *106*, 6289-6297.

CHAPTER 4

A Partitioning Model for Competitive Host-Guest Complexation in ESI-MS

4.1 Introduction

As electrospray ionization (ESI) has grown in popularity, understanding how populations of ions in solution are perturbed by the electrospray process has become a much studied topic (1-21). While ESI offers a snapshot of the various species present in a solution, this view is somewhat distorted by the various solution (2, 6-21), electrochemical (3, 9-12), and gas-phase (7-15) processes occurring as the species are ionized and transferred into the gas phase. Despite some ongoing contention, most generally agree that two competing mechanisms contribute to ion formation in ESI. Ion evaporation, first proposed by Iribarne and Thomson (22), appears to dominate for small species (12), while the charged-residue model put forth by Dole, et al. (23) typically is more active for larger species (9,12). For both of these mechanisms, the ions introduced into the mass spectrometer derive from the offspring droplets of fission events in the first stages of the electrospray (6, 10-12, 24-25). Since these offspring droplets are enriched in both charge (6, 9-11, 18, 24-26) and species from the surface of the parent droplets (5-6, 10-11, 18, 24), compounds that tend to partition to the droplet surface typically yield greater abundances of gas-phase ions than compounds that remain in the bulk solution-like droplet interior (4-6, 11-13, 25).

From this observation and the recognition that the charges in each droplet reside on the surface and are finite in number (5, 11, 24-25), the distribution of species in an electrosprayed droplet and, consequently, the relative abundances of ions generated by electrospray have been modeled as a system at equilibrium (6). Since its development, the equilibrium partitioning model has been the topic of much study (4-5, 15-17, 27-31). In particular, work has been done in such varying areas as extending the model to consider the successive fissions of sprayed droplets (5), examining electrosprayed droplets to verify differing populations on their surfaces and interiors (4, 28), and even linking the ESI efficiency of tri-peptides to their HPLC retention times (30). Such studies, however, have remained fairly limited in the range of analytes studied. Typically, analytes have been chemically simple, permanently charged compounds (5-6, 15-17, 29) or groups of very similar compounds (30-31).

Recently, we presented an extension to the equilibrium partitioning model demonstrating its applicability to the vast field of host-guest chemistry by accurately predicting the observed ESI-MS intensities of different crown ether-metal complexes that formed as the result of an equilibrium process in solution (27). The study of host-guest chemistry marks one of the great successes of electrospray ionization. The relative softness of an electrospray ion source allows many types of weakly-bound complexes to be studied in the gas phase such as those resulting from molecular recognition (1, 32-45), attachment of drugs or other substrates to proteins (8, 46-45) or DNA (48-52), and nucleobase polymerization (53-56). In both qualitative screening applications (1, 34-44, 47-51) and quantitative binding determinations (8, 32-33, 45-46), the speed and

simplicity of analysis make ESI-MS particularly appealing, but questions about the effect of various discrimination effects on experimental results continue to raise concerns (1, 8, 27, 33, 45, 47), often necessitating the application of various empirical corrections (1, 8, 33-34, 37, 43). Conclusions drawn from this partitioning model helped explain in a quantitative manner the relationship between populations of host-guest complexes observed in ESI mass spectra and the species that existed previously in solution (27), but the impact of competing complexation equilibria has not been examined.

In this report, the partitioning model was further extended to consider the more complex yet realistic case where multiple hosts compete to bind one guest or multiple guests compete to bind one host. These cases account for many of the ESI-MS studies that have probed host-guest chemistry (1, 32-46, 49-51). Results from accurately modeling the electrospray of hosts and guests involved in competitive equilibria explain many of the factors leading to errors in the interpretation of ESI-MS analysis, both expanding the applicability and enhancing accuracy of these methods. The application of the equilibrium partitioning model to these more complicated systems was demonstrated, and an analysis of the various factors relevant to many types of ESI-MS analyses of host-guest complexes was performed.

4.2 Experimental

4.2.1 Mathematical Modeling.

Solutions to the partitioning equilibria for the two different electrospray systems studied (i.e. one host with multiple guests or one guest with multiple hosts) were found with custom programs written in the Waterloo Maple 7 (Waterloo, ON, Canada)

computer algebra software package on a Windows-based personal computer. These programs consisted of modules to numerically solve the systems of equations for a given set of parameters and to select the sole physically meaningful solution from the set of all possible solutions.

4.2.2 Electrospray Ionization Mass Spectrometry.

Solutions analyzed contained one or two crown ethers as hosts, one or two alkali metal chlorides as guests, and a tetraalkylammonium iodide salt as a background electrolyte. Hosts included 18-crown-6, dicyclohexano-18-crown-6, benzo-18-crown-6, and dibenzo-18-crown-6, all purchased from the Aldrich Chemical Co. (Milwaukee, WI). The guests used were NaCl and KCl, obtained from EM Science (Gibbstown, NJ), and RbCl and CsCl, both obtained from Aldrich. Tetraethylammonium iodide and tetrapropylammonium iodide were purchased from Aldrich while the third background electrolyte, tetrabutylammonium iodide, was acquired from the Sigma Chemical Co. (St. Louis, MO). Dicyclohexano-18-crown-6 was of 95% purity while all other compounds had purities of 98% or greater. Except where noted, host and guest concentrations were equimolar, and $Bu_4N^+I^-$ was used as the background electrolyte at 10^{-5} M concentration. All solutions were prepared in spectroscopic grade methanol (Fisher Scientific, Fair Lawn, NJ).

Mass spectra for the above solutions were collected on an LCQ Duo quadrupole ion trap mass spectrometer (ThermoFinnigan, San Jose, CA). As was discussed previously, resistors were added to the electrospray to prevent arcing which could damage the source and lead to signal fluctuations (27). The ESI source was operated at a

potential of 4.5 kV, and the source conditions were tuned to minimize fragmentation. To avoid the potential influence of space-charging effects on peak height measurements, all spectra were collected using the automatic gain control feature of the Xcalibur data acquisition software (ThermoFinnigan). Solutions were directly infused into the mass spectrometer at a flow rate of 5 μL/min with a model PHD 2000 syringe pump (Harvard Apparatus, South Natick, MA). Presented spectra are the average of 300 scans.

4.3 Discussion

From the understanding that the distribution of free gas-phase ions produced in an electrospray source depends on the relative amounts of various species on the surfaces of the initial droplets formed at the Taylor cone (5-6, 11, 16, 27), the first equilibrium partitioning model was developed to quantitatively predict abundances of ions in an ESI mass spectrum based on the relative affinities of the different species for these droplet surfaces (6, 16). In its original form, the partitioning model considered the abilities of the various molecules to migrate back and forth between the surface and bulk solution-like interior of the electrospray droplet in a dynamic equilibrium (5, 16). Since the ions formed in ESI largely arise from the surface-enriched offspring droplets from the initial droplet fission events (5-6, 10-12, 18, 24-25), the observed mass spectral ion abundance for a given analyte, A, relates to the portion of the analyte concentration that resides on the droplet surface, $[A^+]_s$, through the equation:

$$A = P\, f\, [A^+]_s \qquad (4\text{-}1)$$

where P is the sampling efficiency of the atmospheric pressure interface (largely dependent on source geometry), and f is the overall efficiency of the ESI source in transferring ions from solution into the gas phase (6, 21). These factors derive from the physical design of the ESI source and are independent of any chemical differences (6, 21).

Justification for the relationship between the proportional concentration of species on the droplet surfaces and the mass spectral abundances lies with several fundamental aspects of the ESI source. First, an ESI source is essentially a controlled-current device (2-3, 6, 9, 11). Electrochemical reactions at the ESI emitter generate an excess of charged species, most of which are neutralized at the front plate of the mass spectrometer that forms the counter-electrode in the circuit. With a known flow rate of solution through the source, Γ, a concentration of the excess charge, [Q], in the droplets prior to any solvent evaporation depends solely on the ESI current, I:

$$[Q] = I / \Gamma F \qquad (4\text{-}2)$$

where F is Faraday's constant (6). The droplet interiors maintain electroneutrality, but electrostatic repulsions ensure that all of the excess charge remains in a thin layer of solution on the surface of the droplets (6). In an ideal conductor like a metal, the excess charge rests entirely on the surface. In a droplet of solution, the conductivity of the solution is something less than the ideal case and the charge carriers (atoms or molecules versus electrons) are significantly larger. As a result, the boundary between surface and interior of the droplets is likely not discrete. Nevertheless, for the purpose of this model, the differences in the chemical environment between the surface and interior are great

enough that they can be treated as distinct phases. Since the ions ultimately formed in ESI must originate from the surface of these droplets initially formed in the electrospray, the observed ion abundances of a given analyte relate not to the concentration of the analyte in solution, but to the concentration of that analyte on the droplet surface (6, 18, 21, 27).

To a rather significant extent the partitioning of species between the droplet surface and interior behaves as a traditional system at equilibrium (5, 16), the only caveat being that the compounds must have a reasonably rapid rate of diffusion in solution to ensure equilibration on timescales relevant to the ESI experiment. As a result, the equilibrium conditions of any additional reactions in the solution must be satisfied simultaneously with the droplet partitioning (27). As demonstrated previously for the simplest host-guest association reactions (27), extending the set of equilibrium equations governing the droplet to incorporate additional reactions poses no fundamental problem in developing a partitioning model and making predictions about the observed ion abundances. Each additional reaction, however, does increase the complexity of both deriving the system of pertinent equilibrium equations and subsequently solving the system. Furthermore, such an analysis has only been experimentally tested for the simplest possible case of a single host binding a single guest (27).

To summarize, the partitioning model follows from several key assumptions and experimental observations: 1) The amount of excess charge in the initial droplets formed by the ESI source is determined by the ESI current and the volume flow rate of the analyte solution (6). 2) Electrostatic repulsions force the excess charge towards the

surfaces of the droplets, creating a chemically different region characterized by both the excess charge and the air-solution interface (6, 27-28). 3) Ions introduced into the mass spectrometer are produced not from the large droplets formed initially, but from the smaller offspring droplets resulting from droplet fission processes (33). 4) The composition of these offspring droplets more nearly matches the surface of the parent droplets rather than the makeup of the bulk solution (24, 26, 33). These factors directly lead to the conclusion that those species which were enriched on the surface of the initial ESI droplets will be enriched in the resulting mass spectrum and *vice versa*. For this reason, analyzing the partitioning equilibrium between the surface and interior of these initial large droplets yields accurate conclusions about the ESI mass spectra obtained for a particular solution.

In early studies of the relationship between solution concentration and ESI-MS abundances, Kebarle and coworkers considered a "sensitivity coefficient" that considered both the equilibrium of analytes between the surface and interior of the ESI droplets and the rate of ion evaporation from the droplet surfaces (21). Assuming that ion evaporation is the dominant mechanism for ion generation, a strict theoretical consideration of ESI would necessarily evaluate both processes. Both the partitioning equilibrium and rate of ion evaporation, however, are driven by the same chemical forces (the greater stability of hydrophilic ions in the polar solvent versus the stability of hydrophobic ions in the non-polar gas phase). For a modeling of the behavior of ions in an electrospray, the difficulty in decoupling these two processes along with the likely limited benefits justify

considering only the partitioning equilibrium with the recognition that some of the observed effects may in fact be due to the two processes acting in concert.

While analyzing solutions where multiple equilibrium reactions are in competition significantly increases the complexity of the partitioning model, the potential benefits are far greater since these systems represent more typical experimental conditions (1, 8, 32-39, 41-43, 45-46, 49-51). As with the more simple models, developing partitioning models for the electrospray of solutions with competitive equilibria begins with an analysis of the equations governing the various equilibria possible in the ESI droplets. This analysis is presented below for two of the possible situations: two charged guests competing to bind a single neutral host and two neutral hosts competing to bind a single charged guest. Although countless other possible systems could be imagined and analyzed, these two paradigms illustrate the range of possible interactions, and the results can be applied, at least in a qualitative sense, to nearly every competitive binding system.

4.3.1 Partitioning Model for Two Guests Competing to Bind One Host.

As with previous models (6, 27), four general types of equations must be used to fully describe the equilibria occurring in an ESI droplet where two charged guests compete to bind to a single host. In the first of these, the charge balance equation, the amount of excess charge in the droplet is related to the concentrations of the different ions on the droplet surface:

$$[Q] = [HG_1^+]_s + [HG_2^+]_s + [G_1^+]_s + [G_2^+]_s + [E^+]_s \qquad (4\text{-}3)$$

where HG_1^+ and HG_2^+ are the two host-guest complexes, G_1^+ and G_2^+ are the two unbound guest ions, and E^+, the background electrolyte, represents any other cations present that are not involved in the binding equilibria. Since all of the excess charge in an ESI droplet must reside at the surface due to electrostatic repulsions, the concentration of excess charge must be composed solely of species on the surface (denoted by the subscript s). This equation illustrates the source of the saturation behavior typically observed in ESI mass spectrometry. The concentration of excess charge on the droplets, [Q], limits the amount of charged species on the droplet surface. Since the ion abundances produced by ESI arise from these ions on the surface, [Q] determines the maximum number of gas-phase ions that can be formed.

The mass balance equations for this system mirror those for a conventional solution equilibrium analysis. The sum of the concentrations of all species containing each of the four primary components, H, G_1^+, G_2^+, and E^+, must equal the formal concentration, C_x, of that species:

$$C_H = [H]_s + [H]_i + [HG_1^+]_s + [HG_1^+]_i + [HG_2^+]_s + [HG_2^+]_i \quad (4\text{-}4)$$

$$C_{G1} = [G_1^+]_s + [G_1^+]_i + [HG_1^+]_s + [HG_1^+]_i \quad (4\text{-}5)$$

$$C_{G2} = [G_2^+]_s + [G_2^+]_i + [HG_2^+]_s + [HG_2^+]_i \quad (4\text{-}6)$$

$$C_E = [E^+]_s + [E^+]_i \quad (4\text{-}7)$$

The subscript i denotes species in the interior of the electrospray droplets while the subscript s indicates that the species are in the thin layer of solvent that makes up the surface of the droplet. Typically, C_H, C_{G1}, and C_{G2} are the prepared concentrations for a solution. C_E, however, represents the concentration of ionic contaminants in the solution,

typically on the order of 1-10 μM (9, 16), but can be elevated through the addition of auxiliary electrolytes.

Since each chemical species can migrate back and forth between the surface and interior of the ESI droplets, the concentrations of the compounds in these two states adhere to equilibrium relationships:

$$K_H = [H]_s / [H]_i \quad (4\text{-}8)$$

$$K_{G1} = [G_1^+]_s / [G_1^+]_i \quad (4\text{-}9)$$

$$K_{G2} = [G_2^+]_s / [G_2^+]_i \quad (4\text{-}10)$$

$$K_{HG1} = [HG_1^+]_s / [HG_1^+]_i \quad (4\text{-}11)$$

$$K_{HG2} = [HG_2^+]_s / [HG_2^+]_i \quad (4\text{-}12)$$

$$K_E = [E^+]_s / [E^+]_i \quad (4\text{-}13)$$

where K_x is the equilibrium constant for the partitioning of species x between the two phases, also called the partitioning constant. These partitioning equilibria, however, do not exist independently. Due to the coupling of these equilibria with the charge balance of the droplets and the competitive nature of the interaction, the ability of each compound to partition to the surface is considered relative to the partitioning ability of the background electrolyte. Taking the ratio of equations 4-8 through 4-12 to equation 4-13 yields five independent equations for the relative partitioning constants, K_{xE}:

$$K_{HE} = K_H / K_E = ([H]_s[E^+]_i) / ([H]_i[E^+]_s) \quad (4\text{-}14)$$

$$K_{G1E} = K_{G1} / K_E = ([G_1^+]_s[E^+]_i) / ([G_1^+]_i[E^+]_s) \quad (4\text{-}15)$$

$$K_{G2E} = K_{G2} / K_E = ([G_2^+]_s[E^+]_i) / ([G_2^+]_i[E^+]_s) \quad (4\text{-}16)$$

$$K_{HG1E} = K_{HG1} / K_E = ([HG_1^+]_s[E^+]_i) / ([HG_1^+]_i[E^+]_s) \quad (4\text{-}17)$$

$$K_{HG2E} = K_{HG2} / K_E = ([HG_2^+]_s[E^+]_i) / ([HG_2^+]_i[E^+]_s) \quad (4\text{-}18)$$

Each relative partitioning constant, designated by the "E" in the subscript since its value is relative to the partitioning ability of the background electrolyte, directly relates to the relative abundances of ions produced by the electrospray. Although all solution equilibria contribute to the concentration of a particular species, the partitioning equilibrium drives the generation of gas-phase ions and is responsible for the differences commonly observed between solution conditions and ESI-MS results.

The final reactions that must be considered are the binding equilibria for the two host-guest complexes. Since the droplet interior is essentially the same as the bulk solution, the binding equilibria there are governed by the same binding constants as those determined for reactions in solution:

$$K_{b1} = [HG_1^+]_i / ([H]_i[G_1^+]_i) \quad (4\text{-}19)$$

$$K_{b2} = [HG_2^+]_i / ([H]_i[G_2^+]_i) \quad (4\text{-}20)$$

On the surface, however, the air interface creates a substantially different chemical environment, potentially shifting the binding equilibria:

$$K_{b1s} = [HG_1^+]_s / ([H]_s[G_1^+]_s) \quad (4\text{-}21)$$

$$K_{b2s} = [HG_2^+]_s / ([H]_s[G_2^+]_s) \quad (4\text{-}22)$$

Substituting equations 4-8, 4-9, 4-11, and 4-19 into equation 4-21 yields the equation:

$$K_{b1s} = (K_H K_{G1}/K_{HG1}) K_{b1} \quad (4\text{-}23)$$

revealing that the binding constant for $[HG_1^+]$ on the surface is simply a combination of Equations 4-8, 4-9, 4-11, and 4-19. As such, Equation 4-21 is not independent

mathematically and must be omitted. Similarly, substituting equations 4-8, 4-10, 4-12, and 4-20 into equation 4-22:

$$K_{b2s} = (K_H K_{G2}/K_{HG2})\, K_{b2} \qquad (4\text{-}24)$$

yields the same results.

The net result of this analysis is a set of twelve equations (equations 4-3 through 4-7 and 4-14 through 4-20) with twelve unknown concentrations. When the equilibrium constants, the formal concentrations, and the ESI current and flow rate are known, the various concentrations can be calculated numerically using a computer algebra program.

4.3.2 Partitioning Model for Two Hosts Competing to Bind One Guest.

Characterizing the equilibria present in an ESI droplet where two neutral hosts are competing to complex a single charged guest ion closely parallels the analysis for cases with two guests competing for a single host. As such, the derivation of the system of equations for this case are not discussed in detail. The differences between the two models rest with the difference in the number and identity of the charged species. This difference first becomes apparent with the charge balance for the system:

$$[Q] = [H_1G^+]_s + [H_2G^+]_s + [G^+]_s + [E^+]_s \qquad (4\text{-}25)$$

The mass balances for a system with two competing hosts account for the formal concentrations of the hosts, H_1 and H_2, the charged guest, G^+, and the background electrolyte, E^+:

$$C_{H1} = [H_1]_s + [H_1]_i + [H_1G^+]_s + [H_1G^+]_i \qquad (4\text{-}26)$$

$$C_{H2} = [H_2]_s + [H_2]_i + [H_2G^+]_s + [H_2G^+]_i \qquad (4\text{-}27)$$

$$C_G = [G^+]_s + [G^+]_i + [H_1G^+]_s + [H_1G^+]_i + [H_2G^+]_s + [H_2G^+]_i \qquad (4\text{-}28)$$

$$C_E = [E^+]_s + [E^+]_i \quad (4\text{-}29)$$

The relative concentration of a particular compound is governed by the affinity of that compound for the droplet surface as described by the partitioning equilibrium equations. For the same reasons discussed above, the relative partitioning constants, obtained by dividing the partitioning equation of the electrolyte into the partitioning equations for each of the other species yields equations 4-30 through 4-34, providing a practical measure of how well each species in the electrospray can compete for the droplet surface relative to the other species present.

$$K_{H1E} = K_{H1} / K_E = ([H_1]_s[E^+]_i) / ([H_1]_i[E^+]_s) \quad (4\text{-}30)$$

$$K_{H2E} = K_{H2} / K_E = ([H_2]_s[E^+]_i) / ([H_2]_i[E^+]_s) \quad (4\text{-}31)$$

$$K_{GE} = K_G / K_E = ([G^+]_s[E^+]_i) / ([G^+]_i[E^+]_s) \quad (4\text{-}32)$$

$$K_{H1GE} = K_{H1G} / K_E = ([H_1G^+]_s[E^+]_i) / ([H_1G^+]_i[E^+]_s) \quad (4\text{-}33)$$

$$K_{H2GE} = K_{H2G} / K_E = ([H_2G^+]_s[E^+]_i) / ([H_2G^+]_i[E^+]_s) \quad (4\text{-}34)$$

Lastly, the association reactions for binding in the droplet interior must also be considered:

$$K_{b1} = [H_1G^+]_i / ([H_1]_i[G^+]_i) \quad (4\text{-}35)$$

$$K_{b2} = [H_2G^+]_i / ([H_2]_i[G^+]_i) \quad (4\text{-}36)$$

Due to the great similarity between the interior of a newly-generated ESI droplet and the bulk solution, the equations and the binding constants used to model are identical to those for traditional solution measurements. Again, the equilibrium equations for binding on the surfaces of the droplets are not independent and thus added no additional information.

As with each partitioning model already developed (6, 16, 27), the model for two hosts competing for a single charged guest yields a system of equations and unknown concentrations that gives exact solutions when solved, if the formal concentrations and various equilibrium constants are known. Alternatively, parameters such as the binding constants or partitioning constants can be determined if enough concentrations are known, a situation likely to result from experimental analysis of the various species in the mixture. In this case, twelve equations make up the system of equations to be solved: equations 4-25 through 4-36. Unfortunately, with a system of equations this large, obtaining a symbolic solution simple enough to be useful for analysis is often difficult, if not impossible. For this reason, the numerical methods available with modern mathematical software were used to solve this system of equations and systematically evaluate the predictions of the mathematical model.

4.3.3 Predictions for Two Charged Guests Competing for a Single Host Molecule.

To evaluate the behavior of this partitioning model under different conditions, the surface concentrations of the two host-guest complexes, HG_1^+ and HG_2^+, were calculated under varying conditions. Recall that these surface concentrations are directly proportional to the observed mass spectral intensities; the proportionality constants depend only on the physical arrangement of the mass spectrometer. For each set of parameters, surface concentrations were calculated across a range of formal concentrations of the host molecule. Then the various parameters were varied independently, and effect of each parameter at different concentrations was considered.

Figure 4-1. Predicted concentrations of host-guest complexes on the surface of electrospray droplets when two guest ions compete for a single neutral host molecule when [Q] (a) or C_E (b) is varied. Black lines represent the more strongly bound complex, HG_1^+, and grey lines represent the less strongly bound complex, HG_2^+.

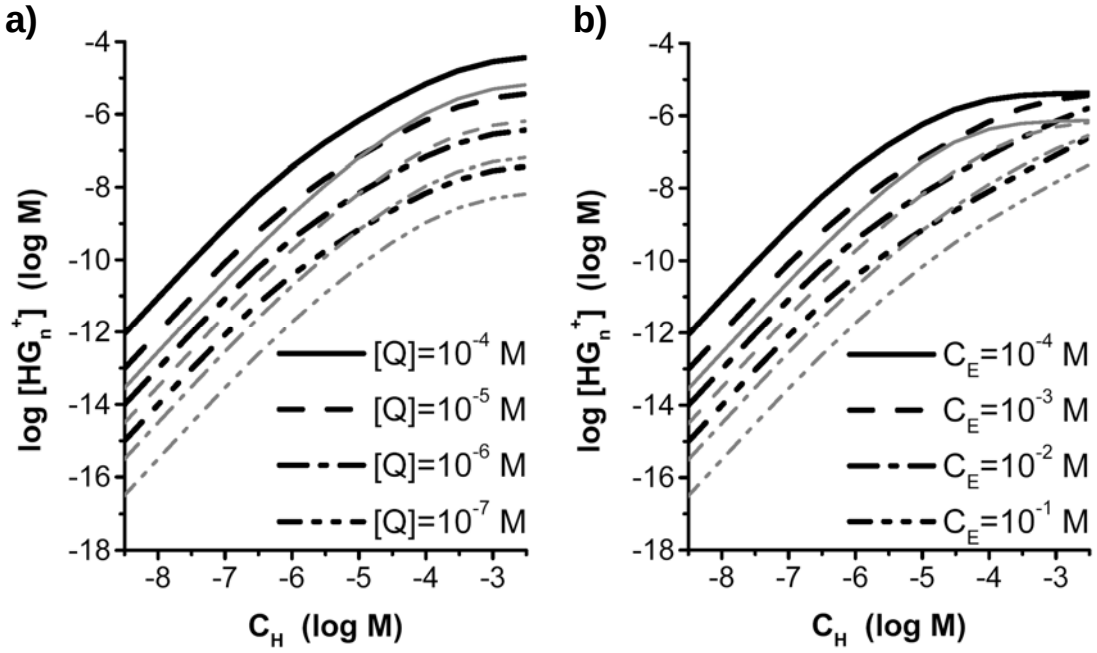

Except when specifically varied, parameters were held constant throughout the evaluation. [Q] and C_E both had concentrations of 10^{-5} M. Relative partitioning constants all had values of one. The two binding constants, K_{b1} and K_{b2}, were 10^6 and $10^{4.5}$, respectively. Additionally, whenever one of the binding constants was varied, K_{b1} was always set to be greater than K_{b2}. In the plots of surface concentration versus formal host concentration, the heavy black lines indicate the more strongly bound complex, HG_1^+, while the thinner grey lines represent the less strongly bound complex, HG_2^+.

The concentration of excess charge, [Q], had the most direct impact on the concentrations of the various species. [Q] dictated the total number of ions which could be produced by an electrospray. Increasing [Q] (Figure 4-1a) resulted in a concomitant

increase in both $[HG_1^+]_s$ and $[HG_2^+]_s$. This increase, though, raises all the surface ion concentrations similarly and has no significant effect on the relative amounts of each ion on the surface of the electrospray droplets. As a result, in a very real sense, [Q] determines the magnitude of the signal observed but has no effect on the qualitative mass spectrum or the quantitative ion abundances relative to each other.

When C_E, the concentration of the electrolyte, changes, both complexes were again affected similarly (Figure 4-1b). Since the electrolyte concentration was present in each of the partitioning equations, equations 4-14 through 4-18, it had no marked influence on the relative concentrations of HG_1^+ and HG_2^+. The magnitude of C_E, however, did have a notable influence on the shape of the concentration response curve that has been noted previously for other systems (27). As C_E was increased, the surface concentrations of both host-guest complexes decreased as long as the formal concentration of the hosts was less than C_E. At higher host concentrations, the surface concentration was saturated and remained unaffected by changes in the background electrolyte concentration. This represented an interesting trade-off between signal intensity and dynamic range that could be manipulated as needed simply by varying the salt concentration of the analyzed samples.

When K_{HG1E}, the partitioning constant of HG_1 relative to the background electrolyte, was varied (Figure 4-2a), the effect on $[HG_1^+]_s$ and $[HG_2^+]_s$ differed at both high and low host concentrations. When C_H was below C_E, $[HG_1^+]_s$ varied linearly with K_{HG1E}. The concentration of HG_2^+, however, did not vary with changes in the partitioning constant of HG_1^+ at these lower concentrations. The difference between

Figure 4-2. Predicted concentrations of host-guest complexes on the surface of electrospray droplets when two guest ions compete for a single neutral host molecule when the partitioning constants are varied. Black lines represent the more strongly bound complex, HG_1^+, and grey lines represent the less strongly bound complex, HG_2^+. The partitioning constants varied are: (a) K_{HG1E}, (b) K_{HG2E}, (c) K_{G1E}, and (d) K_{G2E}.

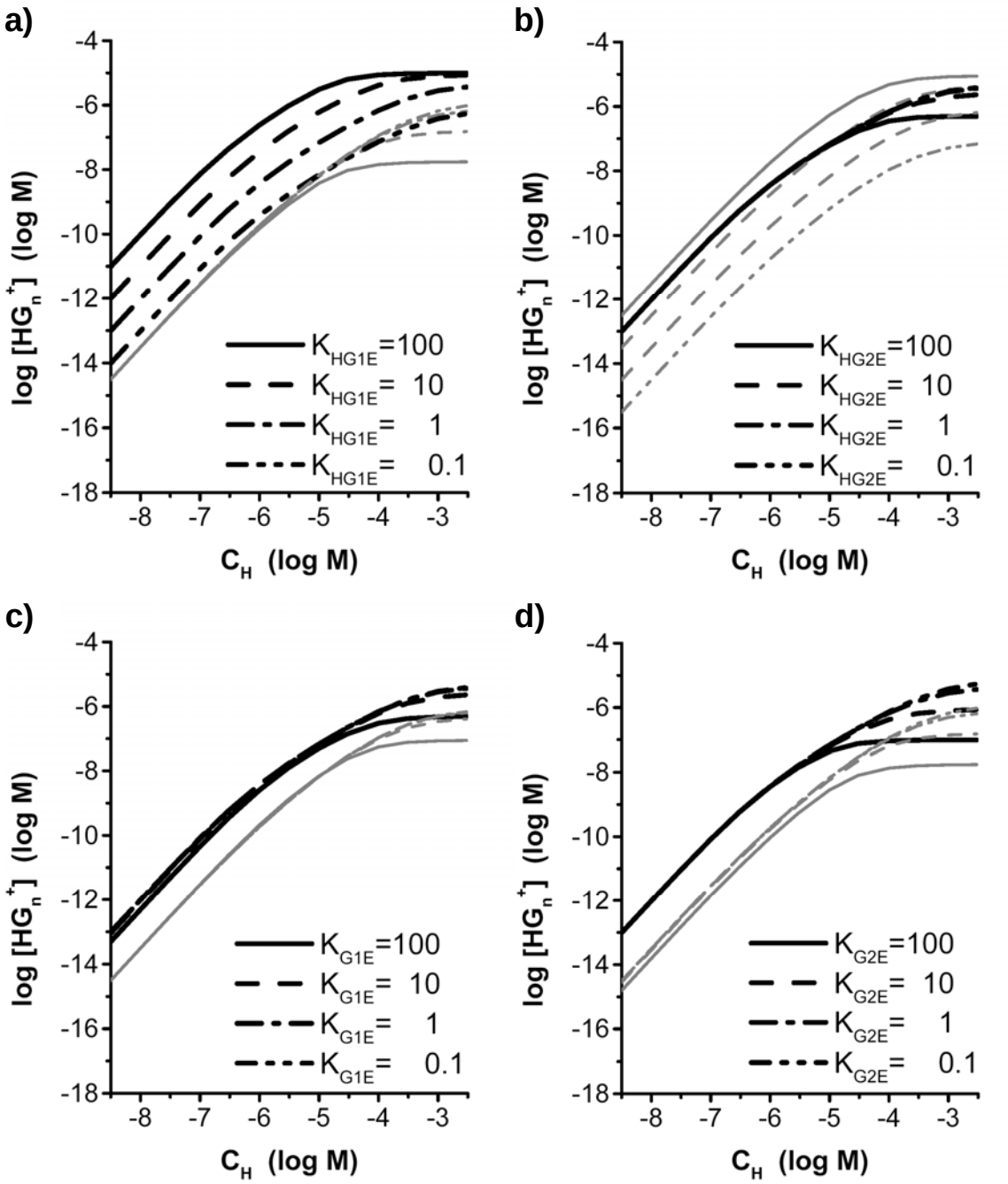

$[HG_1^+]_s$ and $[HG_2^+]_s$ was proportional to the difference between K_{HG1E} and K_{HG2E} Whenever the surface concentration of HG_1^+ reached [Q], both response curves flattened, exhibiting the typical saturation behavior. At lower values of K_{HG1E} the onset of saturation behavior occurred at higher host concentrations. In many cases the ability of complexes to partition to the surface has a greater influence on the distribution of ions generated than the relative binding strengths of the complexes. This is particularly true at concentrations where the surface of the ESI droplets begins to become saturated with analyte ions, where a relatively small change in the relative partitioning constants can easily cause a less strongly bound complex to dominate the mass spectrum.

The results of varying K_{HG2E} (Figure 4-2b) correlate well with the conclusions for when K_{HG1E} was varied. Overall, the effect of varying K_{HG2E} was essentially the reverse of varying K_{HG1E}. At host concentrations below C_E, $[HG_2^+]_s$ varied linearly with K_{HG2E} while $[HG_1^+]_s$ remained constant. At the onset of saturation behavior at higher host concentrations, the response of both complexes leveled simultaneously. At higher host concentrations, when the relative partitioning constant of the more weakly bound complex, K_{HG2E}, was greater than K_{HG1E} by a factor of ten or more, the more weakly bound complex had a greater surface concentration and, by extension, a greater predicted mass spectral intensity than the more strongly bound complex. When the relative partitioning constants differ by a factor of one hundred, the more weakly bound complex had a greater predicted mass spectral intensity at all host concentrations. Taken together, the results of varying K_{HG1E} and K_{HG2E} indicated that at lower host concentrations, i..e concentrations where response was still dynamic and had not yet saturated, the signal

response of the different host-guest complexes in the electrospray were independent of each other.

Increasing K_{G1E} caused a slight drop in $[HG_1^+]_s$ (Figure 4-2c). This effect is very subtle at host concentrations below C_E and became somewhat more prominent at higher host concentrations where competitive effects between analytes become more pronounced. $[HG_2^+]_s$, however, was unaffected by changes in K_{G1E} at lower host concentrations and mirrored the changes predicted for $[HG_1^+]_s$ at higher host concentrations. Increasing K_{G2E} (Figure 4-2d) caused a small decrease in $[HG_2^+]_s$ at lower host concentrations and a somewhat greater decrease at higher host concentrations. K_{G2E} had no effect on $[HG_1^+]_s$ at lower host concentrations, but at higher host concentrations, the variation in $[HG_1^+]_s$ mimicked the variation in $[HG_2^+]_s$. The relative partitioning constants of the guest ions together had only minimal effect on the predicted mass spectra at host concentrations below C_E. Their impact was greatest at the higher analyte concentrations where all charged analytes directly compete for spaces on the surface of ESI droplets.

When considering the effects of K_{HE}, the partitioning constant of the host, the logic of the analysis was necessarily somewhat different. Unlike all the other species examined, the host compound is neutral. The distribution of the host impacted the surface concentrations of the host-guest complexes by driving the binding equilibria and causing indirect shifts in the partitioning equilibria of the charged species. An immediate implication of the host's differing influence is the diminishing change in $[HG_1^+]_s$ and $[HG_2^+]_s$ at higher host concentrations when K_{HE} was varied (Figure 4-3). Since the

Figure 4-3. Predicted concentrations of host-guest complexes on the surface of electrospray droplets when two guest ions compete for a single neutral host molecule when K_{HE} is varied. Black lines represent the more strongly bound complex, HG_1^+, and grey lines represent the less strongly bound complex, HG_2^+.

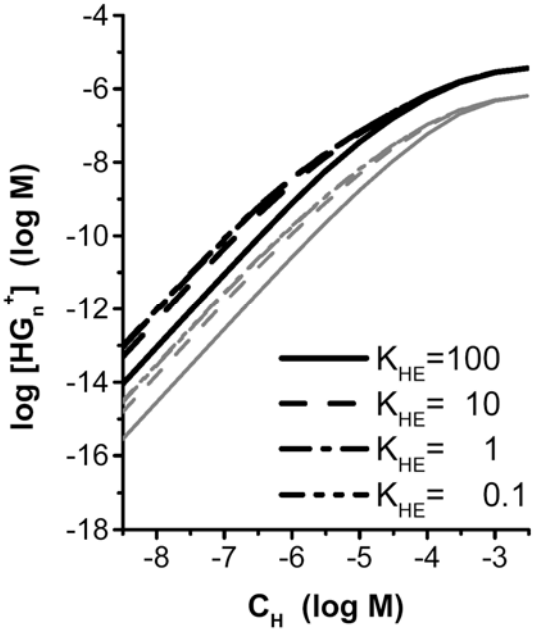

behavior of the surface concentrations in this region was dominated by competition between the ionic species, the distribution of free host simply was not a great factor. At lower host concentrations, an increase in K_{HE} caused a concomitant decrease in both $[HG_1^+]_s$ and $[HG_2^+]_s$. To explain this, when K_H is large, the concentration of hosts in the droplet interior drop,. This in turn drove the dissociation of the host-guest complexes in the droplet interior, leading to a small but similar shift in the distribution of both host-guest complexes from the surface to the interior of the droplets.

Although the binding strength is typically the property of interest in experiments involving host-guest complexation, the binding strengths of the host-guest complexes have no greater influence on the predicted mass spectra than the relative partitioning

Figure 4-4. Predicted concentrations of host-guest complexes on the surface of electrospray droplets when two guest ions compete for a single neutral host molecule when the binding constants are varied. Black lines represent the more strongly bound complex, HG_1^+, and grey lines represent the less strongly bound complex, HG_2^+. The binding constants varied are: (a) K_{b1} (b) K_{b2}.

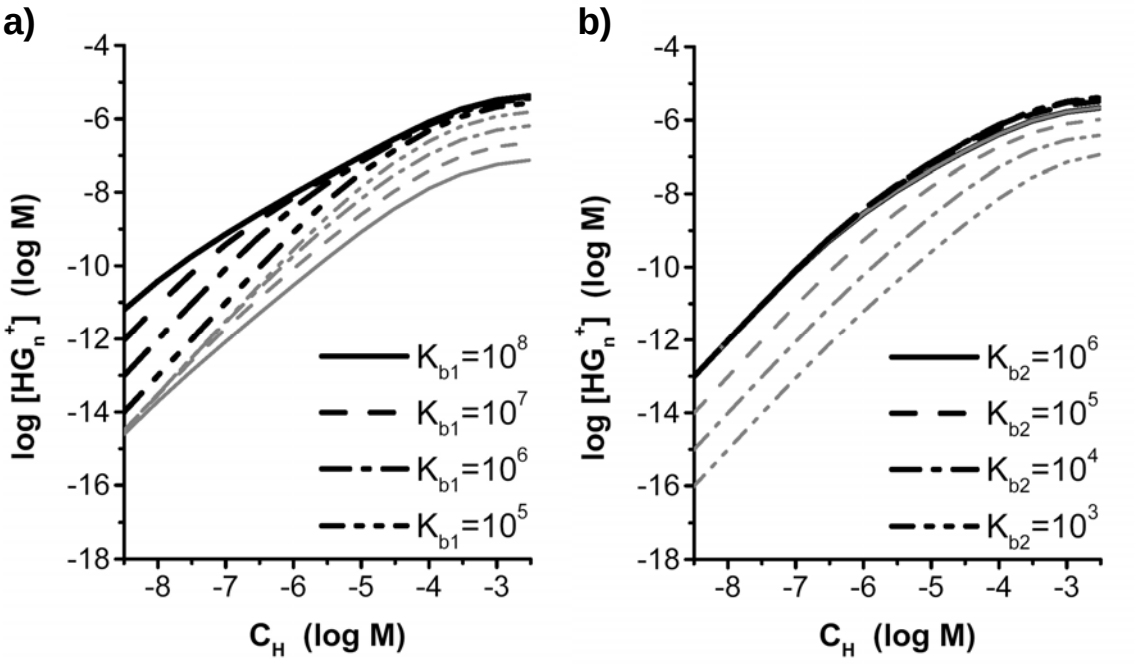

constants of the complexes. When the two binding constants were comparable (for example, log K_{b1} = 5 and log K_{b2} = 4.5 in Figure 4-4a), the surface concentrations of the two complexes were predictably similar, but when the binding constants differed, the concentration response of the two complexes shifted. When K_{b1} was varied while K_{b2} was held constant (Figure 4-4a), two distinct effects were predicted. As K_{b1} increased, at low host concentrations $[HG_1^+]_s$ increased in magnitude and the shape and slope of the response changed as well. In this concentration regime, an increase in the binding strength of one complex causes a roughly proportional increase in the surface concentration of that complex due to the competition with the background electrolyte.

Since more of the host and guest were unbound at these low host concentrations (based on solution equilibrium calculations), a shift in the binding of one complex had a comparatively small, but still significant impact on the coupled equilibria of the second host-guest complex. This coupling caused the effect of varying K_{b1} to depend on concentration as evidenced by the different shapes of the response curves. At higher host concentrations, $[HG_1^+]_s$ was limited by [Q] as expected, but the direct competition between the two complexes forced $[HG_2^+]_s$ to decrease with an increase in K_{b1}.

Interestingly, when the binding strength of the less strongly bound complex varied as shown in Figure 4-4b, $[HG_1^+]_s$ was unaffected when K_{b2} was increased except at the very highest host concentrations. There was, however, a direct correlation between K_{b2} and $[HG_2^+]_s$ that was uniform across the entire range of concentrations. This result indicated that the ESI response to the more strongly bound complex is overwhelmingly independent of the competitive binding equilibrium across the dynamic range of the electrospray source. Neither the second equilibrium nor the partitioning ability of its components had any significant effect on $[HG_1^+]_s$ when the host concentration was less than C_E. $[HG_1^+]_s$ was only affected at high host concentrations where the ESI source was not particularly sensitive to changes in concentration. Similarly, $[HG_2^+]_s$ was largely independent of the equilibria involving the more strongly bound complex, but depended somewhat on K_{b1}, particularly at moderate to high host concentrations.

In general, the partitioning model for two charged guests competing for a single neutral host predicted that the competitive binding equilibria actually have only limited effects on each other at the lower concentrations more useful for ESI-MS analysis. The

distribution of host-guest complexes in the mass spectra, however, cannot be assumed to directly relate to their respective binding strengths since the partitioning constant of a given complex has at least as significant impact on the predicted mass spectral abundance as does the binding strength. When the analyte concentrations surpass the concentration of any background electrolytes, the predictive surface concentrations of the complexes are subject to much wilder fluctuations based on a much wider range of influences. This fact, coupled with the limited response of ESI to concentration in this range, suggested that binding measurements at high concentrations should be particularly prone to error.

4.3.4 Predictions for Two Hosts Competing for a Single Guest Ion.

The same type of analysis was applied to the system of two neutral hosts competing for a single charged guest. Although the results for the two systems were expected to be similar, the competing hosts in this case have a lessened ability to influence the system as a whole since they cannot directly influence the charge balance which governs the production of ions in the electrospray. Varying some of the parameters – [G], C_E, K_{b1}, and K_{b2} – yielded essentially identical changes in the predicted concentrations as with the analysis of their analogues when two guest ions compete for a single host. Additionally, since the justifications given above for the effects of these parameters apply equally well to this case, no further discussion of these parameters is warranted.

Varying K_{H1GE}, the relative partitioning constant for the more strongly bound complex, has a very direct influence on $[H_1G^+]_s$ (Figure 4-5a). As K_{H1GE} increases, a roughly linear increase in $[H_1G^+]_s$ was predicted at low host concentrations while the

Figure 4-5. Predicted concentrations of host-guest complexes on the surface of electrospray droplets when two neutral host molecules compete for a single guest ion when K_{H1GE} (a) or K_{H2GE} (b) is varied. Black lines represent the more strongly bound complex, H_1G^+, and grey lines represent the less strongly bound complex, H_2G^+.

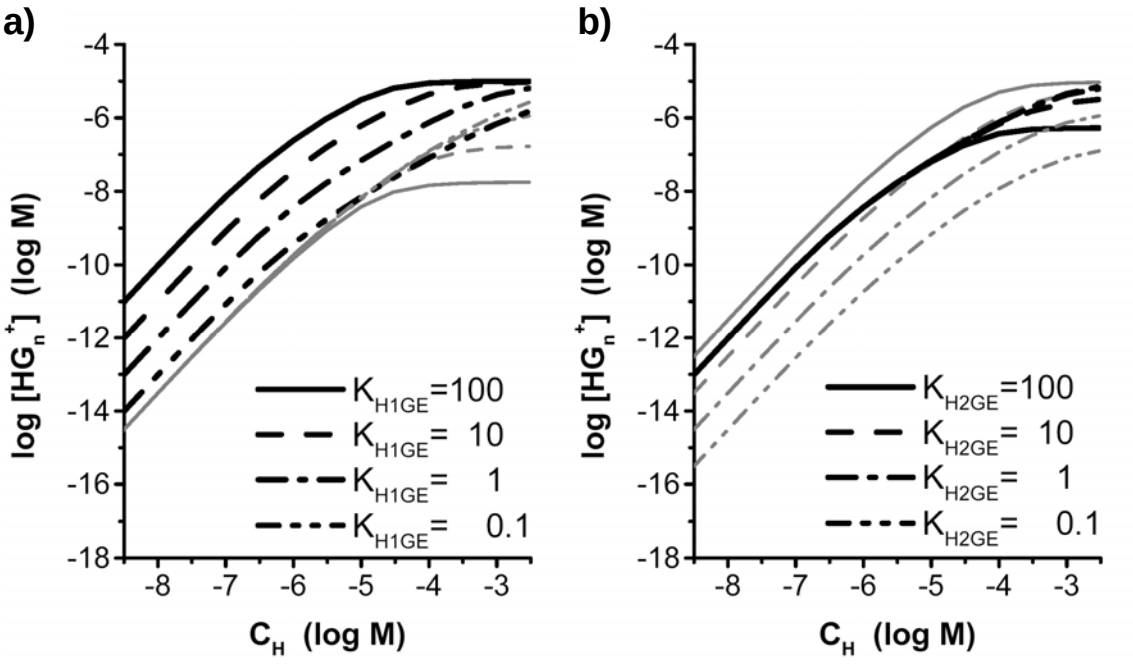

other complex was unaffected. At higher concentrations, however, the effect on both surface concentrations was somewhat more complex. When K_{H1GE} was relatively large, both complexes exhibited the expected saturation behavior. When K_{H1GE} was lower (and more similar to K_{H2GE}), the competition between the two hosts for the guest ion shifts the onset of saturation behavior to higher host concentrations since neither host-guest complex can saturate the surface of the droplets as readily. The net result was that at higher host concentrations, when K_{H1GE} was decreased, $[H_1G^+]_s$ decreased to a somewhat lesser extent than at lower concentrations while $[H_2G^+]_s$ increased, causing the resulting mass spectra to yield qualitatively different results at different concentrations if ion abundances are used as a measure of the relative binding strength of the two complexes.

In a sense, when K_{H2GE} was varied (Figure 4-5b) the model predicted the reverse behavior of when K_{H1GE} was varied. At lower host concentrations, $[H_2G^+]_s$ was proportional to K_{H2GE} while $[H_1G^+]_s$ was unaffected by changes in the relative partitioning constant of the less strongly bound complex. The behavior again became more complicated at higher concentrations. At host concentrations above C_E, $[H_2G^+]_s$ remained roughly proportional to its relative partitioning constant. $[H_1G^+]_s$, on the other hand, increased with decreases in K_{H2GE}. Also, the model predicted again that when K_{H2GE} surpasses K_{H1GE}, the less strongly bound complex could be more abundant in the mass spectrum despite having a lower concentration in the bulk solution.

Changes in the relative partitioning constant of the guest ion had very little effect (Figure 4-6a). Only at very high values of K_{GE} was a slight decrease in the surface concentrations of both complexes predicted. Moreover, the change affected both complexes identically, making K_{GE} largely inconsequential when the relative concentrations of two host-guest complexes are of primary importance.

The effects of varying the relative partitioning constants for the two different hosts were also somewhat muted. When K_{H1} was increased to very large values (Figure 4-6b), $[H_1G^+]_s$ decreased slightly when the host concentration was low. K_{H1} did not affect $[H_1G^+]_s$ at higher concentrations. Additionally, $[H_2G^+]_s$ was independent of K_{H1} at low concentrations, but increased very slightly at high concentrations when K_{H1} was very large.

The effect of varying K_{H2} was slightly more significant than with K_{H1} (Figure 4-6c). While increasing K_{H2} had no influence on $[H_1G^+]_s$, it caused a drop in $[H_2G^+]_s$ that

Figure 4-6. Predicted concentrations of host-guest complexes on the surface of electrospray droplets when two neutral host molecules compete for a single guest ion when K_{GE} (a), K_{H1E} (b), or K_{H2E} (c) is varied. Black lines represent the more strongly bound complex, H_1G^+, and grey lines represent the less strongly bound complex, H_2G^+.

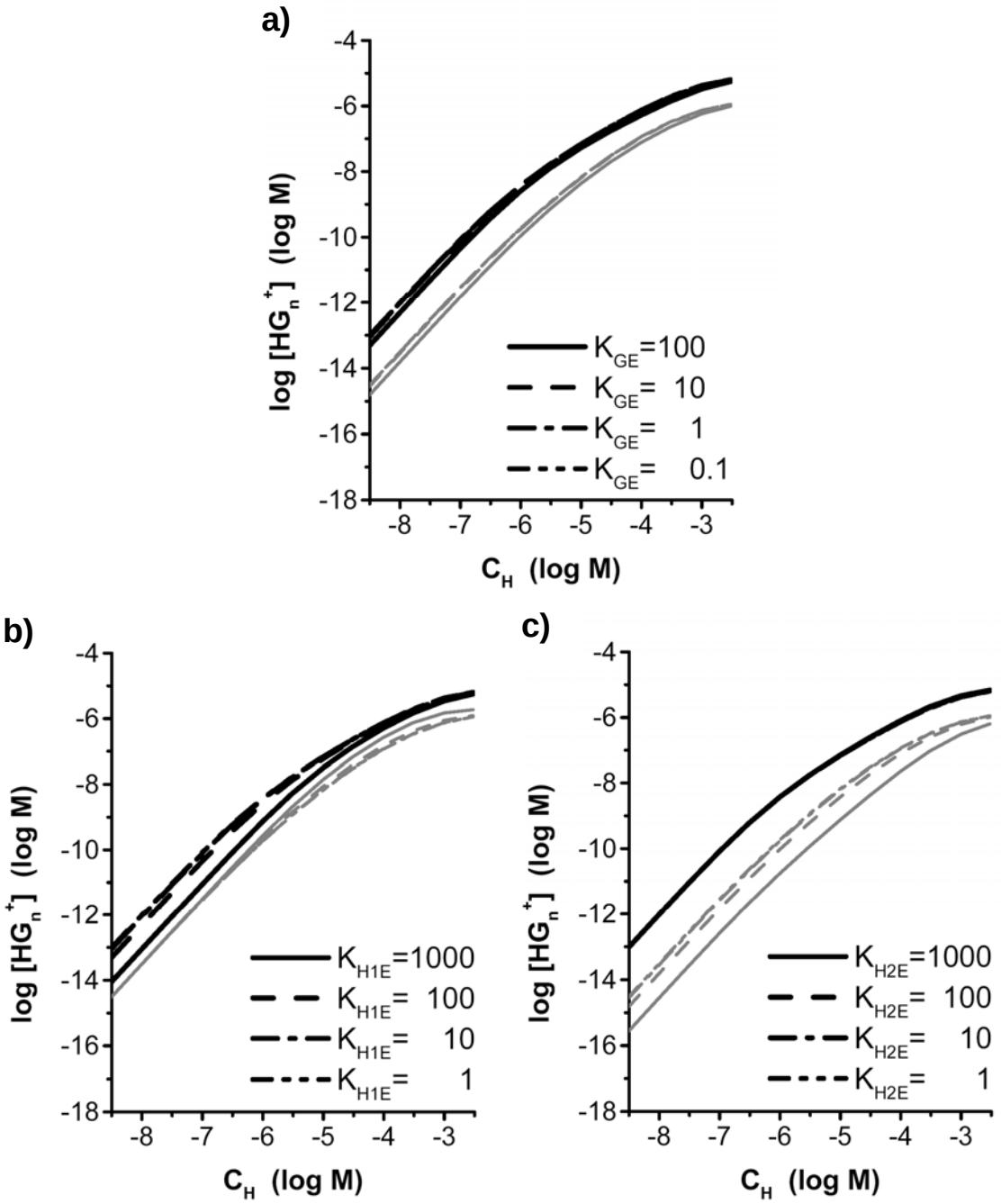

was more pronounced at lower host concentrations but present at all concentrations. This suppression was markedly non-linear, with the drop in signal increasing with higher values of K_{H2}.

Overall, this partitioning model predicted that the relative partitioning constants for the complexes and the bulk solution binding constants have the most significant influence on the relative abundances of host-guest complexes in the mass spectra. This conclusion particularly held true when the formal host concentrations were kept below C_E, where the electrospray source operates in its dynamic range. This concentration range can be manipulated through the addition of background electrolyte, but as long as operation below concentrations where the surface concentrations begin to saturate is ensured, only a limited number of parameters influence the relative predicted surface concentrations of the host-guest complexes. At higher concentrations, the number of parameters significantly affecting the relative values of $[H_1G^+]_s$ and $[H_2G^+]_s$ was much larger. Based on these predictions, deconvoluting the results of experiments conducted in this regime for the deviations caused by each relevant parameter would likely be difficult and error-prone.

4.4 Experimental Results

Although the partitioning model for the two competitive systems could be evaluated very systematically, real experiments are necessarily more complex. A single experimental parameter can rarely be changed in isolation. For example, substituting a different guest ion into a system with one host and two guests causes changes in the

partitioning constant for that guest, the partitioning constant for the complex containing that guest, as well as the binding constant for that complex. The mass spectra collected for this altered system will reflect all of these changes. Nevertheless, such experiments are useful for probing and testing the predictions of the partitioning model if the expected changes can be reasonably estimated. To evaluate the validity of the partitioning model as thoroughly as possible, its predictions were tested with a series of carefully selected experiments. The well-studied crown ether-metal complexes (1, 27, 32-39, 41-44, 57-59) were chosen for these experiments, and the particular conditions for each case tested the model as narrowly as possible to allow for reasonably direct analysis of the influence of each experimental parameter.

4.4.1 Two Charged Guests Competing for a Single Host Molecule.

The concentration of the background electrolyte was varied by analyzing solutions containing 18-crown-6, KCl, and RbCl at equimolar concentrations ranging from 10^{-7} to 10^{-3} M. To control the concentration of the background electrolytes, tetrabutylammonium iodide, Bu_4NI, was added to the solutions at different concentrations. Just as predicted by the partitioning model for this system (Figure 4-1b), an increase in C_E results in a suppression of the ion signal for both host-guest complexes (Figure 4-7). The actual behavior, however, did not vary linearly with the concentration of Bu_4NI as predicted. Rather, at concentrations of Bu_4NI at or below 10^{-5} M, the abundance of (18-crown-6 + $K)^+$ was unchanged, and the abundance of (18-crown-6 + $Rb)^+$ only decreased for a few data points at moderately low host concentrations. At higher Bu_4NI concentrations, the abundances of both complexes decreased significantly.

Figure 4-7. ESI-MS intensities for complexes of 18-crown-6 with K^+ (filled points) or Rb^+ (open points). The concentration of the background electrolyte, $Bu_4N^+I^-$ was varied: 10^{-6} M (—●—),10^{-5} M (− −■− −), 10^{-4} M (− · −♦− · −), and 10^{-3} M (− · · −▲− · · −).

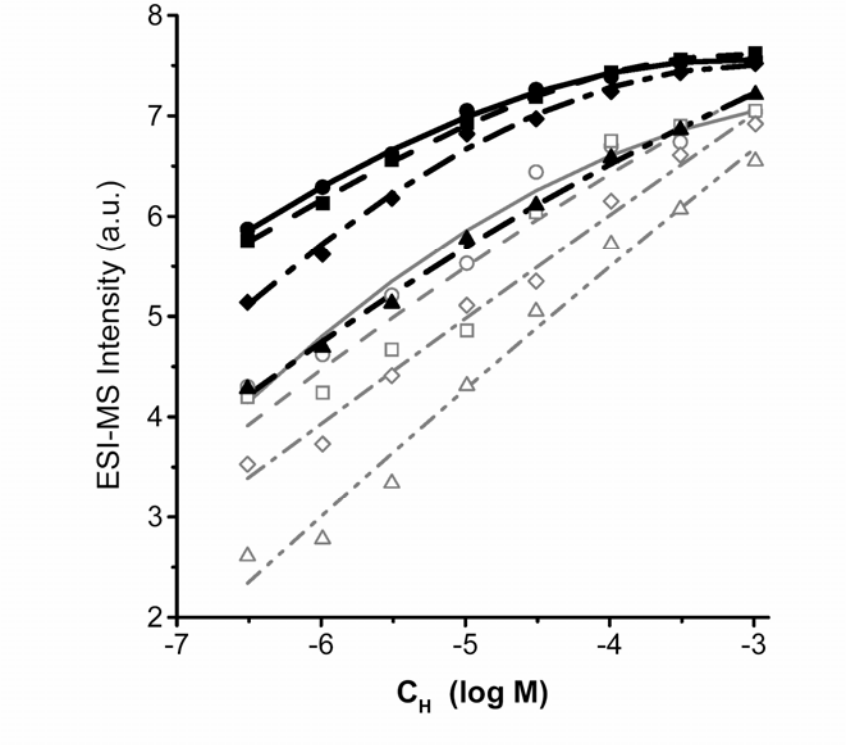

This behavior has been observed previously (27) and resulted from the presence of ionic contaminants in the 1-10 μM range in purchased methanol (9, 16). Despite these deviations, to a large extent varying the Bu_4NI concentration affected both complex ions in a similar manner as expected.

Beyond changing the concentration of the background electrolyte, the identity of the background electrolyte was varied while its concentration was held constant at 10^{-5} M. Three different tetraalkylammonium iodides were selected as background electrolytes since the varying length of their alkyl groups directly correlates with the ability of the cations to partition to the surface of the ESI droplets. Due to their greater

Figure 4-8. ESI-MS intensities for complexes of 18-crown-6 with K^+ (filled points) or Rb^+ (open points). The background electrolyte was varied while its concentration was maintained at 10^{-5} M: $Et_4N^+I^-$ (—●—), $Pr_4N^+I^-$ (– –■– –), and $Bu_4N^+I^-$ (– · –♦– · –).

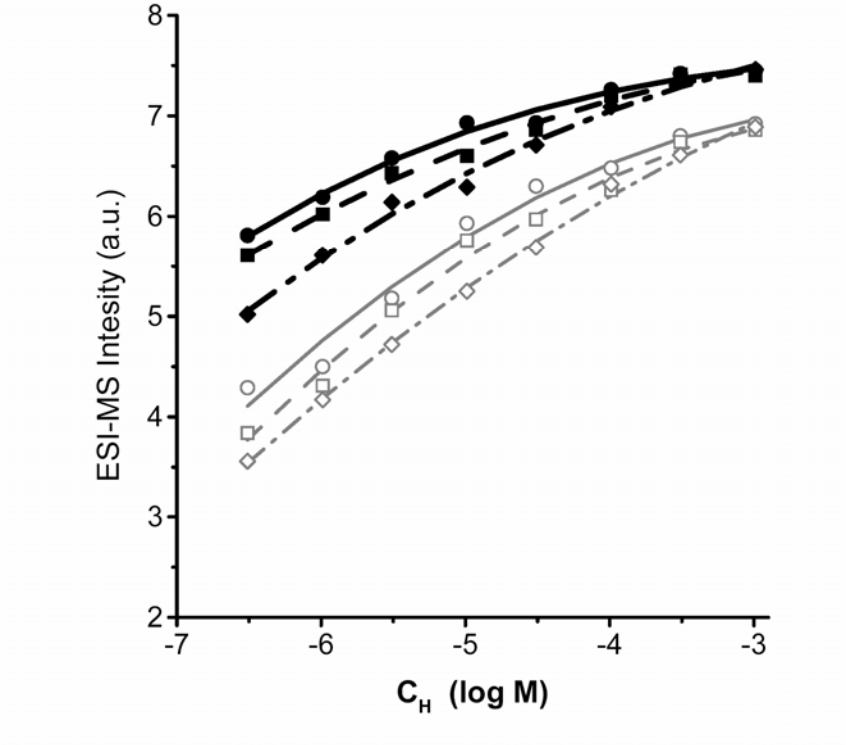

hydrophobic character, the tetraalkylammonium cations with larger alkane groups would be expected to more readily partition to the droplet surface to escape the significantly polar environment inside the droplets (27), resulting in larger K_E values and, as a result, lower relative partitioning constants for all other species. Consistent with predictions, when the background electrolyte has a larger partitioning constant, all other ions had lower intensities in the ESI mass spectra (Figure 4-8).

Mimicking the typical experimental strategy undertaken to evaluate the binding selectivity of a host, solutions containing 18-crown-6, KCl, and various other alkali chlorides were analyzed (Figure 4-9). This represents the often performed experiment where a complex of interest is compared to a competing reference complex. Several

Figure 4-9. ESI-MS intensities for complexes of 18-crown-6 with K^+ (filled points) or a second alkali cation (open points). The second cation in each solution was one of: NaCl (—●—), RbCl (– –■– –), or CsCl (– · –♦– · –).

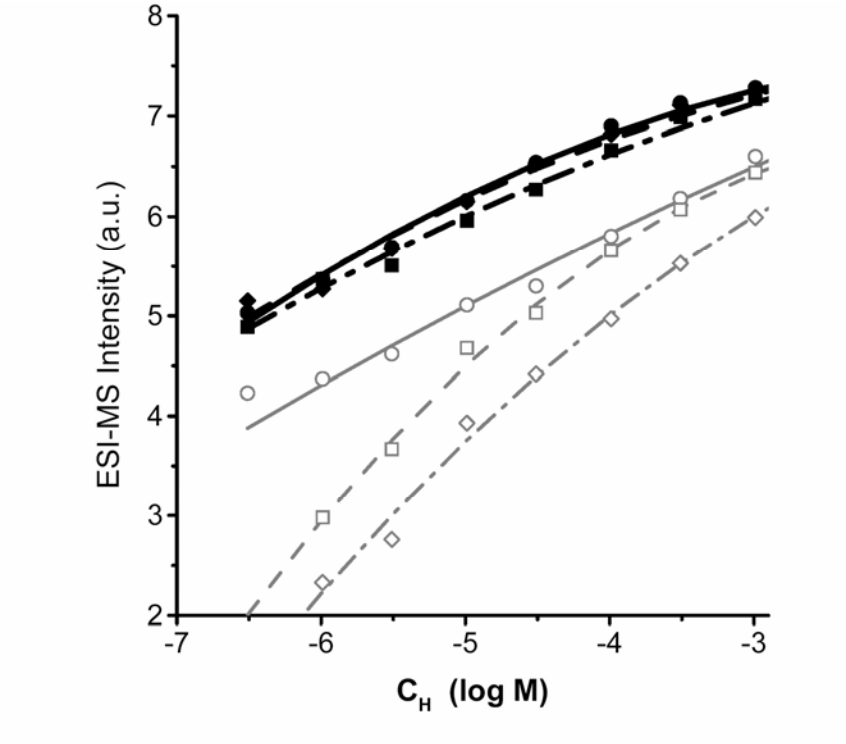

parameters change with the identity of the second guest ion: the binding strength of the second complex, the relative partitioning constant of the second complex, and the relative partitioning constant of the second guest ion. For each of these, the effect on the more strongly bound complex was minimal, consistent with the predictions of the partitioning model (Figures 4-2b, 4-2d, and 4-4b). The same predictions lead to contradictory expectations for the second, less strongly bound complex. In this case, of the less strongly bound complexes (with Na^+, Rb^+, and Cs^+), the Rb^+ complex had the greatest binding constant (Table 4-1). The Na^+ complex, on the other hand, should have the largest partitioning constant since its small size allows its charge to be better encapsulated within the macrocyclic host (27). The partitioning model also suggests a

dependence of the abundance of the second complex ion on the partitioning constant of the guest ion, but the weak dependence predicted was not likely to significantly alter the effects of the other two parameters. The experimental results suggest that the partitioning constant of the second complex determined the relative abundances of the second complex, with the abundances following the size of the guest ions from Na^+ down to Cs^+ which had the lowest abundance. These results confirm that ESI mass spectra may not be reliable indicators of binding strength while considering the effects of partitioning in the ESI droplets can help explain discrepancies observed. The large discrepancy between the results for the Na^+ and Cs^+ complexes despite their nearly identical binding constants (Table 4-1) highlights the possible pitfalls of assuming that ESI mass spectra necessarily reflect binding strength. Based on the results where these cations compete with K^+ to bind with 18-crown-6, the erroneous conclusion that Na^+ bound more strongly could be made.

A common method for correcting the ESI-MS results of a competitive binding experiment for the partitioning effects, typically referred to simply as "differences in ESI efficiency," is to analyze a solution containing an excess of the host to minimize binding selectivity (34, 37). The relative abundances in the mass spectra are then assumed to be independent of differences in binding strength, allowing the ratio of these abundances to serve as a "correction factor." To evaluate how accurately this procedure accounts for the partitioning effects, solutions containing 18-crown-6, KCl, and RbCl were analyzed with equimolar concentrations, a five-to-one excess of 18-crown-6, and a five-to-one excess of both KCl and RbCl (Figure 4-10). Changes in the relative concentrations of the

Table 4-1. Binding Constants[a] for Crown Ether-Metal Host-Guest Complexes

	Guest Ion			
Host	**Na+**	**K+**	**Rb+**	**Cs+**
18-crown-6[b]	4.37	6.05	5.56	4.43
benzo-18-crown-6[c]	4.03	5.27	4.62	3.66
dibenzo-18-crown-6[d]	4.37	4.93	4.47	3.36
dicyclohexano-18-crown-6[e]		5.61		

[a] Binding constants are the log of the values for each complex determined in methanol listed in the indicated references. Where multiple values were reported, the average is given.
[b] From reference 57.
[c] From reference 58.
[d] From reference 56.
[e] From reference 59.

host and guests had very little effect on the ion abundances observed when the guests were in excess, despite the increased concentrations of the two guest ions at a given host concentration. When the host, 18-crown-6, was present in excess to decrease the selectivity towards the two guest ions, the ion abundance of both host-guest complexes dropped. To some extent, this could be attributed to the decrease in the overall number of complex ions that could form due to the reduction in the number of guest ions, but the observed decrease was greater for the less strongly bound rubidium complex than for the potassium complex. As was discussed above, the rubidium complex had a lower partitioning constant than the potassium complex. The additional decrease in the abundance of (18-crown-6 + Rb)$^+$, therefore, can be explained as the influence of partitioning effects towards the overall behavior of this system in the electrospray and may, in fact, provide a useful way to analyze the solution binding interactions. As such, the predictions of the partitioning model support the method determining a correction

Figure 4-10. ESI-MS intensities for complexes of 18-crown-6 with K^+ (filled points) or Rb^+ (open points) from solutions with different relative concentrations of the host and guests. The ratios of the formal concentrations (18-crown-6:KCl:RbCl) were: 5:1:1 (—●—), 1:1:1 (– –■– –), or 1:5:5 (– · –♦– · –).

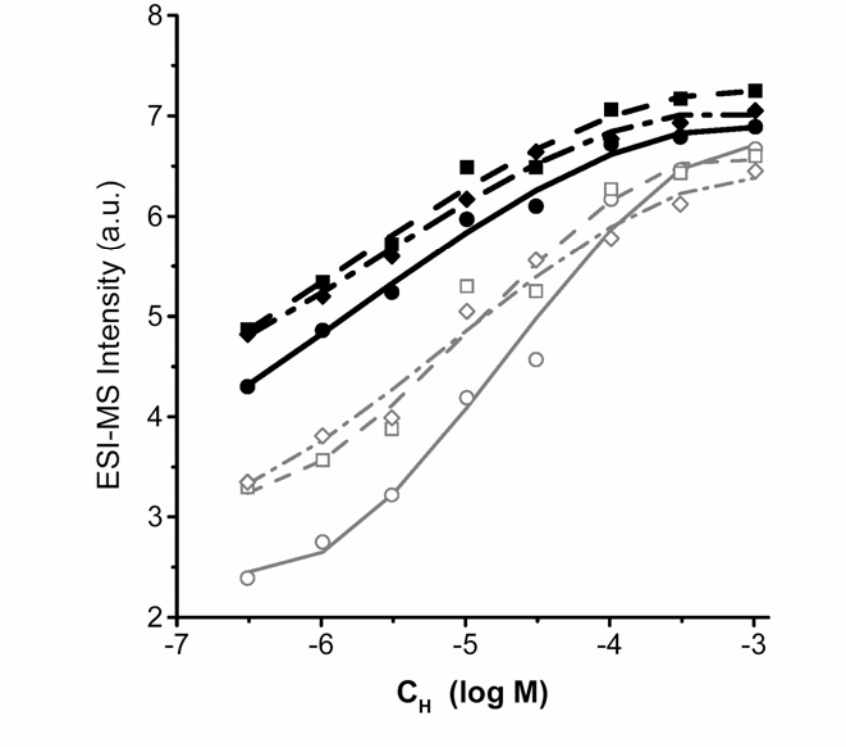

factor by raising the concentration of a neutral host while holding the concentration of competing guest ions constant.

4.4.2 Two Neutral Hosts Competing for a Single Guest Ion.

To gauge the effect of the background electrolyte on a system with two host molecules in competition for a guest ion, several experiments analogous to those described above were performed with 18-crown-6, KCl, and a second crown ether. When either the concentration of the background electrolyte or its identity was varied, the results obtained (not shown) were nearly identical to those for the one host / two guest system (Figures 4-7 and 4-8).

Figure 4-11. ESI-MS intensities for complexes of 18-crown-6 with K^+ (filled points) or a second macrocyclic host (open points). The second host in each solution was one of: dicyclohexano-18-crown-6 (—●—), benzo-18-crown-6 (− −■− −), or dibenzo-18-crown-6 (− · −♦− · −).

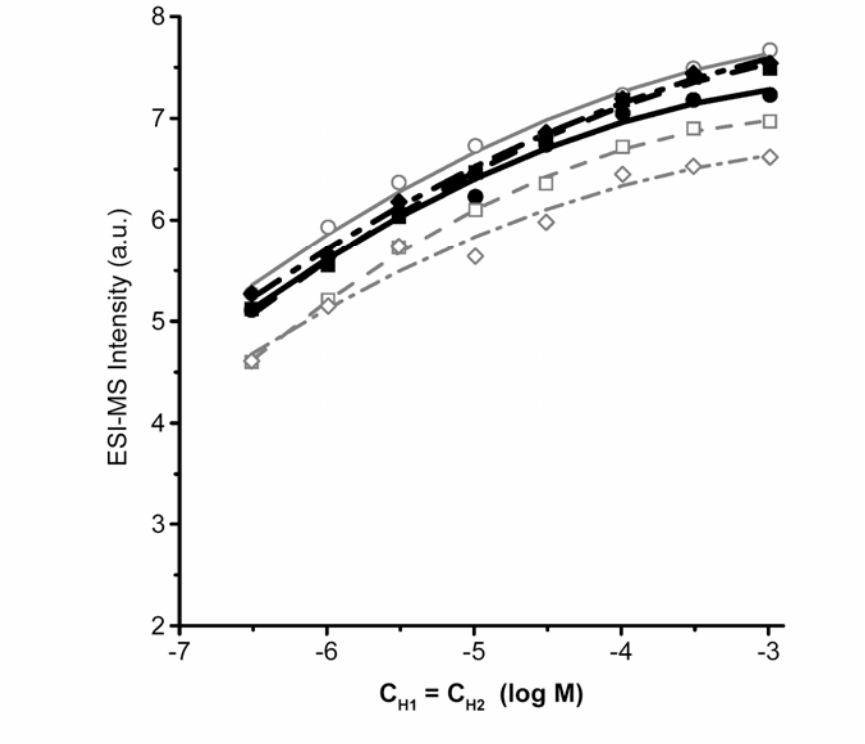

In experiments where the host molecules were varied, the results were both more complicated and more interesting due to the parallels with methods commonly used for characterizing novel ligands (1,32-44,49-51). When 18-crown-6 and KCl were mixed with one of dicyclohexano-18-crown-6, benzo-18-crown-6, or dibenzo-18-crown-6, (Figure 4-11) the abundance of (18-crown-6 + $K)^+$, the complex known to have the greatest binding constant (Table 4-1), was not affected significantly. The abundance of the second crown ether–potassium complex varied with the identity of the crown ether. The abundance was greatest with dicyclohexano-18-crown-6 and lowest with dibenzo-18-crown-6. Among the complexes bound less strongly in each of these mixtures, the abundances of the complexes in the mass spectra reflected the binding strengths of the

Figure 4-12. ESI-MS intensities for complexes of 18-crown-6 (filled points) or dibenzo-18-crown-6 (open points) with K^+ from solutions with different relative concentrations of the host and guests. The ratios of the formal concentrations (18-crown-6:dibenzo-18-crown-6:KCl) were: 5:5:1 (—●—), 1:1:1 (− −■− −), or 1:1:5 (− · −♦− · −).

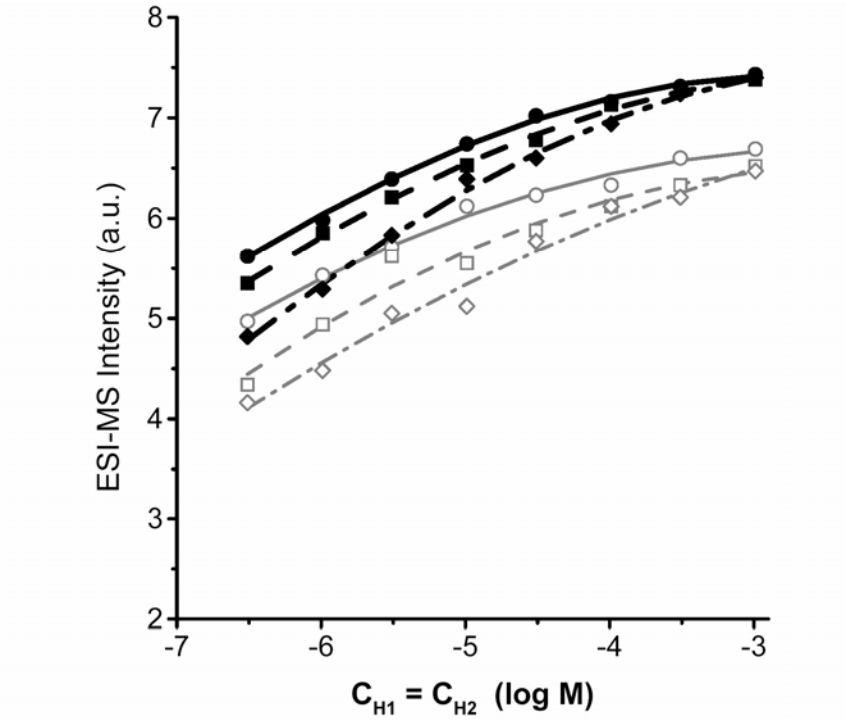

complexes (Table 4-1). These less strongly-bound complexes did not necessarily have lower abundances than the more strongly bound complex; the abundance of (dicyclohexano-18-crown-6 + K)$^+$ surpassed that of (18-crown-6 + K)$^+$ despite the greater binding constant of the latter complex. This indicates that, while competitive binding experiments between different hosts may sometimes yield useful results, allowing both hosts to compete against another more strongly-binding ligand rather than against each other can produce results reflecting the actual binding strengths of the complexes.

While changes in the relative concentrations of the species in experiments with one host and two guests supported the idea that the formal concentrations in an

experiment could be carefully selected to measure partitioning effects independently of the binding interactions, an analogous experiment with two macrocyclic hosts competing for a single guest ions yielded very different results when the relative concentrations were changed (Figure 4-12). When the guest ion, K^+, was in excess, the decreased binding selectivity towards 18-crown-6 and dibenzo-18-crown-6 allowed any shift in the relative abundances of the two complexes to be attributed to differences in electrospray efficiencies. In this case, the relatively non-polar benzo- groups give (dibenzo-18-crown-6 + K)$^+$ a greater partitioning constant than the more strongly bound (18-crown-6 + K)$^+$, leading to a prediction that the differences in the abundances will diminish relative to the equimolar mixtures, particularly at higher host concentrations, consistent with the experimental results. When the hosts were in excess, competition between them for the limited number of guest ions likely enhanced the apparent binding selectivity. As a result, the difference in the abundances of the two complexes was pronounced, especially at higher concentrations where the partitioning effects would also lead to heightened competition.

4.5 Conclusions

The development of partitioning models of the electrospray of solutions containing competitive host-guest binding equilibria further extends the applicability of the partitioning theory while explaining many of the nuances inherent to the use of ESI mass spectrometry to probe host-guest binding. Evaluation of the partitioning models, both through systematic evaluation of the relevant parameters and testing of the

predictions through experiments with crown ether–alkali metal complexes, revealed that certain factors such as the concentration of the background electrolyte, binding strength, and partitioning ability of the host-guest complex all had a significant impact on the ion abundances produced by an electrospray. On the other hand, factors such as the partitioning abilities of the individual hosts and guests had only limited influence on the relative abundances observed for the host-guest complexes. A key finding was the fact that in many situations the relative abundances of different complexes to differ significantly from trends expected from solution binding strengths, consistent with the prediction that differences in the ability of complexes to partition to the surface of ESI droplets could supersede the influence of binding strengths. Preliminary experiments support the practice of using carefully designed experiments to "correct" for ESI efficiencies using these partitioning effects. The predictions of the partitioning models provide the understanding necessary to explain deviations in ion abundances resulting from the electrospray and allow more confident use of ESI-MS for the evaluation of host-guest binding interactions.

4.6 References

(1) Young, D.-S.; Hung, H.-Y.; Liu, L. K. *J. Mass Spectrom.* **1997**, *32*, 432-437.

(2) Tang, L.; Kebarle, P. *Anal. Chem.* **1993**, *65*, 3654-3668.

(3) Van Berkel, G. J.; Zhou, F. *Anal. Chem.* **1995**, *67*, 2916-2923.

(4) Tang, K.; Smith, R. D. *J. Am. Soc. Mass Spectrom.* **2001**, *12*, 343-347.

(5) Cech, N. B.; Enke, C. G. *Anal. Chem.* **2001**, *73*, 4632-4639.

(6) Enke, C. G. *Anal. Chem.* **1997**, *69*, 4885-4893.

(7) Ikonomou, M. G.; Blades, A. T.; Kebarle, P. *Anal. Chem.* **1990**, *62*, 957-967.

(8) Tjernberg, A.; Carnö, S.; Oliv, F.; Benkestock, K.; Edlund, P.-O.; Griffiths, W. J.; Hallén, D. *Anal. Chem.* **2004**, *76*, 4325-4331.

(9) Cole, R. B. *J. Mass Spectrom.* **2000**, *35*, 763-772.

(10) Kebarle, P.; Tang, L. *Anal. Chem.* **1993**, *65*, 972A-986A.

(11) Cech, N. B.; Enke, C. G. *Mass Spectrom. Rev.* **2001**, *20*, 362-387.

(12) Kebarle, P.; Peschke, M. *Anal. Chim. Acta.* **2000**, *406*, 11-35.

(13) King, R.; Bonfiglio, R.; Fernandez-Metzler, C.; Miller-Stein, C.; Olah, T. *J. Am. Soc. Mass Spectrom.* **2000**, *11*, 942-950.

(14) Zook, D. R.; Bruins, A. P. *Int. J. Mass Spectrom.* **1997**, *162*, 129-147.

(15) Sjoberg, P. J. R.; Bokman, C. F.; Bylund, D.; Markides, K. E. *J. Am. Soc. Mass Spectrom.* **2001**, *12*, 1002-1010.

(16) Constantopoulos, T. L.; Jackson, G. S.; Enke, C. G. *Anal. Chim. Acta.* **2000**, *406*, 37-52.

(17) Constantopoulos, T. L.; Jackson, G. S.; Enke, C. G. *J. Am. Soc. Mass Spectrom.* **1999**, *10*, 625-634.

(18) Zhou, S.; Cook, K. D. *J. Am. Soc. Mass Spectrom.* **2001**, *12*, 206-214.

(19) Fenn, J. B. *J. Am. Soc. Mass Spectrom.* **1993**, *4*, 524-535.

(20) Wang, G.; Cole, R. B. *Anal. Chem.* **1994**, *66*, 3702-3708.

(21) Tang, L.; Kebarle, P. *Anal. Chem.* **1991**, *63*, 2709-2715.

(22) Iribarne, J. V.; Thomson, B. A. *J. Chem. Phys.* **1976**, *64*, 2287-2294.

(23) Dole, M.; Mack, L. L.; Hines, R. L.; Mobley, R. C.; Ferguson, L. D.; Alice, M. B. *J. Chem. Phys.* **1968**, *49*, 2240-2249.

(24) Gomez, A.; Tang, K. *Phys. Fluids.* **1994**, *6*, 404-414.

(25) Tang, K.; Smith, R. D. *Int. J. Mass Spectrom.* **1999**, *185/186/187*, 97-105.

(26) Taflin, D. C.; Ward, T. L.; Davis, E. J. *Langmuir*. **1989**, *5*, 376-384.

(27) Sherman, C. L.; Brodbelt, J. S. *Anal. Chem.* **2003**, *75*, 1828-1836.

(28) Haddrell, A. E.; Agnes, G. R. *Anal. Chem.* **2004**, *76*, 53-61.

(29) Sjoberg, P. J. R.; Bokman, C. F.; Bylund, D.; Markides, K. E. *Anal. Chem.* **2001**, *73*, 23-28.

(30) Cech, N. B.; Krone, J. R.; Enke, C. G. *Anal. Chem.* **2001**, *73*, 208-213.

(31) Cech, N. B. *Anal. Chem.* **2000**, *72*, 2717-2723.

(32) Kempen, E. C.; Brodbelt, J. S. *Anal. Chem.* **2000**, *72*, 5411-5416.

(33) Young, D.-S.; Hung, H.-Y.; Liu, L. K. *Rapid Commun. Mass Spectrom.* **1997**, *11*, 769-773.

(34) Blair, S. M.; Kempen, E. C.; Brodbelt, J. S. *J. Am. Soc. Mass Spectrom.* **1998**, *9*, 1049-1059.

(35) Williams, S.; Blair, S. M.; Brodbelt, J. S.; Huang, X.; Bartsch, R. A. *Int. J. Mass Spectrom.* **2001**, *212*, 389-401.

(36) Blair, S. M.; Brodbelt, J. S.; Marchand, A. P.; Kumar, K. A.; Chong, H.-S. *Anal. Chem.* **2000**, *72*, 2433-2445.

(37) Williams, S. M.; Brodbelt, J. S.; Marchand, A. P.; Cal, D.; Mlinaric-Majerski, K. *Anal. Chem.* **2002**, *74*, 4423-4433.

(38) Kempen, E. C.; Brodbelt, J. S.; Bartsch, R. A.; Jang, Y.; Kim, J. S. *Anal. Chem.* **1999**, *71*, 5493-5500.

(39) Blair, S. M.; Brodbelt, J. S.; Reddy, G. H.; Marchand, A. P. *J. Mass Spectrom.* **1998**, *33*, 721-728.

(40) Schalley, C. A.; Castellano, R. K.; Brody, M. S.; Rudevich, D. M.; Siuzdak, G.; Rebek, Jr., J. *J. Am. Chem. Soc.* **1999**, *121*, 4568-4579.

(41) Wu, H.-F.; Huan, S.-M.; Wu, C.-F. *Eur. J. Mass Spectrom.* **2002**, *8*, 375-380.

(42) Oshima, T.; Matsuda, F.; Fukushima, K.; Tamura, H.; Matsubayashi, G.; Arakawa, R. *J. Chem. Soc., Perkin Trans. 2*. **1998**, 145-148.

(43) Brodbelt, J. S.; Kempen, E. C.; Reyzer, M. *Struct. Chem.* **1999**, *10*, 213-219.

(44) Allain, F.; Virelizier, H.; Moulin, C.; Jankowski, C. K.; Dozol, J. F.; Tabet, J. C. *Spectroscopy (Amsterdam)*. **2000**, *14*, 127-139.

(45) Daniel, J. M.; Friess, S. D.; Rajagopala, S.; Wendt, S.; Zenobi, R. *Int. J. Mass Spectrom.* **2002**, *216*, 1-27.

(46) Jorgensen, T. J. D.; Roepstorff, P.; Heck, A. J. R. *Anal. Chem.* **1998**, *70*, 4427-4432.

(47) Loo, J. A. *Mass Spectrom. Rev.* **1997**, *16*, 1-23.

(48) Beck, J. L.; Colgrave, M. L.; Ralph, S. F.; Sheil, M. M. *Mass Spectrom. Rev.* **2001**, *20*, 61-87.

(49) Reyzer, M. L.; Brodbelt, J. S.; Kerwin, S. M.; Kumar, D. *Nucleic Acids Res.* **2001**, *29*, e103.

(50) Wan, K. X.; Shibue, T.; Gross, M. L. *J. Am. Chem. Soc.* **2000**, *122*, 300-307.

(51) Gabelica, V.; De Pauw, E.; Rosu, F. *J. Mass Spectrom.* **1999**, *34*, 1328-1337.

(52) Vairamani, M.; Gross, M. L. *J. Am. Chem. Soc.* **2003**, *125*, 42-43.

(53) Sessler, J. L.; Jayawickramarajah, J.; Sherman, C. L.; Brodbelt, J. S. *J. Am. Chem. Soc.* **2004**, *126*, 11460-11461.

(54) Sessler, J. L.; Jayawickramarajah, J.; Sathiosatham, M.; Sherman, C. L.; Brodbelt, J. S. *Org. Lett.* **2003**, *5*, 2627-2630.

(55) Sakamoto, S.; Nakatani, K.; Saito, I.; Yamaguchi, K. *Chem. Commun.* **2003**, 788-789.

(56) Manet, I.; Francini, L.; Masiero, S.; Pieraccini, S.; Spada, G. P.; Gottarelli, G. *Helv. Chim. Acta.* **2001**, *84*, 2096-2107.

(57) Izatt, R. M.; Pawlak, K.; Bradshaw, J. S.; Bruening, R. L. *Chem. Rev.* **1991**, *91*, 1721-2085.

(58) Ercolani, G.; Mandolini, L.; Masci, B. *J. Am. Chem. Soc.* **1981**, *103*, 7484-7489.

(59) Yamato, K.; Fernandez, F. A.; Vogel, H. F.; Bartsch, R. A.; Dietz, M. L. *Tetrahetron Lett.* **2002**, *43*, 5229-5232.

CHAPTER 5

Electrospray Ionization Mass Spectrometric Detection of Self-Assembly of a Crown Ether Complex Directed by Pi-Stacking Interactions

5.1 Introduction

In recent years, molecular self-assembly has become a key tool for developing novel chemical structures. Applications as diverse as patterned deposition of metallic monolayers (1), creation of ordered light-harvesting arrays (2), and creation of new biological materials based on self assembled peptide structures (3), have revolutionized the development of materials with nanoscale features. Various types of chemical interactions have been used to direct the assembly of individual sub-units into the desired products. In the present report, electrospray ionization mass spectrometry (ESI-MS) results on a novel crown ether are presented which demonstrate that donor-acceptor π-stacking interactions can be used to direct the self-assembly of non-covalent macrocycle-metal complexes.

For probing metal complexation of macrocyclic systems, ESI-MS has proven to be an invaluable tool. Since ESI is capable of transferring even very weakly bound non-covalent complexes to the gas phase, mass spectrometry can be used to qualitatively and quantitatively evaluate the binding selectivities of the hosts or the relative binding constants of the resulting host-guest complexes (4-22). Furthermore, many studies have

demonstrated that the results of ESI-MS analysis of these host-guest complexes correlate well with measurements of the equilibria in solution (8-9, 14-17). Crown ether-metal complexes in particular have been the subject of much study, and the binding properties of many types of these macrocyclic complexes have been evaluated through both ESI-MS (4-5, 7-14, 16-17, 22-25) and more traditional solution analyses (26-31). While most such studies have focused on the 1:1 crown ether:metal complexes, 2:1 crown ether:metal:crown ether "sandwich" complexes are well known (23-25, 28-31) and have been studied successfully by ESI-MS (23-25).

Although binding of the second ligand in a sandwich complex in solution is typically not as strong as for the first ligand for unsubstituted crown ethers (27), it is expected that the addition of certain functional groups on the macrocycle could enhance the formation of sandwich complexes. An analogous result has been observed for the formation of bis-crown ether-metal complexes studied by ESI-MS (13, 23, 28). For these macrocycles, the pre-organization offered by the covalently linked crown ethers results in very strong metal complexation in which the metal cation is simultaneously coordinated by both crown ethers.

Rather than rely on covalently linked structures such as those used in bis-crown ethers, other chemical interactions must be leveraged to create sandwich complexes which can self-assemble. Pi-stacking interactions, present in many biological systems and having demonstrated utility in strengthening other types of molecular interactions (32-35), represent a novel means of enhancing the formation of macrocycle-metal sandwich complexes. In contrast to the well-studied interactions between metal ions and

π-orbital systems (36-38), the inclusion of aromatic moieties on the macrocycles in this report is expected to result in π-stacking interactions between the π-orbital systems on different macrocycles. These interactions should enhance the formation of sandwich complexes when the π-orbitals have appropriate overlap by allowing the detection of sandwich complexes incorporating larger macrocycles or smaller metal ions, ones not typically observed.

Pi-stacking interactions can be further enhanced through the presence of donor-acceptor interactions between the π-orbitals. Including electronegative heteroatoms such as nitrogen or oxygen in an aromatic system creates an electron-deficient π-system in a manner similar to the effect of including an electron-withdrawing substituent on the aromatic ring (32). The net result is a change in the polarization of the π-orbitals relative to an aromatic moiety without such heteroatoms, causing an additional attractive force as some electron density from the electron-rich π-system is donated to the electron-deficient π-system, strengthening the overall interaction (32, 39). In the present work, an electron-deficient quinoxaline moiety was incorporated into a crown ether macrocycle, **1** (shown in Scheme 5-1), to enhance the sandwich complex formation with benzo-crown ethers as

Scheme 5-1.

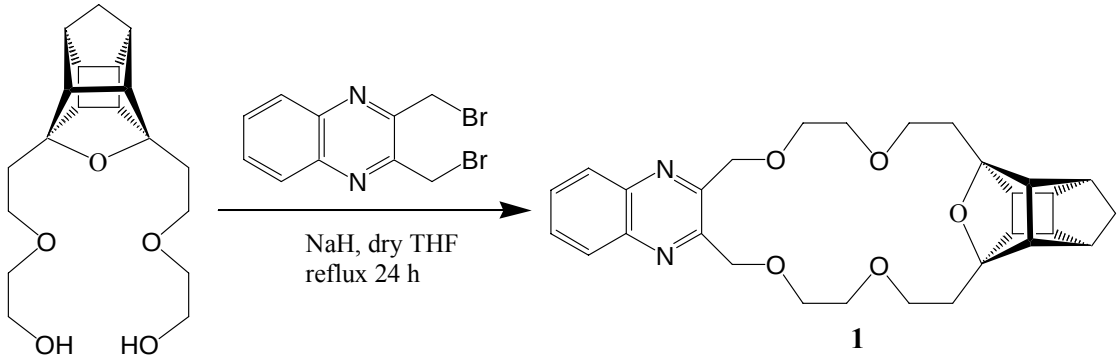

2 **1**

a potential building block for self-assembled structures. The size-selectivity of sandwich formation was evaluated based on comparative studies involving different metal ions, and the impact of the donor-acceptor interactions was investigated by use of a variety of reference macrocycles. Additionally, the impact of various solvent systems on sandwich complex formation was studied.

5.2 Experimental

5.2.1 Instrumentation.

Mass spectra were collected on a LCQ Duo quadrupole ion trap mass spectrometer equipped with an ESI source (ThermoFinnigan, San Jose, CA). Instrumental parameters were optimized for transmission of the 2:1 crown ether:metal complexes, and the heated capillary was kept at 80ºC to minimize in-source fragmentation. The same parameters were used for all solutions to minimize instrumental deviations. Presented spectra are averages of one hundred scans. High-resolution mass spectral data reported herein for compound **1** were obtained by personnel at the Mass Spectrometry Facility at the Department of Chemistry and Biochemistry, University of Texas at Austin by using a ZAB-E double sector high-resolution mass spectrometer (Micromass, Manchester, England) that was operated in the chemical ionization mode. Elemental microanalysis of **1** was performed by personnel at M-H-W Laboratories, Inc., Phoenix, AZ.

5.2.2 Synthesis of 1.

The quinoxaline-containing caged 19-crown-5, **1,** was prepared by the base-promoted reaction of 2,3-bis(bromomethyl)quinoxaline with **2** as shown in Scheme 5-1. A mixture of NaH (obtained as a 60% dispersion in mineral oil, 400 mg, 9.0 mmol) and dry THF (40 mL) was refluxed with stirring under argon. To this refluxing mixture was added dropwise with stirring a solution of **2** (40) (504 mg, 1.5 mmol) and 2,3-bis(bromomethyl)quinoxaline (498 mg, 1.6 mmol) in dry THF (15 mL). After the addition of reagents had been completed, the resulting mixture was refluxed under argon for 24 h. The stirred reaction mixture was allowed to cool gradually to ambient temperature and then was quenched via careful dropwise addition of water (2 mL) until a clear solution resulted. An additional quantity of water (15 mL) was added, and the resulting aqueous solution was extracted with EtOAc (3 × 20 mL). The combined organic layers were washed with brine (20 mL), dried (Na_2SO_4) and filtered, and the filtrate was concentrated *in vacuo*. The residue was purified via column chromatography on silica gel by eluting with 40% EtOAc-hexane. Workup of the chromatography fractions thereby obtained afforded crude **1** (335 mg, 46%); fractional recrystallization of this material from EtOAc afforded pure **1** as a colorless microcrystalline solid: mp 140-141°C; IR (KBr) 2961 (m), 2941 (m), 2894 (m), 2865 (m), 2850 (m), 1295 (m), 1118 (vs), 1102 (vs), 978 (s), 909 (s), 771 cm^{-1} (s); ^1H NMR ($CDCl_3$) δ 1.43 (AB, J_{AB} = 10.3 Hz, 1 H), 1.75 (AB, J_{AB} = 10.3 Hz, 1 H), 1.94-2.01 (m, 4 H), 2.32 (br s, 2 H), 2.51-2.60 (m, 6 H), 3.64-3.82 (m, 12 H) , 4.99 (s, 4 H), 7.68-7.73 (upfield half of a centrosymmetric AA'BB' spin pattern, 2 H), 8.04-8.09 (lowfield half of a centrosymmetric AA'BB' spin pattern, 2

H); ^{13}C NMR ($CDCl_3$) δ 32.2 (t), 41.3 (d), 43.4 (t), 43.8 (d), 48.0 (d), 58.9 (d), 68.0 (t), 70.0 (t), 71.1 (t), 72.5 (t), 94.3 (s), 128.9 (d), 129.7 (d), 141.1 (s), 152.2 (s). Exact Mass (CI HRMS) Calc'd for $C_{29}H_{34}N_2O_5$: $(M_r + H)^+$ m/z 491.2546. Found: $(M_r + H)^+$ m/z 491.2539. Anal. calc'd for $C_{29}H_{34}N_2O_5$: C, 71.00; H, 7.00. Found: C, 71.24; H, 6.80.

5.2.3 Reagents.

18-Crown-6, aza-18-crown-6, benzo-18-crown-6, dibenzo-18-crown-6, and dicyclohexano-18-crown-6 and the RbCl, CsCl, $SrCl_2$, and $BaCl_2$ salts were obtained from the Aldrich Chemical Co. (Milwaukee, WI). NaCl, KCl, and NH_4Cl salts were obtained from EM Science (Gibbstown, NJ). $AgNO_3$ was obtained from Alfa Aesar (Ward Hill, MA). Aside from the aza-18-crown-6 and dicyclohexano-18-crown-6 which had purities of 95% and 90%, respectively, all reagents were of at least 98% purity. All were used without further purification. Analyzed solutions contained **1**, an additional macrocycle, and a salt in a 1:1:1 ratio with concentrations of 5×10^{-5} M using spectroscopic grade OmniSolv methanol (EM Science) as the solvent. Solvent studies were performed using 1:1:1 solutions as described above using as solvents 1:1 water:methanol (water purified in house, OmniSolv methanol), Omnisolv methanol, HPLC grade acetonitrile purchased from Fisher Scientific (Pittsburgh, PA), and Optima grade chloroform, also from Fisher.

5.3 Results and Discussion

To evaluate the importance of π-stacking interactions in the self-assembly process, ESI-MS was used to examine solutions containing an equimolar quantity of **1**, a

second ligand, and a cation. For each solution, the distribution of complexes containing a single macrocycle and cation (i.e. 1:1 complexes), two of the same macrocycles with one cation (i.e. 2:1 complexes or homo-ligand sandwiches), or two different macrocycles with one cation (i.e. mixed-ligand sandwich complexes) was monitored. The distribution of complexes was then correlated with the structures of the macrocycles, the presence of appropriate donor-acceptor interactions, and the type of cation.

As a semi-quantitative means of evaluating the contribution of π-stacking towards any observed enhancement in the amount of the mixed-ligand complex, a hypothetical ligand exchange reaction was considered:

$$A_2M^+ + B_2M^+ \Leftrightarrow 2ABM^+ \qquad (5\text{-}1)$$

where A and B are two different macrocyclic ligands and M is the cation bound between the ligands. Regardless of whether or not the direct ligand exchange reaction is kinetically feasible, if the system is at equilibrium, the concentrations of the complexes must adhere to the thermodynamic equilibrium:

$$K_{EX} = \frac{[ABM^+]^2}{[A_2M^+][B_2M^+]} \qquad (5\text{-}2)$$

where K_{EX} is the equilibrium constant for Reaction 1. ESI mass spectral abundances, A_X, relate to solution concentrations through the use of an ESI efficiency correction, C_X:

$$[X] = C_X A_X \qquad (5\text{-}3)$$

K_{EX} can then be calculated directly from the ESI mass spectral abundances, A_X, of the complex ions:

$$K_{EX} = \left(\frac{C_{ABM^+}{}^2}{C_{A_2M^+} C_{B_2M^+}} \right) \left(\frac{A_{ABM^+}{}^2}{A_{A_2M^+} A_{B_2M^+}} \right) \qquad (5\text{-}4)$$

Previous studies suggest that ESI efficiencies for similar host-guest complexes, including ones involving macrocyles or even large biological molecules, are often close enough to ignore (8, 12, 14-15, 41-46). When considering this ligand exchange reaction, even if the ESI efficiencies of the different sandwich complexes were very different, they would have only minimal influence on the measured K_{EX} values. Since the mixed-ligand sandwich complex contains one ligand from each of the two homo-ligand complexes, its ESI efficiency should be somewhere midway between the efficiencies of the homo-ligand complexes. As a result, the ratio of ESI efficiencies in equation 5-4 is near unity, allowing simplification of equation 5-4 into:

$$K_{EX} = \frac{A_{ABM^+}{}^2}{A_{A_2M^+} A_{B_2M^+}} \qquad (5\text{-}5)$$

From K_{EX}, the Gibb's free energy of the ligand exchange reaction can be calculated from:

$$\Delta G_{EX} = -RT \ln K_{EX} \qquad (5\text{-}6)$$

where R is the ideal gas constant and T is the temperature. For an electrospray experiment, T is simply the room temperature. This change in free energy represents the extent to which a mixed-ligand complex is energetically favored relative to the two homo-ligand complexes. The ΔG_{EX} values in this study were calculated from ESI mass spectra obtained for solutions containing two different macrocycles, thus allowing direct comparison of the abundances of each homo-ligand sandwich complex to the single

mixed-ligand sandwich complex and providing a self-consistent standardization of the spectra. Large positive ΔG_{EX} values signify that the homo-ligand complexes are favored, near-zero values mean that the homo-ligand and mixed-ligand complexes are equally

Chart 5-1.

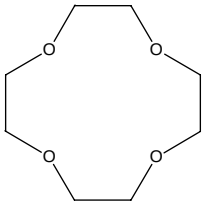

12-crown-4
(176 Da)

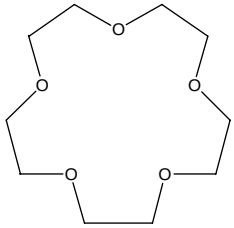

15-crown-5
(220 Da)

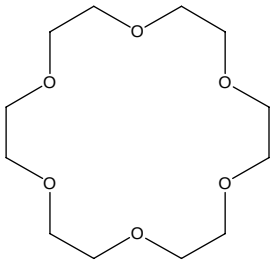

18-crown-6
(264 Da)

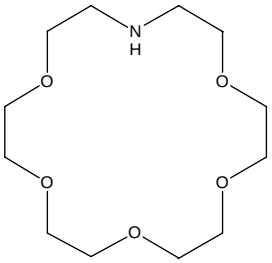

aza-18-crown-6
(263 Da)

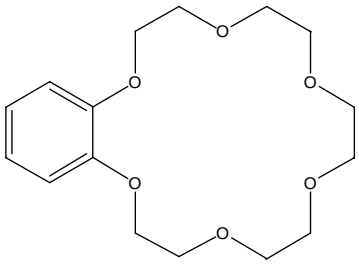

benzo-18-crown-6
(312 Da)

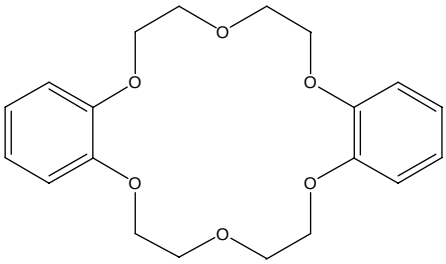

dibenzo-18-crown-6
(360 Da)

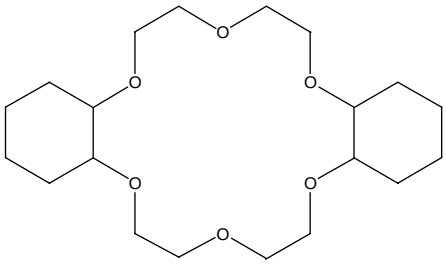

dicyclohexano-18-crown-6
(372 Da)

favored, and large negative values reflect a strong preference for formation of mixed-ligand sandwich complexes.

To differentiate the importance of π-stacking interactions from other types of electrostatic interactions, several reference macrocycles were chosen for comparison of their interactions with **1** (see Chart 5-1). 18-Crown-6 and aza-18-crown-6 were selected because these ligands have no functional groups capable of interacting with the quinoxaline moiety of **1**. Benzo-18-crown-6 and dibenzo-18-crown-6 were selected as reference ligands because they have similar metal binding properties, but their aromatic substituents could promote π-stacking interactions with **1**. Dicyclohexano-18-crown-6 has a similar size and shape to that of dibenzo-18-crown-6 but its substituents are not aromatic, thus allowing a way to evaluate the possibility that favorable steric interactions enhance sandwich formation rather than interactions between the aromatic groups. Admittedly, the three-dimensional structure of cyclohexane bears little resemblance to benzene, but as substituents on 18-crown-6 both would add a similar degree of structural rigidity and have approximately the same degree of "bulk" extending from the crown ether.

As nearly ideal singly-charged spheres, the alkali metals Li^+, Na^+, K^+, Rb^+, and Cs^+ were analyzed with all combinations of macrocycles in solution to evaluate the periodic trends in the size-selectivity of sandwich formation. Other metals studied included the alkaline earths Sr^{2+} and Ba^{2+}, chosen because their ionic radii are similar to Na^+ and K^+ yet with much greater charge densities, as well as Ag^+ which is known to have particular affinity for nitrogen-containing compounds (47-48) and has a size

Figure 5-1. ESI-mass spectrum of (a) **1** in methanol, and (b) **1** with equimolar LiCl, NaCl, KCl, RbCl, and CsCl in methanol.

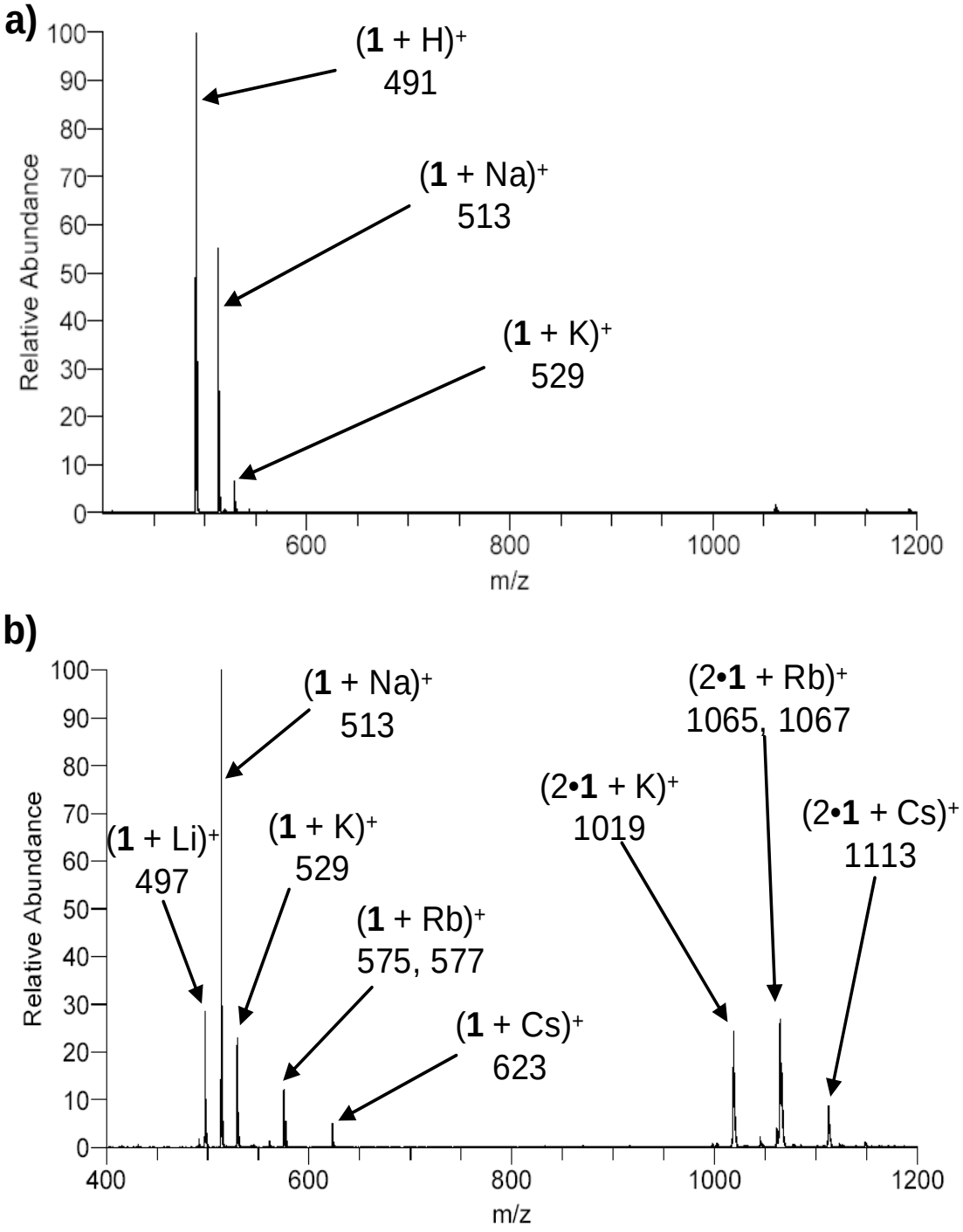

between that of Na^+ and K^+. Finally, formation of sandwich complexes with NH_4^+, a non-metallic ion with a size similar to that of Rb^+, were examined in order to evaluate the activity of the self-assembly process over a wider range of cations.

As an initial control experiment, **1** was analyzed alone in methanol as shown in Figure 5-1a. In this spectrum, protonated **1** was the dominant ion, and lesser amounts of (**1** + Na^+) and (**1** + K^+) complexes were also observed, presumably due to the presence of background solvent contaminants or ionic contaminants leached from the glassware used (Figure 5-1a). The complete absence of sandwich complexes demonstrated that the levels of ionic contaminants in the solvents used are not sufficient to promote sandwich complex formation, eliminating the possibly of contaminant-related errors.

ESI-MS analysis of **1** alone in solution with alkali metal ions added at equimolar concentrations indicates that in the formation of 1:1 macrocycle:metal complexes, **1** has a greater affinity for Na^+ over that of Li^+, K^+, Rb^+, or Cs^+ assuming similar electrospray efficiencies (Figure 5-1b). (2•**1** + K)$^+$, (2•**1** + Rb)$^+$, and (2•**1** + Cs)$^+$ sandwich complexes are also formed, but sandwiches incorporating Li^+ or Na^+ are not observed because the smaller sizes of Li^+ and Na^+ allow them to be encapsulated within the cavity of **1**, thus preventing the favorable coordination of a second ligand. The larger sizes of K^+, Rb^+, and Cs^+ make them perch partially out of the cavity of **1** and permit the complexation of a second ligand.

5.3.1 Analysis of Model Sandwich Complexes.

To confirm the validity of the approach outlined above for evaluating the formation of mixed-ligand sandwich complexes, two model systems were evaluated:

Table 5-1. Reported binding constants in methanol for the first and second attachment of either 12-crown-4 (A) or 15-crown-5 (B) to Na^+ or K^+ and free energy change for the ligand exchange reaction for solutions containing both ligands with one of the cations calculated from the ESI-MS measurements. Errors reflect statistical deviation over three replicate measurements.

Cation	log K[a]				ΔG_{EX} (kJ/mol)
	MA	MA_2	MB	MB_2	
Na^+	1.5	2.2	3.32	2.5	-0.5 ± 0.2
K^+	1.60	1.45[b]	3.5	2.5	-1.5 ± 0.1

[a] From reference 27 except where noted.
[b] From reference 49.

sandwich complexes of 12-crown-4, 15-crown-5, and either Na^+ or K^+. Both ligands are known to form homo-ligand sandwich complexes readily (27). Furthermore, these two ligands are both small and likely have little interaction with the adjacent ligand in a sandwich complex. In an ideal case, if the binding of ligands to a metal were completely independent, the first and second binding constants, K_1 and K_2, would be equal. As seen in Table 5-1, for each of these ligands with either Na^+ or K^+, K_1 and K_2 values are close to each other. Absent any specific interactions between the ligands, the binding in the analogous mixed-ligand sandwich complexes should be nearly independent as well. As a consequence, there should be no significant difference energetically between the homo- and mixed-ligand complexes in a ligand exchange reaction like in equation 5-1. In other words, with 12-crown-4, 15-crown-5, and either Na^+ or K^+, the value of ΔG_{EX} measured from the ESI mass spectra and calculated with equation 5-6 should be near zero. As summarized in Table 5-1, with Na^+, a ΔG_{EX} of -0.5 kJ/mol was measured, and for K^+, ΔG_{EX} was -1.5 kJ/mol, with both values validating this approach.

5.3.2 Sandwich Complexes of Dibenzo-18-crown-6 with Different Macrocycles.

As a first step towards evaluating the propensity of the various crown ethers to form mixed-ligand sandwich complexes, ESI mass spectra were collected for mixtures of dibenzo-18-crown-6, KCl, and various other reference macrocycles, all crown ethers. In these, and all spectra used for quantitative measurements of the sandwich complexes, the mass ranges were restricted to the region containing the sandwich to avoid space-charge effects in the ion trap from the often abundant 1:1 complexes. From these spectra, the free energy of each ligand exchange reactions between the mixed- and homo-ligand complexes was calculated using equation 5-6 and listed in Table 5-2. Of the five other crown ether ligands evaluated, four yielded ΔG_{EX} values near zero, indicating nearly equal preference for formation of both the homo- and mixed-ligand complexes and suggesting the lack of any special ligand interactions that specifically favor formation of mixed-ligand complexes. The smaller size of 15-crown-5 prevents it from fully encapsulating K^+, thus allowing the formation of both mixed-ligand and homo-ligand

Table 5-2. Free energy change for the ligand exchange reaction for solutions of either **1** or dibenzo-18-crown-6, K^+ and a second macrocycle. Errors reflect statistical deviation over three replicate measurements.

	ΔG_{EX} (kJ/mol)	
Second Macrocycle	**1**	**dibenzo-18-crown-6**
15-crown-5	8.6 ± 0.8	0.0 ± 0.7
18-crown-6	7.2 ± 0.8	11 ± 1
aza-18-crown-6	7.6 ± 0.2	0.0 ± 0.5
dicyclohexano-18-crown-6	3.74 ± 0.08	1.3 ± 1.3
benzo-18-crown-6	-8.57 ± 0.03	-0.7 ± 0.3
dibenzo-18-crown-6	-7.8 ± 0.1	– –

complexes in the presence of dibenzo-18-crown-6 For experiments involving aza-18-crown-6 and dibenzo-18-crown-6, the amino proton on aza-18-crown-6 introduces a degree of electrostatic repulsion between the crown and the metal, thus preventing complete encapsulation of K^+ and allowing formation of stable mixed-ligand complexes. With either dicyclohexano-18-crown-6 or benzo-18-crown-6, the substituents make both ligands more rigid, resulting in no significant difference in stability of the homo-ligand complexes relative to the mixed-ligand complexes as evidenced by the ΔG_{EX} values near zero (Table 5-2). None of these four ligands displayed any special enhancement in the formation of mixed-ligand complexes with K^+ and dibenzo-18-crown-6, in striking contrast to the results described below (and also summarized in Table 5-2) for sandwich formation involving ligand **1**.

The one notable exception in the propensity for formation of mixed-ligand sandwich complexes was for the experiments involving dibenzo-18-crown-6 and 18-crown-6 with K^+ in which the spectra exhibited a marked preference against formation of the mixed-ligand complexes (i.e. (dibenzo-18-crown-6 + 18-crown-6 + K^+)), with a ΔG_{EX} value of 11 kJ/mol calculated from the mass spectrum. 18-Crown-6 is both large enough and flexible enough to encapsulate the potassium cation, thus prohibiting the coordination of a second ligand and quenching the formation of sandwich complexes

5.3.3 Sandwich Complexes Involving 1 with Different Macrocycles.

To determine the degree of enhancement in the formation of mixed-ligand sandwich complexes due to π-stacking interactions, solutions containing KCl, **1** and various other reference macrocycles were analyzed. The ESI mass spectra shown in

Figure 5-2. ESI-mass spectra of **1**, a second macrocycle, and a metal ion in methanol. (a) **1**, 18-crown-6 (18c6) and K^+, (b) **1**, dibenzo-18-crown-6 (db18c6) and K^+, and (c) **1**, dibenzo-18-crown-6 and Rb^+. No data was collected below 700 Th in (c) to allow the complexes to be analyzed without peak broadening due to space-charge effects.

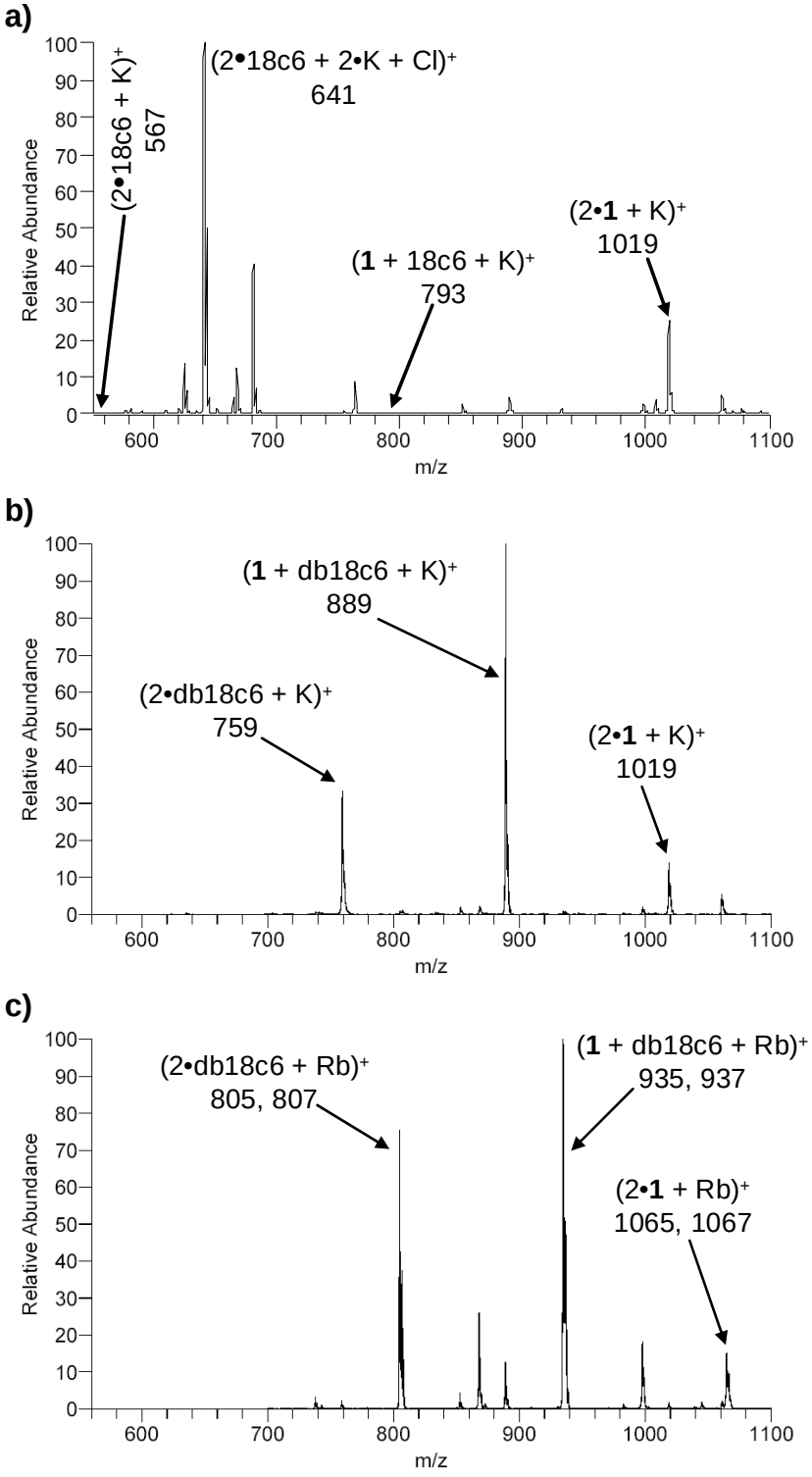

Figure 5-2 display the types of product ion distributions observed upon analysis of solutions containing **1**, a second macrocycle, and an alkali metal salt, all at equimolar concentrations. For example, in the spectrum shown in Figure 5-2a for **1**, 18-crown-6, and KCl, the homo-ligand $(2\bullet\mathbf{1} + K)^+$ complex is abundant, but the abundances of the sandwich complexes containing 18-crown-6, i.e. $(2\bullet\text{18-crown-6} + K)^+$ and $(\mathbf{1} + \text{18-crown-6} + K)^+$, are very low. The ΔG_{EX} value calculated from this mass spectrum is 7.2 kJ/mole (Table 2), and the large positive value conveys the preference for formation of the homo-ligand $(2 \bullet \mathbf{1} + K)^+$ complexes over the mixed-ligand $(\mathbf{1} + \text{18-crown-6} + K)^+$ complexes. When the solution containing **1**, dibenzo-18-crown-6 and K^+ was analyzed (Figure 2b), the mixed ligand complex, $(\mathbf{1} + \text{dibenzo-18-crown-6} + K)^+$, dominated the spectrum. Its greater abundance relative to the homo-ligand complexes, $(2 \bullet \text{dibenzo-18-crown-6} + K)^+$ and $(2 \bullet 1 + K)^+$, results in a ΔG_{EX} of –7.8 kJ/mole that reflects the marked enhancement of the mixed-ligand sandwich complexes due to cooperative interactions between the quinoxaline group on **1** and one of the benzene groups on dibenzo-18-crown-6. For the solution containing **1** and dibenzo-18-crown-6 with RbCl instead of KCl (Figure 5-2c), the mixed-ligand sandwich complex, i.e. $(\mathbf{1} + \text{dibenzo-18-crown-6} + Rb)^+$, again dominated the spectrum, but the preference for formation of the mixed-ligand sandwiches was not as great as observed in Figure 5-2b, and the calculated ΔG_{EX} value was lower (-4.9 kcal/mole in Table 5-3). The ΔG_{EX} value diminishes on going from K^+ to Rb^+, possibly because the greater size of Rb^+ reduces the overlap of the pi-orbitals between **1** and dibenzo-18-crown-6.

The ΔG_{EX} values obtained from this series of ESI-MS experiments are summarized in Table 5-2. For 15-crown-5, 18-crown-6, and aza-18-crown-6, the ΔG_{EX} values are positive, indicating that the formation of mixed-ligand sandwiches is disfavored relative to the formation of the homo-ligand complexes. With no additional functional groups on these three macrocycles, these were not expected to engage in any special interactions with **1**, other than the typical electrostatic interactions between the positive metal ion and the heteroatom donor groups, that would specifically strengthen the mixed-ligand sandwich complexes. Dicyclohexano-18-crown-6, of similar size as dibenzo-18-crown-6, was evaluated to ensure that a particularly favorable steric situation was not responsible for any observed enhancement. The ΔG_{EX} with dicyclohexano-18-crown-6 was +3.74 kJ/mole, again indicating that the formation of the mixed-ligand sandwich complex is disfavored.

Table 5-3. Effect on ΔG_{EX} values for mixed-ligand sandwich complexes of **1** and either dibenzo-18-crown-6 or 18-crown-6 with various cations in methanol. Concentrations were 50 μM in all cases. Errors reflect statistical deviation over three replicate measurements.

Cation	**Ionic Radii[a] (pm)**	**ΔG_{EX} (kJ/mol)**	
		dibenzo-18-crown-6	**18-crown-6**
Na^+	116	-2.6 ± 0.5	7.9 ± 0.8
K^+	152	-7.8 ± 0.1	7.2 ± 0.8
Rb^+	166	-4.9 ± 0.3	3.6 ± 0.4
Cs^+	181	-0.6 ± 0.8	5.7 ± 0.3
Sr^{2+}	127	0.5 ± 0.7	-10.9 ± 0.7
Ba^{2+}	143	-3.0 ± 0.3	-5.2 ± 0.9
Ag^+	129	2.4 ± 0.5	4 ± 2
NH_4^+	161	-5.4 ± 0.5	3.6 ± 0.9

[a] From reference 50.

The complexation of **1** and K^+ with two macrocycles possessing aromatic functional groups was also examined: benzo-18-crown-6 and dibenzo-18-crown-6. These two macrocycles have benzene groups capable of donating electron density to the quinoxaline moiety on **1**. With benzo-18-crown-6, a ΔG_{EX} of -8.57 kJ/mol was found (Table 5-2), indicating a significant enhancement in the formation of mixed-ligand sandwiches over that observed for the previous macrocycles. For dibenzo-18-crown-6 with **1** and K^+, a ΔG_{EX} of -7.8 kJ/mol was measured. These values indicate that with either benzo-18-crown-6 or dibenzo-18-crown-6 the mixed-ligand sandwich complexes with **1** are very strongly favored. We speculate that the small increase in ΔG_{EX} for the sandwich formation involving **1** and benzo-18-crown-6 versus **1** and dibenzo-18-crown-6 is due to steric hindrance between the bulky cage group on **1** and the second benzo-group on dibenzo-18-crown-6 – a hindrance not present with benzo-18-crown-6. The reactions of **1** with benzo-18-crown-6 and dibenzo-18-crown-6 also suggest that the cage group on **1**, included as an anchor point to allow attachment of the macrocycle to a polymer or surface, does not interfere with the π-stacking interactions.

In addition to the positive ΔG_{EX} values obtained upon reaction of **1** and K^+ with the three reference macrocycles that did not possess aromatic groups, all of the observed sandwich complexes with the reference macrocycles had very low abundances in the mass spectra. These abundances were typically one to two orders of magnitude less than that of sandwich complexes formed with macrocycles containing aromatic functional groups, leading to the conclusion that even without any enhancement due to donor-

Figure 5-3. ΔG_{EX} for mixed-ligand sandwich complexes of **1** and either dibenzo-18-crown-6 (solid line) or 18-crown-6 (dotted line) with different alkali metal cations in methanol.

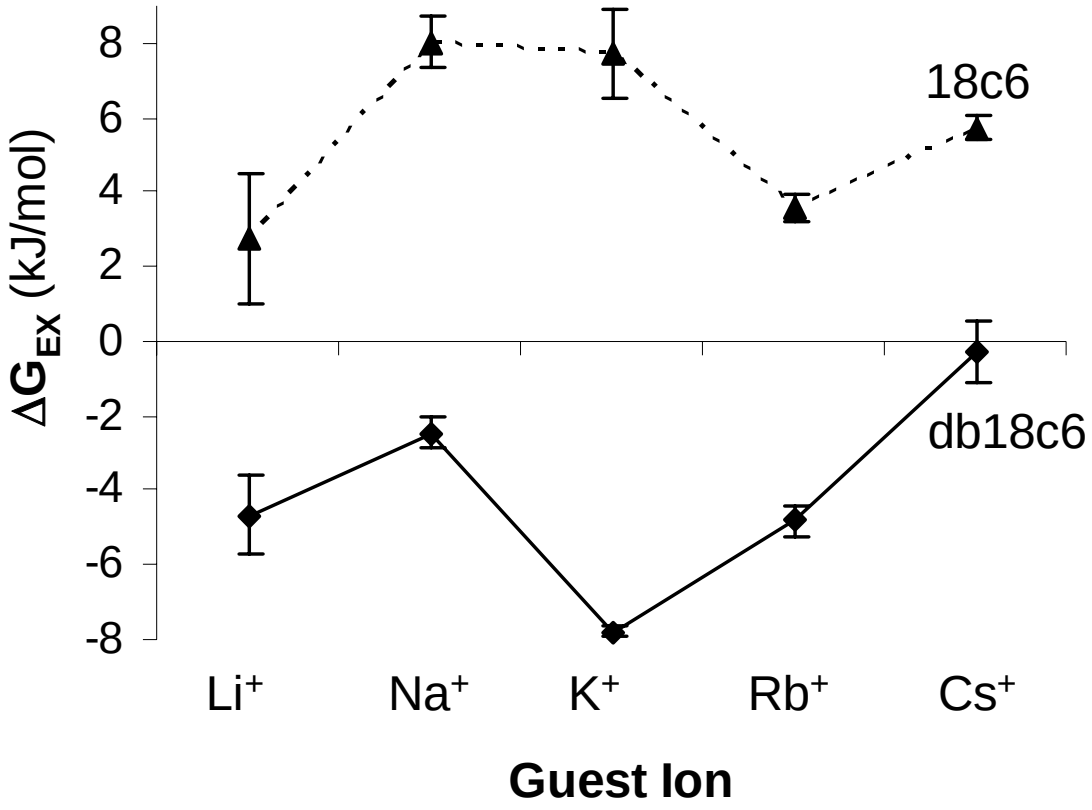

acceptor interactions, π-stacking interactions significantly stabilize the formation of crown ether-metal sandwich complexes.

5.3.4 Sandwich Complexes Involving 1 with Different Cations.

The formation of sandwich complexes containing different cations was examined in order to investigate the influence of the size and charge density of the cation on the self-assembly process. The Pauling ionic radii of the cations are listed in Table 5-3. When solutions containing **1**, dibenzo-18-crown-6, and each of the alkali metal chlorides

were analyzed, a clear periodic trend emerged in the distribution of mixed-ligand sandwiches relative to the homo-ligand complexes as shown by the data in Figure 5-3 and Table 5-3. For the largest ion, Cs^+, the ΔG_{EX} value was near zero, indicating that there was no significant preference for the formation of mixed-ligand sandwiches. The smallest ion, Li^+, resulted in complexes that had very low abundances in the mass spectra, likely due to the poor ability of large crown ethers to form sandwich complexes with Li^+ (27), presumably due to a mismatch between the ion and cavity sizes. Due to the low abundances of complexes, ΔG_{EX} values could not be calculated in most cases and were therefore omitted from Table 5-3. The largest enhancement was seen with K^+, reaching a ΔG_{EX} value of -7.8 kJ/mol, while Na^+ and Rb^+ showed more modest enhancements in the formation of the mixed-ligand sandwich complexes. These results contrast starkly with solutions containing **1** and 18-crown-6 (Table 5-3, last column). The ΔG_{EX} values obtained upon analysis of solutions containing **1**, 18-crown-6 and an alkali metal ion, summarized graphically in Figure 5-3, were significantly positive with all the alkali metals, indicating a consistent preference against formation of the mixed-ligand complexes regardless of the size of the metal ion. The large enhancement of mixed-ligand sandwich complexes between **1** and dibenzo-18-crown-6 when K^+ is the cation is likely the result of several size-related effects. Periodic trends are well known for 1:1 crown ether:metal complexes (7, 11, 24, 26-28), with binding affinities in solution typically increasing as ions become large enough to interact optimally with more of the potential coordinating sites (oxygen heteroatoms). This size-selective effect is even more pronounced for sandwich complexes because larger ions are not encapsulated by a single

macrocycle, thus facilitating coordination by two ligands. As a countering effect seen in the present work, with very large ions, such as Cs^+, the spacing between the macrocyclic rings increases, reducing the overlap between the π-orbitals on the aromatic substituents of the benzo-crown ethers and **1** and decreasing the strength of their interactions.

In addition to the alkali metals, sandwich formation involving several other cations was evaluated as well. The alkaline earth cation Sr^{2+}, with an ionic radius comparable to Na^+, demonstrated no significant preference for the formation of mixed-ligand sandwiches involving **1** and dibenzo-18-crown-6, while with Ba^{2+}, similar in size to K^+, only a modestly negative ΔG_{EX} was observed. Both metals, however, resulted in lower ΔG_{EX} values for sandwich complexes incorporating **1** and 18-crown-6 (Table 5-3). The greater charge of these cations likely results in a shift in the relative contributions of the binding modes. Due to stronger electrostatic attractions between the doubly charged metal ions and the coordinating oxygen atoms, each macrocycle in a sandwich complex would be drawn closer to the metal ion and closer to the second coordinating ligand. The expected steric hindrance between the quinoxaline and cage groups on **1** and the benzene groups of dibenzo-18-crown-6 likely becomes a punitive factor, causing a decrease in the formation of mixed-ligand sandwiches. 18-Crown-6 lacks any bulky substituents, and thus the enhancement in sandwich formation due to the higher charge density of the alkaline earth metal ion is not mitigated by counterproductive steric effects.

To evaluate whether the complexation of **1** was influenced directly by the quinoxaline moiety on **1**, sandwich complex formation with Ag^+ was examined (Table 5-3). With silver's known affinity for nitrogen heteroatoms (47-48), an enhancement of

sandwich formation might be expected relative to that observed for complexation of K^+, which has a similar ionic radius and no special affinity for nitrogen. No such enhancement is observed, however, and the positive ΔG_{EX} values observed for Ag^+ with **1** and either dibenzo-18-crown-6 (2.4 kJ/mol) or 18-crown-6 (4 kJ/mol) indicate that silver is a poor choice overall for mixed-ligand sandwich complex formation. This result may be related to the general preference of Ag^+ to adopt a linear coordination geometry which creates an orbital alignment problem when forming sandwich complexes (50).

Finally, to determine whether cations other than metals could result in enhancement in mixed-ligand sandwich formation, solutions containing **1**, a second macrocycle, and the ammonium ion were analyzed. With an ionic radius similar to Rb^+, a roughly spherical shape, and a closed valence, NH_4^+ led to a significantly negative ΔG_{EX} value (-5.4 kJ/mol) for the mixed-ligand sandwich complexes containing **1** and dibenzo-18-crown-6, its enhancement second only to K^+ in this study (Table 5-3). Since NH_4^+ binds to crown ethers though hydrogen bonding interactions rather than metal-ligand coordination, this result suggests that the use of donor-acceptor π-stacking to direct self-assembly of sandwich complexes might be possible with a wide range of cations.

5.3.5 Concentration Dependence of ΔG_{EX} Measurements.

A common endeavor when evaluating the binding of novel ligands is to examine how the binding behavior changes with different relative concentrations of the individual species (7-8, 10, 14, 16-17). One of the advantages of evaluating the binding information thermochemically, however, is that the results should display no dependence on solution

Figure 4. Result of measuring ΔG_{EX} at different relative concentrations of the ligands (dibenzo-18-crown-6 and **1**) and alkali metal cations. Errors reflect statistical deviation over three replicate measurements.

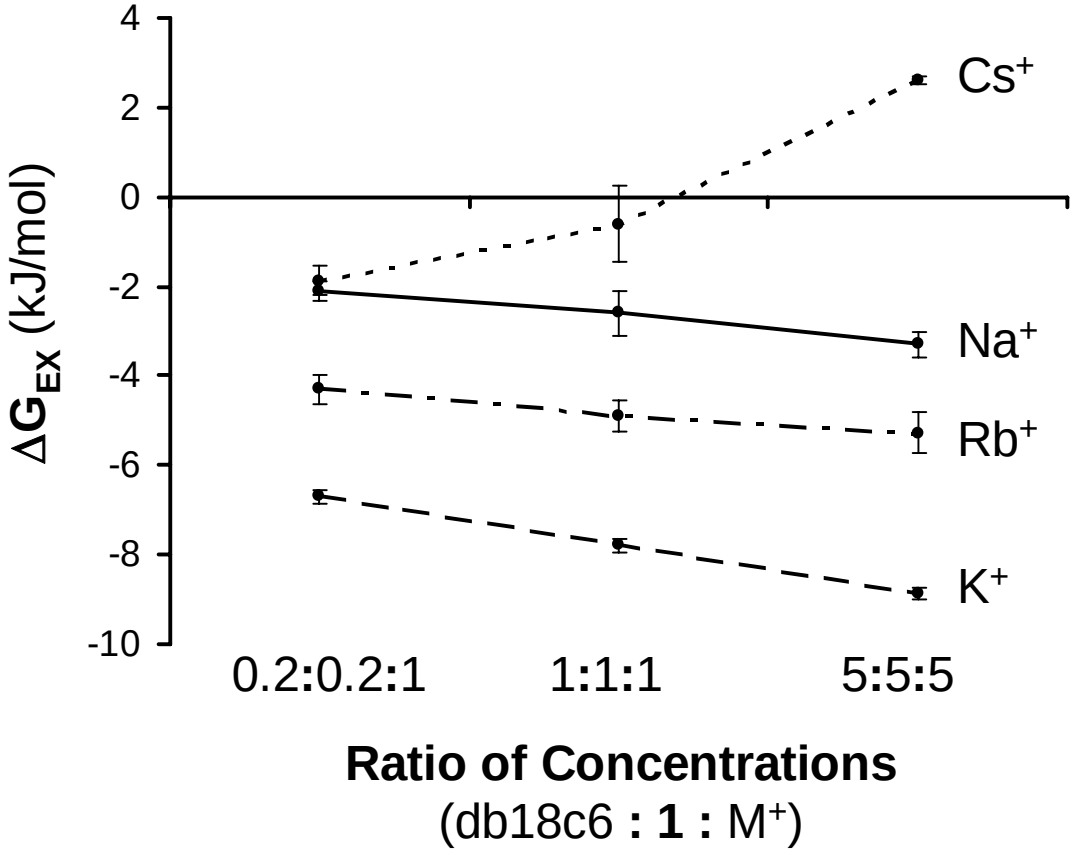

concentrations. Accordingly, as a final test of the experimental method, **1** and dibenzo-18-crown-6 were again analyzed with the alkali metals as described above. This time, however, while the metal concentrations remained unchanged, solutions were analyzed in which the ligand concentrations were both increased and decreased five-fold. With Na^+, K^+, and Cs^+ the three metal cations that most readily formed mixed-ligand complexes, increasing ligand concentrations caused very small decreases in the calculated ΔG_{EX} values that were barely significant with respect to variations among the replicate measurements (Figure 4). With Cs^+, however, an increase in ΔG_{EX} was observed with

increasing ligand concentrations, possibly the result of in-source fragmentation of the fairly weak Cs^+ sandwich complexes. Changing the relative concentration had virtually no effect on the measured values of ΔG_{EX} in most cases, illustrating the validity of these thermochemical measurements, particularly for the mixed-ligand complexes displaying the greatest enhancement in stability.

5.4 Conclusions

Through ESI-MS experiments, the novel crown ether **1** containing an electron-poor quinoxaline moiety was demonstrated to form 2:1 macrocycle:cation sandwich complexes preferentially with secondary macrocycles containing electron-rich benzene substituents through donor-acceptor π-stacking interactions between the aromatic side groups. The magnitude of the enhancement of these mixed-ligand sandwich complexes was found to be highly dependent on the size of the encapsulated cation, with a preference for cations that maximize the effective interactions of each macrocycle with the cation yet minimize steric effects between the macrocycles. Similar experiments with dibenzo-18-crown-6 and K^+ yielded no additional stabilization of the mixed ligand complexes with any of the other crown ethers examined. That such donor-acceptor π-stacking interactions so readily enhance the formation of crown ether sandwich complexes confirms their utility as building blocks in self-assembled molecular structures.

5.5 References

(1) Ho, P. K.-H.; Filas, R. W.; Abusch-Magder, D.; Bao, Z. *Langmuir* **2002**, *18*, 9625-9628.

(2) Ahrens, M. J.; Sinks, L. E.; Rybtchinski, B.; Liu, W.; Jones, B. A.; Giaimo, J. M.; Gusev, A. V.; Goshe, A. J.; Tiede, D. M.; Wasielewski, M. R. *J. Am. Chem. Soc.* **2004**, *126*, 8284-8294.

(3) Zhang, S. *Biotech. Adv.* **2002**, *20*, 321-339.

(4) Schalley, C. A. *Int. J. Mass Spectrom*. **2000**, *194*, 11-39.

(5) Dearden, D.V.; Liang, Y.; Nicoll, J. B.; Kellersberger, K. A. *J. Mass Spectrom*. **2001**, *36*, 989-997.

(6) Przybylski, M.; Glocker, M. O. *Angew. Chem. Int. Ed. Engl*. **1996**, *35*, 807-826.

(7) Williams, S.; Blair, S. M.; Brodbelt, J. S.; Huang, X.; Bartsch, R. A. *Int. J. Mass Spectrom.* **2001**, *212*, 389-401.

(8) Blair, S. M.; Brodbelt, J. S.; Marchand, A. P.; Kumar, K. A.; Chong, H. S. *Anal. Chem.* **2000**, *72*, 2433-2445.

(9) Kempen, E. C.; Brodbelt, J. S. *Anal. Chem.* **2000**, *72*, 5411-5416.

(10) Williams, S. M.; Brodbelt, J. S.; Marchand, A. P.; Cal, D.; Mlinaric-Majerski, K. *Anal. Chem.* **2002**, *74*, 4423-4433.

(11) Sherman, C. L.; Brodbelt, J. S. *Anal. Chem.* **2003**, *75*, 1828-1836.

(12) Kempen, E. C.; Brodbelt, J. S.; Bartsch, R. A.; Jang, Y.; Kim, J. S. *Anal. Chem.* **1999**, *71*, 5493-5500.

(13) Blair, S. M.; Brodbelt, J. S.; Reddy, G. M.; Marchand, A. P. *J. Mass Spectrom.* **1998**, *33*, 721-728.

(14) Blair, S. M.; Kempen, E. C.; Brodbelt, J. S. *J. Am. Soc. Mass Spectrom.* **1998**, *9*, 1049-1059.

(15) Jorgensen, T. J. D.; Roepstorff, P.; Heck, A. J. R. *Anal. Chem.* **1998**, *70*, 4427-4432.

(16) Young, D.-S.; Hung, H.-Y.; Liu, L. K. *Rapid Commun. Mass Spectrom.* **1997**, *11*, 769-773.

(17) Young, D.-S.; Hung, H.-Y.; Liu, L. K. *J. Mass Spectrom.* **1997**, *32*, 432-437.

(18) Schalley, C.A.; Catellano, R.K.; Brody, M.S.; Rudkevich, D. M.; Siuzdak, G.; Rebek, J. Jr. *J. Am. Chem. Soc*. **1999**, *121*, 4568-4579.

(19) Mansikkamaki, H.; Nissinen, M.; Schalley, C. A.; Rissanen, K. *New J. Chem*. **2003**, *27*, 88-97.

(20) Nuutinen, J. M. J.; Irico, A.; Vincenti, M.; Dalcanale, E.; Pakarinen, J. M. H.; Vainiotalo, P. *J. Am. Chem. Soc*. **2000**, *122*, 10090-10100.

(21) Zhang, H.; Paulsen, E.; Walker, K. A.; Krzysztof, E.; Dearden, D. V. *J. Am. Chem. Soc*. **2003**, *125*, 9284-9285.

(22) Nicoll, J. B.; Dearden, D.V. *Int. J. Mass Spectrom*. **2001**, *204*, 171-183.

(23) Wu, H.-F.; Huan, S.-M.; Wu, C.-F. *Eur. J. Mass Spectrom*. **2002**, *8*, 375-380.

(24) Shen, N.; Pope, R. M.; Dearden, D. V. *Int. J. Mass Spectrom*. **2000**, *195/196*, 639-652.

(25) Oshima, T.; Matsuda, F.; Fukushima, K.; Tamura, H.; Matsubayashi, G.; Arakawa, R. *J. Chem. Soc., Perkin Trans. 2* **1998**, 145-148.

(26) Marchand, A. P.; Kumar, K. A.; McKim, A. S.; Alihodzic, S.; Chong, H.-S.; Krishnudu, K.; Takhi, M.; Mlinaric-Majerski, K.; Kragol, G.; Sumanovac, T. *Kem. Ind.* **2001**, *50*, 129-138.

(27) Arnaud-Neu, F.; Delgadoand, R.; Chaves, S. *Pure Appl. Chem*. **2003**, *75*, 71-102.

(28) Seyedi, S. M.; Gouran, A.; Malekshah, T. *Heterocycles* **2003**, *60*, 113-119.

(29) Izatt, R. M.; Bradshaw, J. S.; Nielsen, S. A.; Lamb, J. D.; Christensen, J. J.; Sen, D. *Chem. Rev*. **1985**, *85*, 271-339.

(30) Marchand, A. P.; Reddy, G. M.; Zaragoza, F.; Bartsch, R. A.; Eley, M. D. *Tetrahedron Lett.* **1993**, *34*, 5377-5380.

(31) Bartsch, R. A.; Eley, M.; Marchand, A. P.; Shukla, R.; Kumar, K. A. *Tetrahedron* **1996**, *52*, 8979-8988.

(32) Hunter, C. A.; Lawson, K. R.; Perkins, J.; Urch, C. J. *J. Chem. Soc., Perkin Trans. 2* **2001**, *5*, 651-669.

(33) Kamieth, M.; Burkert, U.; Corbin, P. S.; Dell, S. J.; Zimmerman, S. C.; Klärner, F.-G. *Eur. J. Org. Chem.* **1999**, *11*, 2741-2749.

(34) Cloninger, M. J.; Whitlock, H. W. *J. Org. Chem.* **1998**, *63*, 6153-6159.

(35) Reek, J. N. H.; Priem, A. H.; Engelkamp, H.; Rowan, A. E.; Elemans, J. A. A. W.; Nolte, R. J. M. *J. Am. Chem. Soc.* **1997**, *119*, 9956-9964.

(36) Gokel, G. W., De Wall, S. L., Meadows, E. S. *Eur. J. Org. Chem.* **2000**, 2967-2978.

(37) Zacharias, N.; Dougherty, D. A. *Trends Pharmacol. Sci.* **2002**, *23*, 281-287.

(38) Meyer, E. A.; Castellano, R. K.; Diederich, F. *Angew. Chem. Int. Ed.* **2003**, *42*, 1210-1250.

(39) Ferguson, S. B.; Sanford, E. M.; Seward, E. M.; Diederich, F. *J. Am. Chem. Soc.* **1991**, *113*, 5410-5419.

(40) Marchand, A. P.; Chong, H.-S.; Alihodzic, S.; Watson, W. H.; Bodige, S. G. *Tetrahedron* **1999**, *55*, 9687-9696.

(41) Wang, W.; Kitova, E. N.; Klassen, J. S. *Anal. Chem.* **2003**, *75*, 4945-4955.

(42) Zampronio, C. G.; Giannakaopulous, A. E.; Zeller, M.; Bitziou, E.; Macpherson, J. V.; Derrick, P. J. *Anal. Chem*. **2004**, *76*, 5172-5179.

(43) Sannes-Lowery, K. A.; Griffey, R. H.; Hofstadler, S. A. *Anal. Biochem*. **2000**, *280*, 264-271.

(44) Greig, M. J.; Gaus, H.; Cummins, L. L.; Sasmor, H.; Griffey, R. H. *J. Am. Chem. Soc.* **1995**, *117*, 10765-10766.

(45) Loo, J. A.; Hu, P.; McConnell, P.; Mueller, W. T.; Sawyer, T. K.; Thanabal., V. *J.Am. Soc. Mass Spectrom.* **1997**, *8*, 234-243.

(46) Lim, H. K.; Hsieh, F. Y. L.; Ganem, B.; Henion, J. *J. Mass Spectrom*. **1995**, *30*, 708-714.

(47) El Aribi, H.; Rodriquez, C. F.; Shoeib, T.; Ling, Y.; Hopkinson, A. C.; Siu, K. W. M. *J. Phys. Chem. A* **2002**, *106*, 8798-8805.

(48) Ma, N. L. *Chem. Phys. Lett.* **1998**, *297*, 230-238.

(49) Buschmann, H.-J. *J. Sol. Chem.* **1987**, *16*, 181-190.

(50) Cotton, F. A.; Wilkinson, G.; Murillo, C. A.; Bochmann, M. *Advanced Inorganic Chemistry*, 6th ed., John Wiley & Sons, New York, **1999**.

CHAPTER 6

ESI-MS Characterization of a Pyrrole-Inosine Nucleoside That Selectively Targets Quadruplex DNA

6.1 Introduction

In the ongoing search for more effective anti-tumor drugs, researchers have targeted a wide range of biological molecules for drug interaction. Activity of the enzyme telomerase has been implicated as a factor in tumorigenesis (1-6), and as such much work has focused on identifying (2-9) and blocking (2, 4-7, 10-18) its function. One avenue for disrupting telomerase activity is through the attachment of a drug to its primary substrate, telomeric DNA (4-6, 8, 10-21). Having been identified as one of the mechanisms by which tumor cells attain immortality (3-4, 6), the lengthening of telomeres by telomerase represents one of the critical aspects of tumorigenesis. Modifying the telomeric DNA in such a way as to block its recognition by telomerase has the potential to halt tumorigenesis completely (3-6, 10-14). Guanine-rich DNA sequences like those found in the telomere have long been known to associate into quadruplex structures via Hoogsteen-type interactions (22-23) *in vitro* (5, 14, 19, 24-26). More recently, similar types of quadruplex DNA structures have been identified in biological systems (7, 27-29), and it is thought that the first step in the lengthening of telomeres by telomerase involves the unfolding of the telomeric quadruplex (4, 9-10).

Prior to the recent reports that have verified the existence of quadruplex DNA in biological systems (7, 27-29), extensive fundamental knowledge about quadruplex structure and chemical behavior had been obtained through various experiments with short guanine-rich oligonucleotides (4, 10-16, 18-21, 24-25, 30-37). Such studies remain a powerful means of probing the underlying chemistry. For instance, NMR spectroscopic (4, 18, 21, 24, 30, 32, 37-39) and X-ray crystallography studies (24, 26, 33, 38-41) have both served to confirm that quadruplexes are formed from stacked arrays of guanine tetrads (4, 18, 24, 26, 32-33, 37, 40-41). These structures can be formed through simple annealing procedures (11, 13, 15, 17, 19-20) from four parallel oligonucleotides (a G4 quadruplex), from a single oligonucleotide strand folded back on itself four times (a G4' quadruplex), or from two strands where each strand contributes two guanines to each tetrad (a G'2 quadruplex) (1, 4, 24, 34, 42). The resulting model systems have permitted a range of DNA quadruplex properties to be studied, including their ability to chelate metal cations (4, 9, 24, 26, 32, 37-38, 40, 43), to assemble into extended guanine assemblies (24, 30, 35-36), and to interact with various drug candidates (4, 10-16, 20-21, 24-25, 31).

Electrospray ionization mass spectrometry (ESI-MS) is now widely used to evaluate interactions between many different classes of biological species (10-11, 13-15, 19-20, 25, 30, 43-44). Mass spectrometric studies of these interactions have been demonstrated to be effective in characterizing binding selectivity and specificity (11, 13, 15, 19, 44), establishing the mode of binding (10-11, 13, 19, 44), and correlating specific binding patterns with *in vitro* antitumor and antibacterial cytotoxicity (44). Recently,

Chart 6-1. Structures of synthetic nucleosides, **1**-**3**, and the 2',3',5'-tri-O-acetyl nucleosides, **4**-**7**.

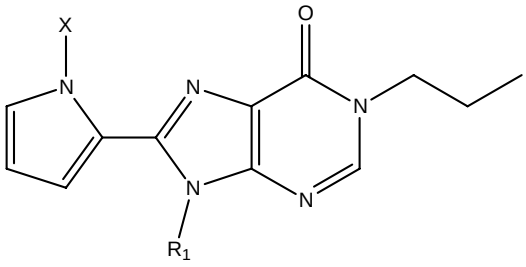

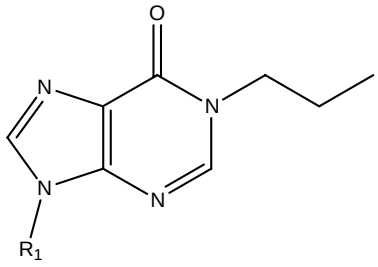

1: X = H
2: X = *tert*-butoxycarbonyl

3

R_1 = 2',3',5',-tri-O-(*tert*-butyldimethylsilyl)-β-D-ribofuranoside

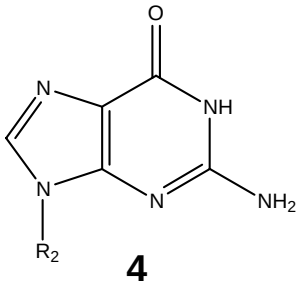

4
guanine

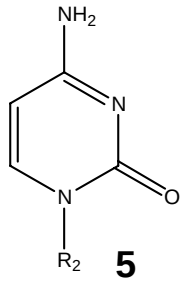

5
cytosine

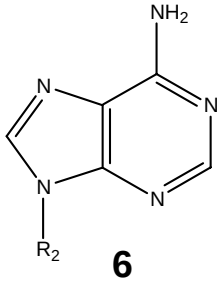

6
adenine

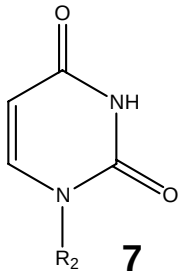

7
uracil

R_2 = 2',3',5',-tri-O-acetyl-β-D-ribofuranoside

work presented by the Brodbelt group (19) and others (10-11, 13-14, 20) has established the utility of using ESI-MS to evaluate the activity of potential quadruplex-interactive ligands. The observation of quadruplex-drug complexes with ESI-MS in particular has been demonstrated to be a rapid and accurate screening tool for novel drug candidates (10-11, 13-15, 19-20) and has been shown to correlate with *in vivo* telomerase inhibition (10-11).

The function of many of the quadruplex-interactive ligands described to date has been attributed to intercalation in or end-stacking on the quadruplex structure (13, 19-20, 24). These ligands, typically large poly-aromatics, stabilize the quadruplex, thus

Scheme 6-1. Hoogsteen binding in guanine tetrads and between **1** and 2',3',5'-tri-O-acetylguanosine, **4**.

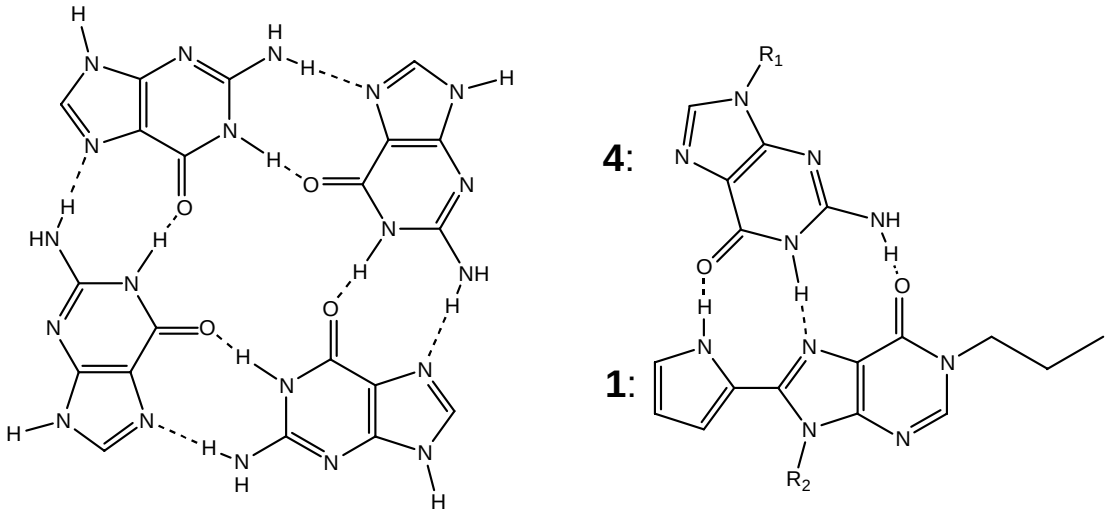

R_1 = 2',3',5',-tri-O-acetyl-β-D-ribofuranoside
R_2 = 2',3',5',-tri-O-(*tert*-butyldimethylsilyl)-β-D-ribofuranoside

preventing the action of telomerase. Herein, we present a ligand with a different functional modality; a pyrrole-inosine based synthetic nucleoside, **1**, that has previously demonstrated the ability to recognize and bind to guanine via an extended Hoogsteen-type interaction (45). In this study, the interactions of **1** with the individual nucleosides were evaluated with ESI-MS to determine the selectivity and specificity of **1** towards each of the natural nucleobases and the guanine tetrads that form the core of quadruplex DNA (Scheme 6-1). Subsequent experiments with two different quadruplex-forming oligonucleotides, dT_2G_5T and $d(TTAGGG)_2$, two repeats of the human telomeric DNA sequence, as well as an assortment of single-stranded and self-complementary oligonucleotide sequences characterized the interactions of **1** with various DNA structures. Furthermore, control experiments were carried out to evaluate the binding of

structures analogous to **1** where the pyrrole NH was either blocked, **2**, or removed, **3**. While neither **2** nor **3** was found to interact with quadruplex DNA, the specific binding observed between **1** and quadruplex structures illustrates the potential usefulness of these compounds.

6.2 Experimental

6.2.1 Reagents.

Preparation of the synthetic nucleosides **1**, **2**, and **3** was described previously.[45] 2',3',5'-Tri-*O*-acetylguanosine, **4**, 2',3',5'-tri-*O*-acetylcytidine, **5**, 2',3',5',-tri-*O*-acetyladenosine, **6**, and 2',3',5',-tri-*O*-acetyluridine, **7**, were purchased from the Sigma Chemical Company (St. Louis, MO) with purities of 95% or greater. Ammonium acetate (97% purity) was acquired from EM Science (Gibbstown, NJ). Oligonucleotides were prepared and purified by reverse-phase HPLC in an ammonium acetate buffer by TriLink BioTechnologies (San Diego, CA). A.C.S. Grade Spectranalyzed methanol and A.C.S. Grade chloroform were both obtained from Fisher Scientific (Fair Lawn, NJ). All purchased chemicals were used without further purification. Water was purified in house with an EASYpure UV deionizer (Barnstead International, Dubuque, IA).

6.2.2 Preparation of Samples for Analysis.

Solutions of triacetyl nucleosides **4**-**7** were prepared in methanol at 50 μM both with and without each of the synthetic nucleosides **1**-**3** in equimolar concentrations. dT_2G_5T was annealed to form the quadruplex structure through three successive freeze-thaw cycles in water at 800 μM (19). The annealed dT_2G_5T was then diluted to 10 μM

with 50 μM of either **1** or **2** in a final solvent composition of 10% water, 65% methanol, and 25% chloroform to ensure complete solubility of the synthetic nucleosides. Annealing of $dT_2AG_3T_2AG_3$ and self-complementary oligonucleotides was performed by heating a 1 mM solution of the oligonucleotide in 1 M ammonium acetate to 90°C followed by cooling to room temperature at a rate of 10°C per hour (15, 20, 30). The annealed oligonucleotides were then diluted to concentrations of 20 μM with final ammonium acetate concentrations of 25 mM for $dT_2AG_3T_2AG_3$ and 40 mM for self-complementary sequences with a solvent of 20% water, 55% methanol, and 25% chloroform. Non-self-complementary oligonucleotides were prepared identically to the self-complementary ones with the exception that no heating and cooling was performed.

The formation of the duplex and quadruplex DNA structures in this unusual solvent system was confirmed by comparing mass spectra and energy-variable collisionally activated dissociation of the oligonucleotides electrosprayed from this solvent and from the water-methanol mixtures typically used for analysis of DNA (10-11, 13-14, 19-20, 25, 30, 43-44) (results not shown). In no case was any appreciable difference between the different solvent systems observed. No sodium was added to any solution. Sodium adducts observed in the mass spectra likely resulted from low-level contaminants in the solvents used or reflected cations leached from glassware. Their presence was consistent from day-to-day and among different experimental procedures.

6.2.3 Methods and Instrumentation.

Mass spectrometric analyses were performed on an LCQ Duo quadrupole ion trap mass spectrometer equipped with the stock ESI source (ThermoFinnigan, San Jose, CA).

Triacetyl nucleosides were analyzed in the positive ion mode with the heated capillary set at 80°C. Source conditions were tuned to minimize in-source fragmentation of complexes with a needle voltage of 4.5 kV and a nitrogen sheath gas of 30 arbitrary units. Solutions were infused directly at 5 μL/min, and the spectra presented represent the average of 300 scans. Oligonucleotide solutions were analyzed in the negative ion mode. Otherwise, conditions were similar to those described above.

6.3 Results and Discussion

6.3.1 Behavior of Acetylated Nucleosides.

Positive ESI-MS analysis of the four triacetyl nucleosides **4**-**7** in methanol yielded mass spectra consistent with previous results (45-48). In the spectrum of the triacetylguanosine, **4** (Figure 6-1a), both the sodium-cationized monomeric and dimeric ions dominated, but significant abundances of higher order complexes were also observed. In particular, an ion corresponding to $(\mathbf{4}_8 + 2\ Na)^{2+}$, whose charge state was confirmed by examining the spacing of carbon isotopes, was present in a significant abundance. In fact, on a molar basis the population of this ion contained nearly as much **4** as the dimer. The large amount of **4** present as an octamer bound to sodium cations reflects the high relative stability of this complex and is in agreement with the body of literature describing the ability of guanine to form tetrad structures (46-50). In contrast, monomeric and dimeric species again dominated the mass spectra of **5**-**7** with weakly abundant trimeric species present for all three as well (Figures 6-2a, 6-3a, and 6-4a), but no higher-order aggregates were observed for these nucleosides.

Figure 6-1. ESI-mass spectra of 2',3',5'-tri-*O*-acetylguanosine, **4**, alone (a), and with each of **1** (b), **2** (c), and **3** (d).

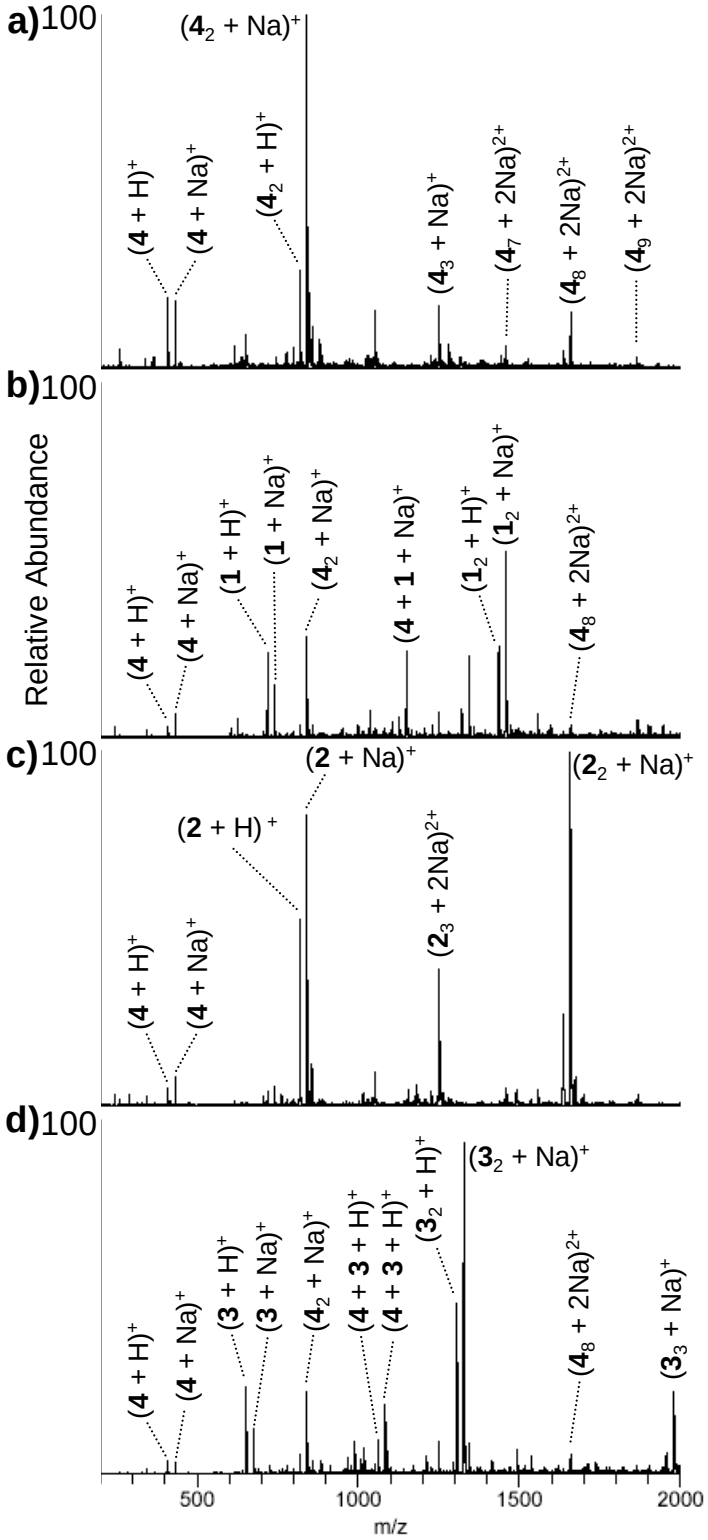

6.3.2 *Interactions between Acetylated Nucleosides and Pyrrole-Inosine Nucleosides.*

The pyrrole-inosine nucleoside, **1**, was designed to interact directly with guanine through a proposed extended Hoogsteen interaction as shown in Scheme 6-1 (45). The third hydrogen bond in this interaction serves to strengthen the interaction between **1** and guanine. It also prevents guanine from binding with a second guanine molecule through Hoogsteen interactions as occurs in guanine tetrads. In accord with such expectations, the addition of **1** to a solution of **4** led to two significant changes in the resulting mass spectrum (Figure 6-1b). In addition to the ions related to **1** and **4** individually, an abundant ion corresponding to $(\mathbf{4} + \mathbf{1} + Na)^+$ was observed which we interpret to indicate a significant degree of binding between **1** and **4**. Additionally, under these conditions the abundance of octameric **4** decreased by about a third relative to the dominant dimer species (a twelve-fold decrease in the relative number of moles of **4** present as the octamer). Together, these two differences lead us to propose that **1** disrupts the formation of the guanine tetrad by binding to **4**.

As a control experiment, the interaction of **2** with **4** was studied. This compound was designed to be nearly identical to **1** except for the addition of a *tert*-butoxycarbonyl (BOC) blocking group on the pyrrole NH (Chart 6-1). Through steric hindrance, the BOC moiety should prevent **2** from engaging in a three-point Hoogsteen interaction in contrast to what is possible with **1**. When a solution containing both **2** and **4** was analyzed, ions corresponding to various complexes of either **2** or **4** were detected (Figure 6-1c). Although similar in mass, many of the ions corresponding to various complexes of **2** differ from the complexes of **4** of similar mass/charge by a full Thompson, allowing

them to be distinguished. The octameric form of **4**, however, had too low an abundance to be distinguished from the first carbon isotope of $(\mathbf{2}_2 + Na)^+$. Theoretical calculations of the expected isotopic distribution for the two overlapping ions indicated that little if any of the $(\mathbf{4}_8 + 2\ Na)^{2+}$ ion was present. The same held true for the $(\mathbf{4}_2 + Na)^+$ and $(\mathbf{2} + Na)^+$ ions; only the $(\mathbf{2} + Na)^+$ ion was present in any appreciable amount. Additionally, the $(\mathbf{2}_3 + 2\ Na)^{2+}$ and $(\mathbf{4} + \mathbf{2} + Na)^+$ complexes were isobaric within the resolution of the mass spectrometer at 1249 Th. Collisionally activated dissociation of this ion (results not shown) indicated that it contained little if any **4**, making $(\mathbf{2}_3 + 2\ Na)^{2+}$ the correct assignment. The absence of **4** ions in the mass spectrum was a consequence of the lack of any interaction between **2** and **4**. With no complexes present, the ions of **2** alone dominated the spectrum and suppressed the signal for the ions of **4**. The inability of **2**, with its blocked Hoogsteen face, to bind **4** supports the conclusion that the interaction between **1** and **4** occurs on the Hoogsteen binding face of **1**.

The design of **3**, containing only the inosine portion and not the pyrrole part of the synthetic nucleobase, gives it the possibility of forming a two-point hydrogen bond with guanine that is weaker than the interaction between **1** and guanine. As expected, the mass spectrum of a solution of **3** and **4** contained a reasonably abundant ion corresponding to $(\mathbf{4} + \mathbf{3} + Na)^+$ (Figure 6-1d). No significant reduction in the octameric form of **4** relative to the other complexes containing **4** was observed. Furthermore, the dimer of **3** was significantly more abundant than the corresponding dimers formed from either **1** or **2**, indicating its preference for self-aggregation over binding with guanine.

Figure 6-2. ESI-mass spectra of 2',3',5'-tri-O-acetylcytidine, **5**, alone (a), and with each of **1** (b), **2** (c), and **3** (d).

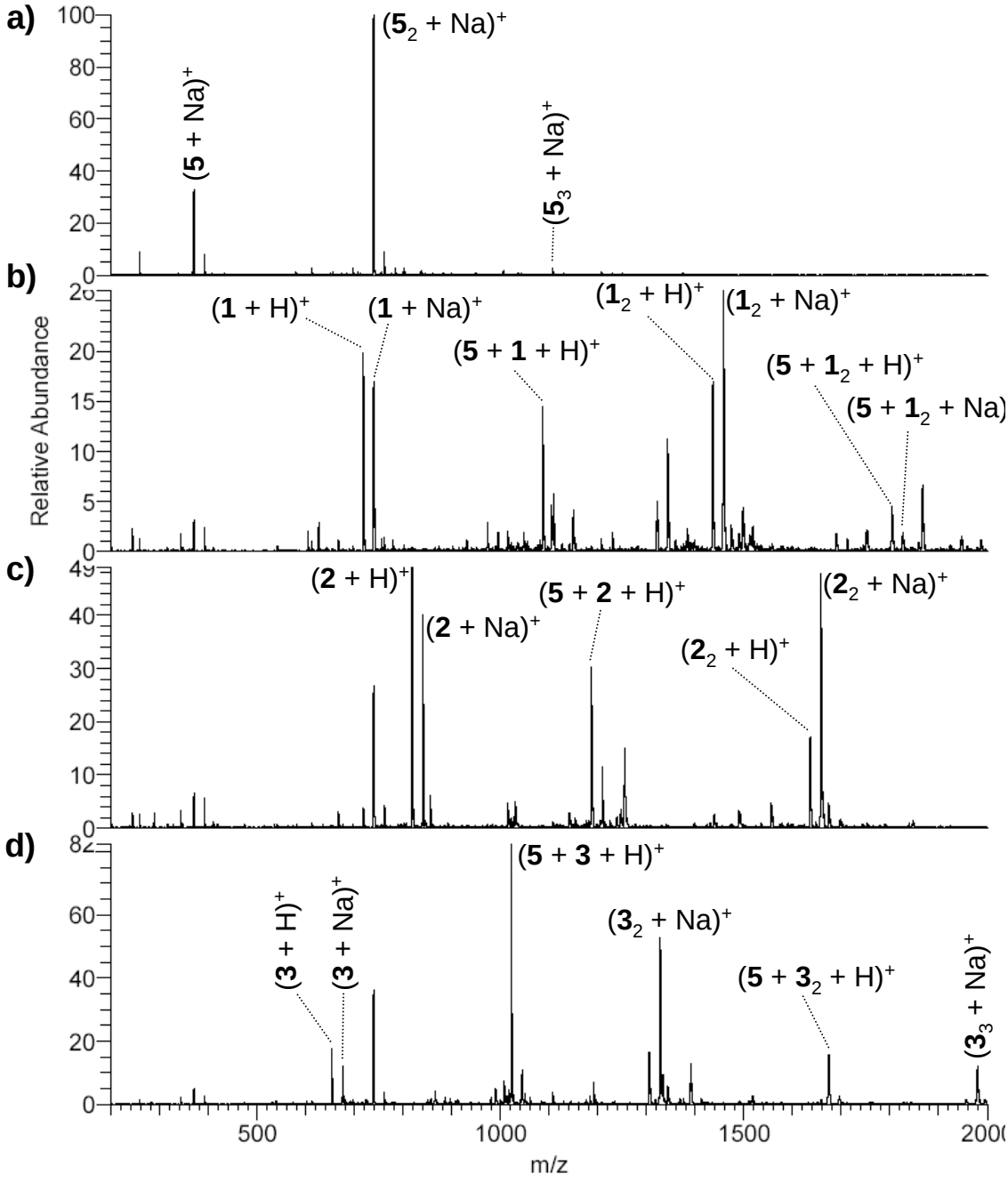

Figure 6-3. ESI-mass spectra of 2',3',5'-tri-O-acetyladenosine, **6**, alone (a), and with each of **1** (b), **2** (c), and **3** (d).

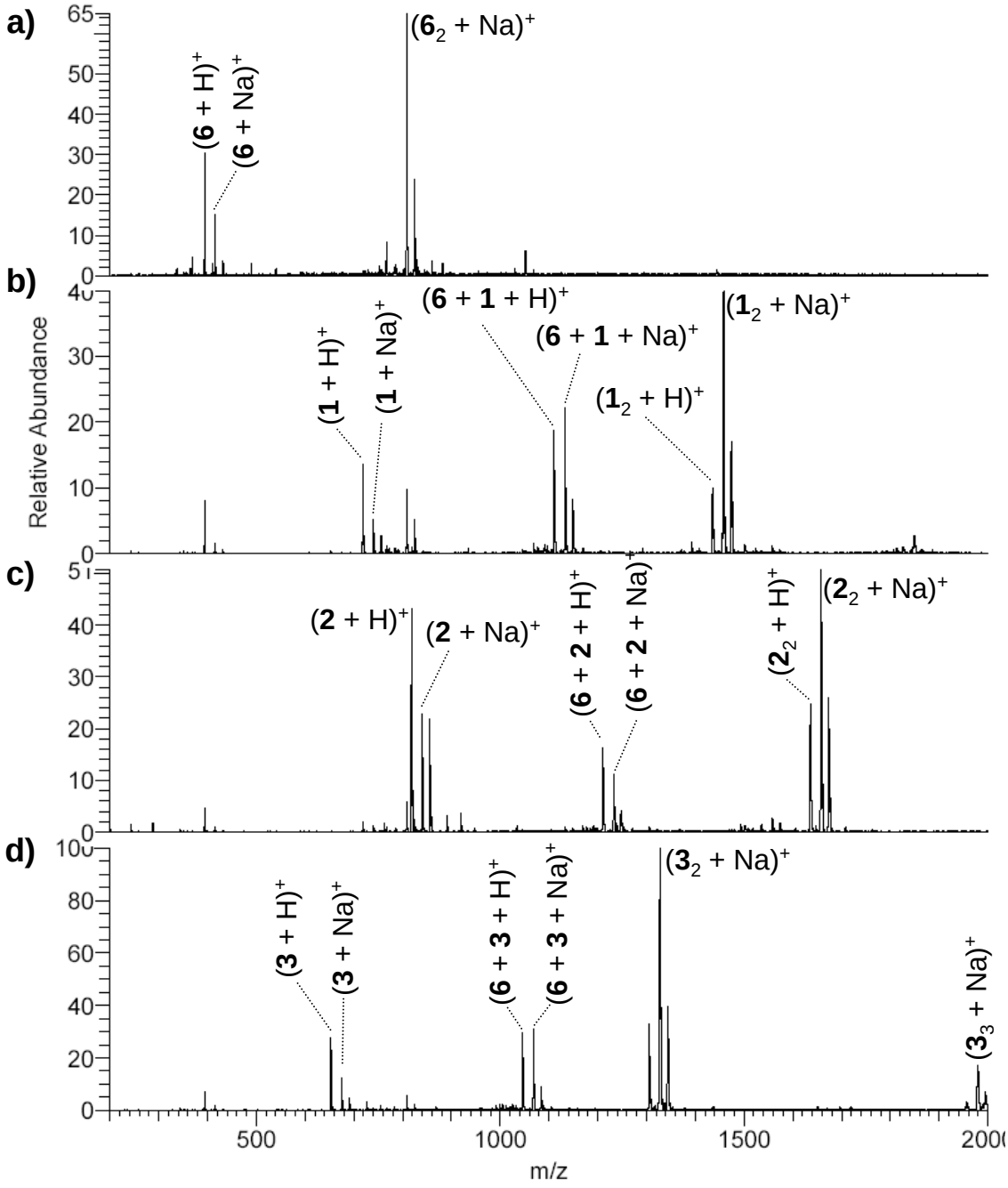

Figure 6-4. ESI-mass spectra of 2',3',5'-tri-O-acetyluridine, **7**, alone (a), and with each of **1** (b), **2** (c), and **3** (d).

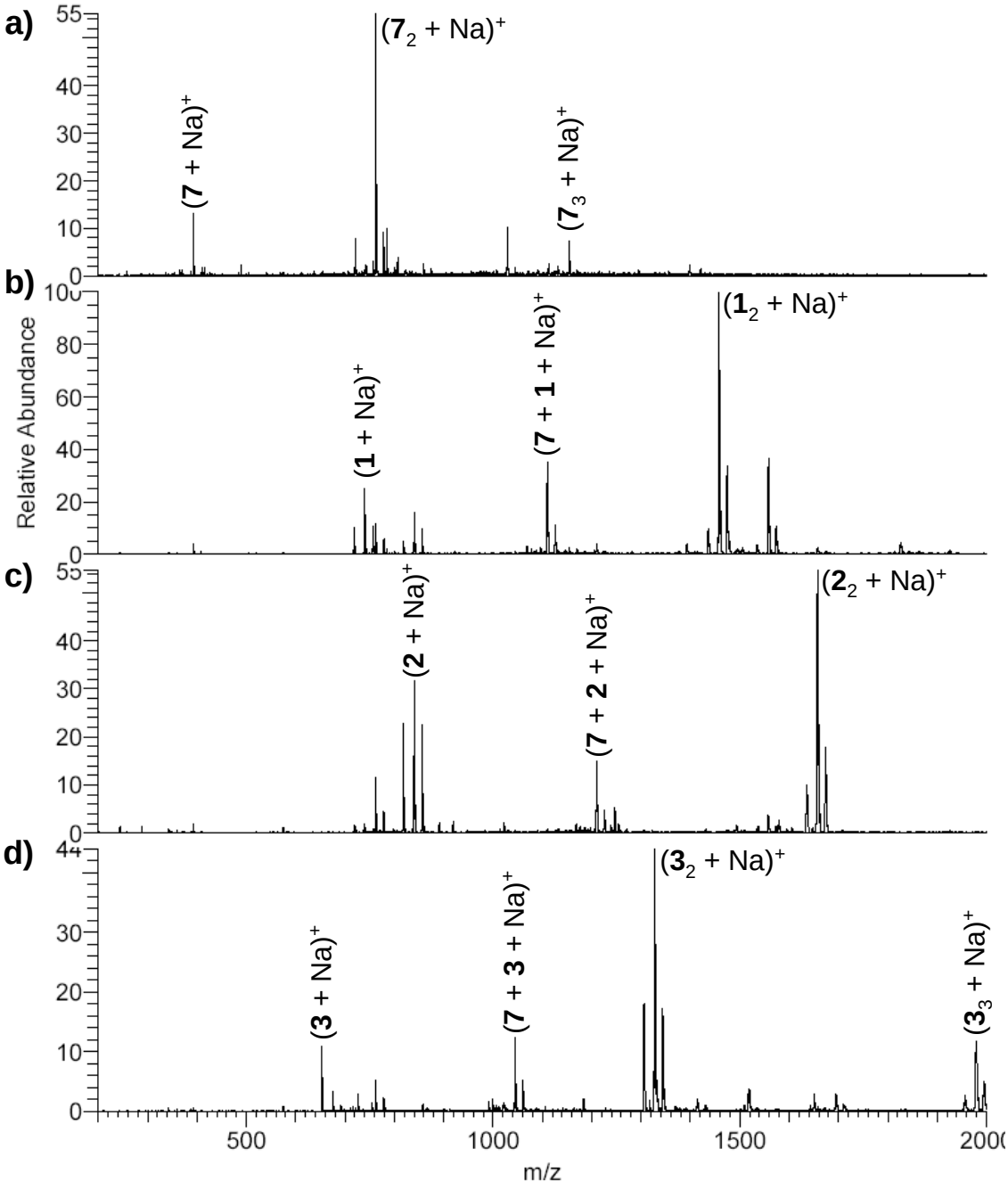

Analogous experiments were performed for solutions containing one of each of **5**, **6**, or **7** and each of **1**, **2**, or **3** (Figures 6-2 to 6-4). For each of the triacetyl nucleosides **5** to **7**, significant binding to **1** was observed. More telling, however, was the fact that each nucleoside also bound to **2** to an extent comparable to **1**. That the BOC blocking group on **2** apparently had no influence on the binding of the pyrrole-inosine nucleosides to **5**-**7** suggests that these complexes have a different structure which is unaffected by steric effects near the pyrrole unit. Likely, these complexes are the result of non-specific hydrogen-bonded clusters. This argument is bolstered by the presence of $(\mathbf{5} + \mathbf{1}_2 + H)^+$ and the corresponding sodium complex which would not be possible with the binding proposed in Scheme 6-1 for **1** and **4**. **1** and **5** simply appear to aggregate, forming complexes of stoichiometries different than those observed when complexes result from specific interactions. Lastly, the interactions of **5**, **6** and **7** with **3** offered no surprises; complexes observed by ESI-MS with all three of these triacetyl nucleosides were comparable with those observed with **1** and **2**.

6.3.3 Interactions between Quadruplex DNA and Pyrrole-Inosine Nucleosides 1 and 2.

Previous experiments have demonstrated the utility of ESI-MS for analyzing quadruplex DNA structures formed from short oligonucleotides (10-11, 13-14, 19-20, 25, 30, 43, 51). Two of these oligonucleotides were selected to evaluate the interactions between quadruplex DNA and the two pyrrole-inosine nucleosides, **1** and **2**. The first oligonucleotide, dT_2G_5T, has been used previously to determine the interactions of drugs with G4 quadruplex DNA (19). The second model sequence, $dT_2AG_3T_2AG_3$, consists of

Figure 6-5. ESI-mass spectra of dT_2G_5T alone (a) and with either **1** (b) or **2** (c). Single stranded species are denoted by ss, and quadruplex structures are labeled as Q.

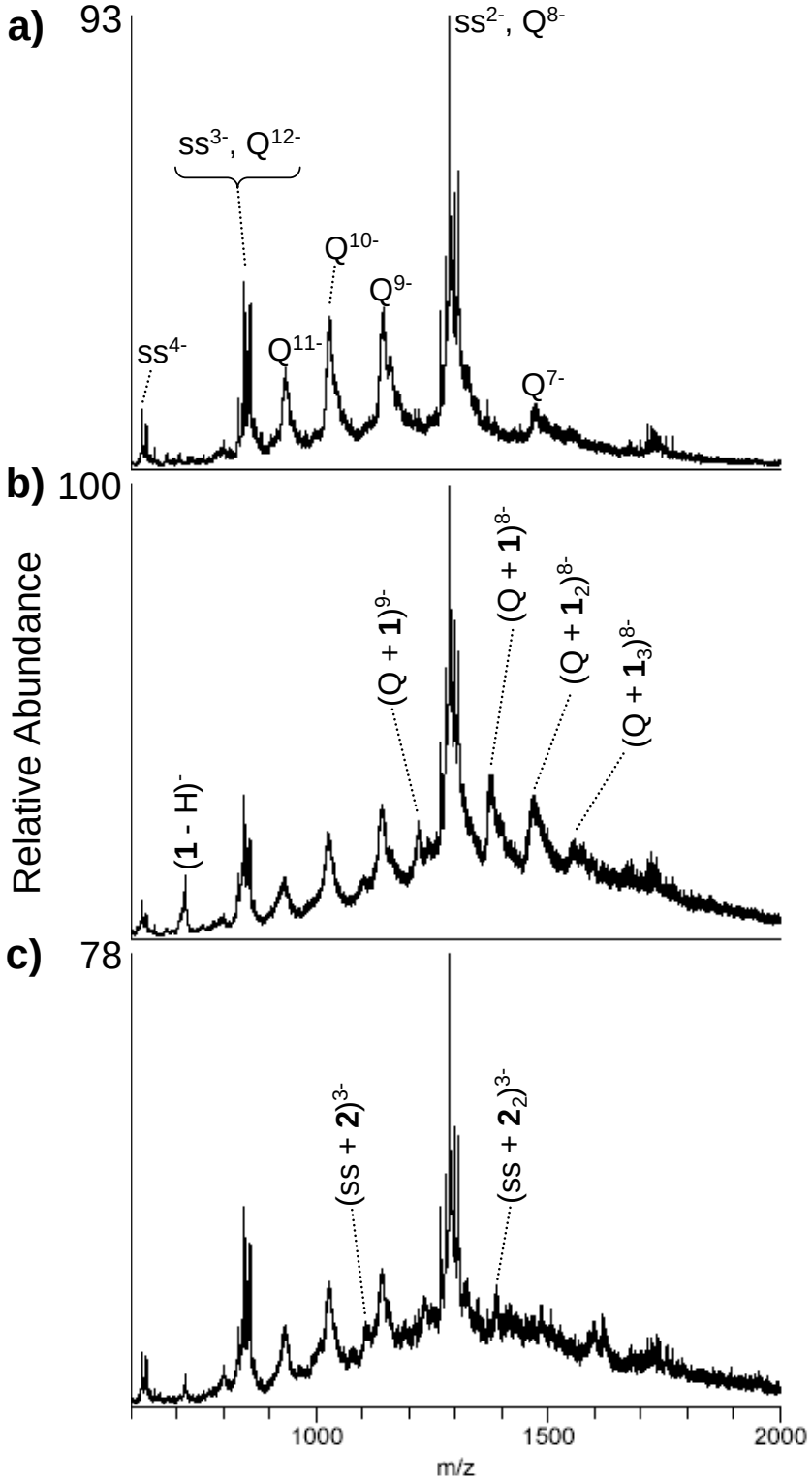

two repeats of the human telomeric oligonucleotide sequence and can form a G'2 quadruplex.

When dT_2G_5T was electrosprayed, ions corresponding to both single stranded and quadruplex species were observed (Figure 6-5a). Although the single strands and quadruplex ions with $4n^-$ charge states (integer values of n) overlapped, other charge states of the quadruplex were unambiguously assigned such as Q^{7-}, Q^{9-}, Q^{10-}, and Q^{11-}. On addition of **1** to the solution (Figure 6-5b), several ions corresponding to complexes of **1** and $(dT_2G_5T)_4$ were observed, a finding that again is taken to indicate binding between the two species. No complexes were observed between **1** and the single-stranded oligonucleotide; binding was only observed to the quadruplex. On addition of **2** to the quadruplex solution (Figure 6-5c), two ions of low abundance ascribed to the complex between **2** and the singly-stranded dT_2G_5T were detected. No adducts to the $(dT_2G_5T)_4$ quadruplex structure, however, were observed. Together these spectra indicate that **1** binds $(dT_2G_5T)_4$ selectively over dT_2G_5T, and that the BOC blocking group on **2** suppresses binding as it did with the individual nucleosides.

In the analogous experiments with $dT_2AG_3T_2AG_3$, similar results were obtained (Figure 6-6). Both quadruplex and single-stranded species were observed in the ESI-mass spectra of the oligonucleotide alone (Figure 6-6a). For this oligonucleotide sequence, the G'2 quadruplex ions (i.e. $(dT_2AG_3T_2AG_3)_2$) possessing even charge states overlap with single strand $dT_2AG_3T_2AG_3$ ions, but the odd charged quadruplexes are unambiguously assigned. When **1** was added to the solution, two new complexes were detected, $(Q + \mathbf{1})^{5-}$ and $(Q + \mathbf{1}_2)^{5-}$. No complexes involving **1** and single-stranded

Figure 6-6. ESI-mass spectra of dT2AG3T2AG3 alone (a) and with either **1** (b) or **2** (c). Single stranded species are denoted by ss, and quadruplex structures are labeled as Q.

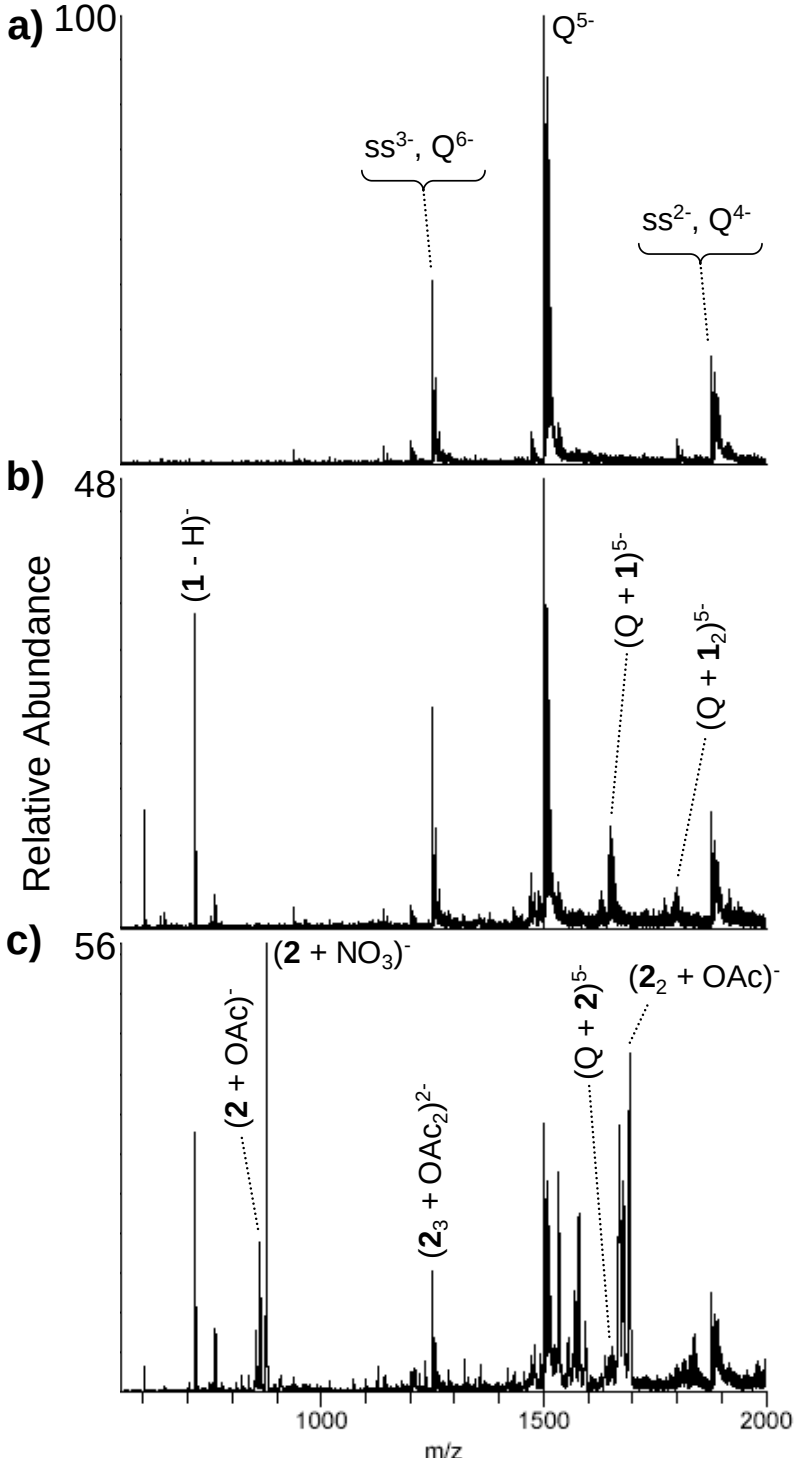

Figure 6-7. ESI-mass spectra of dT_2G_5T alone (a) and with varying concentrations of **1**. Concentrations were (b) 10 μM, (c) 20 μM, (d) 50 μM, (e) 100 μM, (f) 200 μM, and (g) 500 μM. Single stranded species are denoted by ss, and quadruplex structures are labeled as Q.

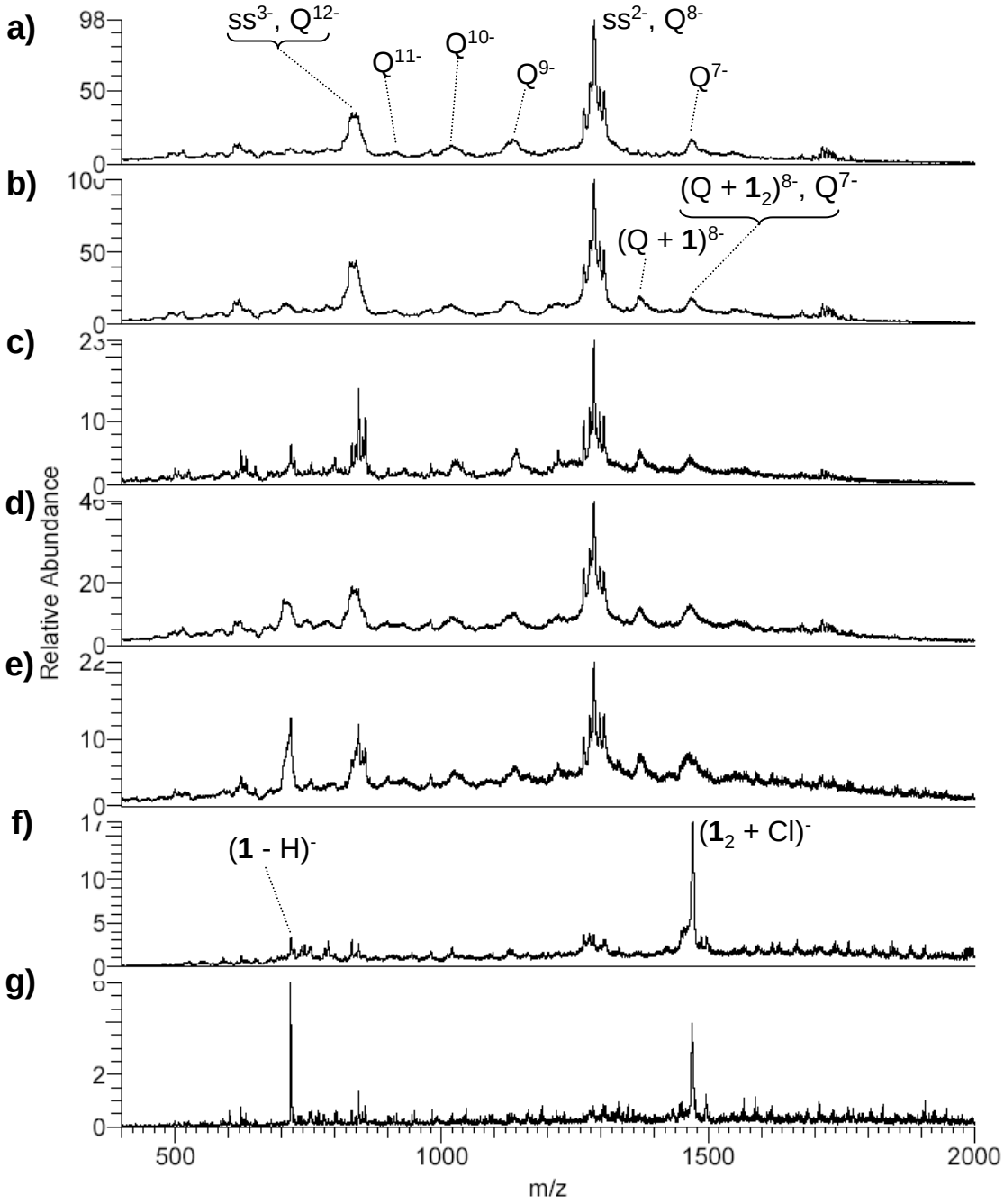

$dT_2AG_3T_2AG_3$ were detected. In contrast, **2** aggregated preferentially with the acetate anions from the buffer in which $dT_2AG_3T_2AG_3$ was annealed rather than interacting with the oligonucleotide itself (Figure 6-6c). Only a small amount of the corresponding $[(dT_2AG_3T_2AG_3)_2 + \mathbf{2}]^{5-}$ complex was observed, further supporting the conclusion that **1** selectively binds to quadruplex DNA structures and that the pyrrole NH proton plays a crucial role in stabilizing the observed complexes formed with quadruplex DNA.

6.3.4 Concentration Dependence of Quadruplex-1 Adduction.

To verify that the interaction between **1** and quadruplex DNA was a specific association and not simply a non-specific aggregation occurring either in solution or in the ESI source, solutions containing dT_2G_5T with varying concentrations of **1** were analyzed (Figure 6-7). From equimolar mixtures to solutions with **1** in ten-fold excess, the extent of adduction between **1** and dT_2G_5T remained unchanged. Deprotonated **1** and a $(\mathbf{1}_2 + Cl)^-$ aggregate dominated the mass spectra at higher concentrations of **1**, but no further adduction to dT_2G_5T was observed. The independence of the extent of adduct formation from the concentration of **1** provides evidence against non-specific aggregation.

6.3.5 Interactions between Single-Stranded or Duplex DNA and Pyrrole-Inosine Nucleosides.

The various experiments described above confirm that **1** specifically binds quadruplex DNA. To evaluate the selectivity, both **1** and **2** were analyzed with several different oligonucleotide sequences. Two sequences were analyzed as singly-stranded oligonucleotides: dGGCACG and dGACTACAAGT (Figures 6-8 and 6-9). Adducts of

Figure 6-8. ESI-mass spectra of dGGCACG alone (a) and with either **1** (b) or **2** (c). Single stranded species are denoted by ss.

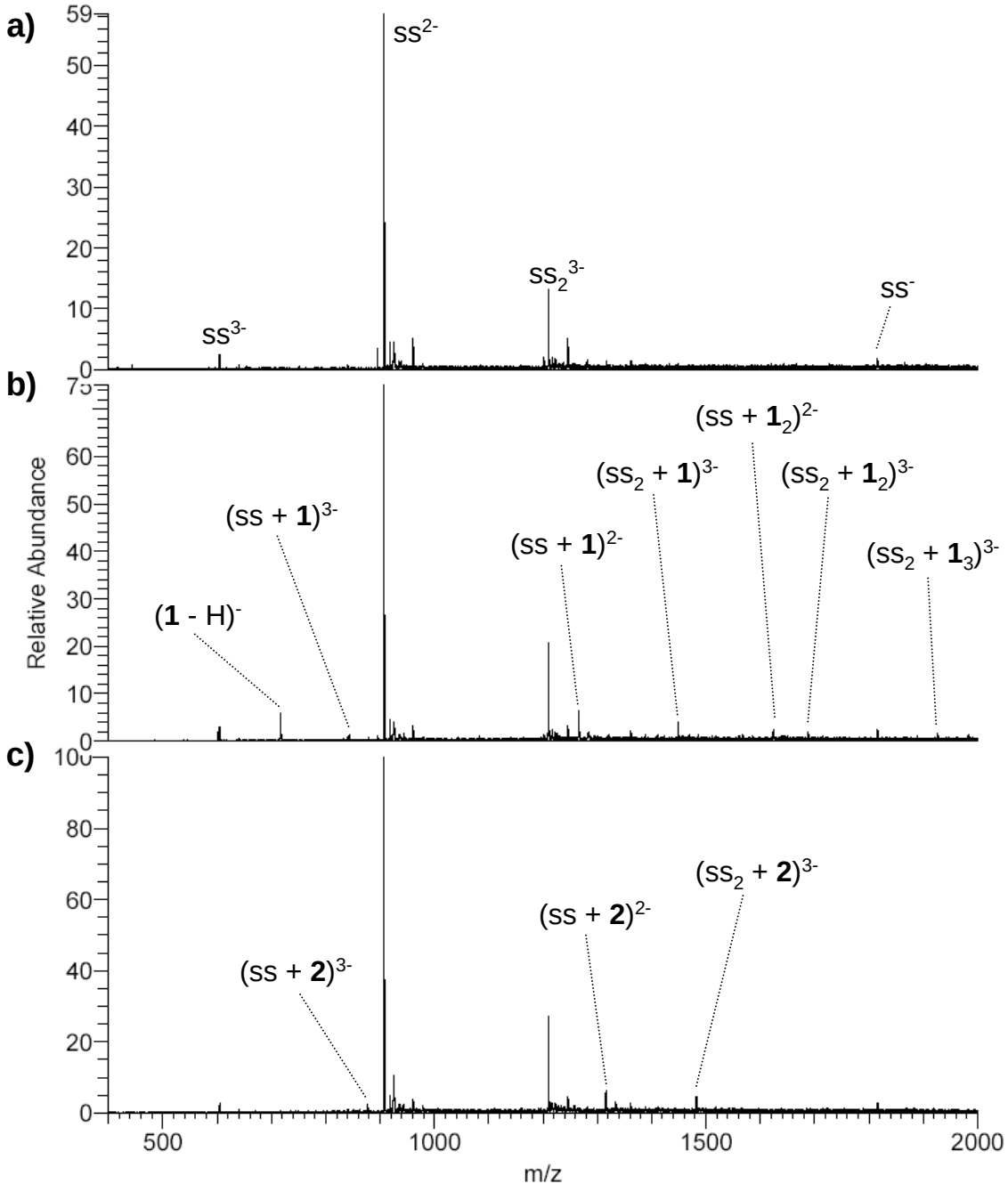

Figure 6-9. ESI-mass spectra of dGACTACAAGT alone (a) and with either **1** (b) or **2** (c). Single stranded species are denoted by ss.

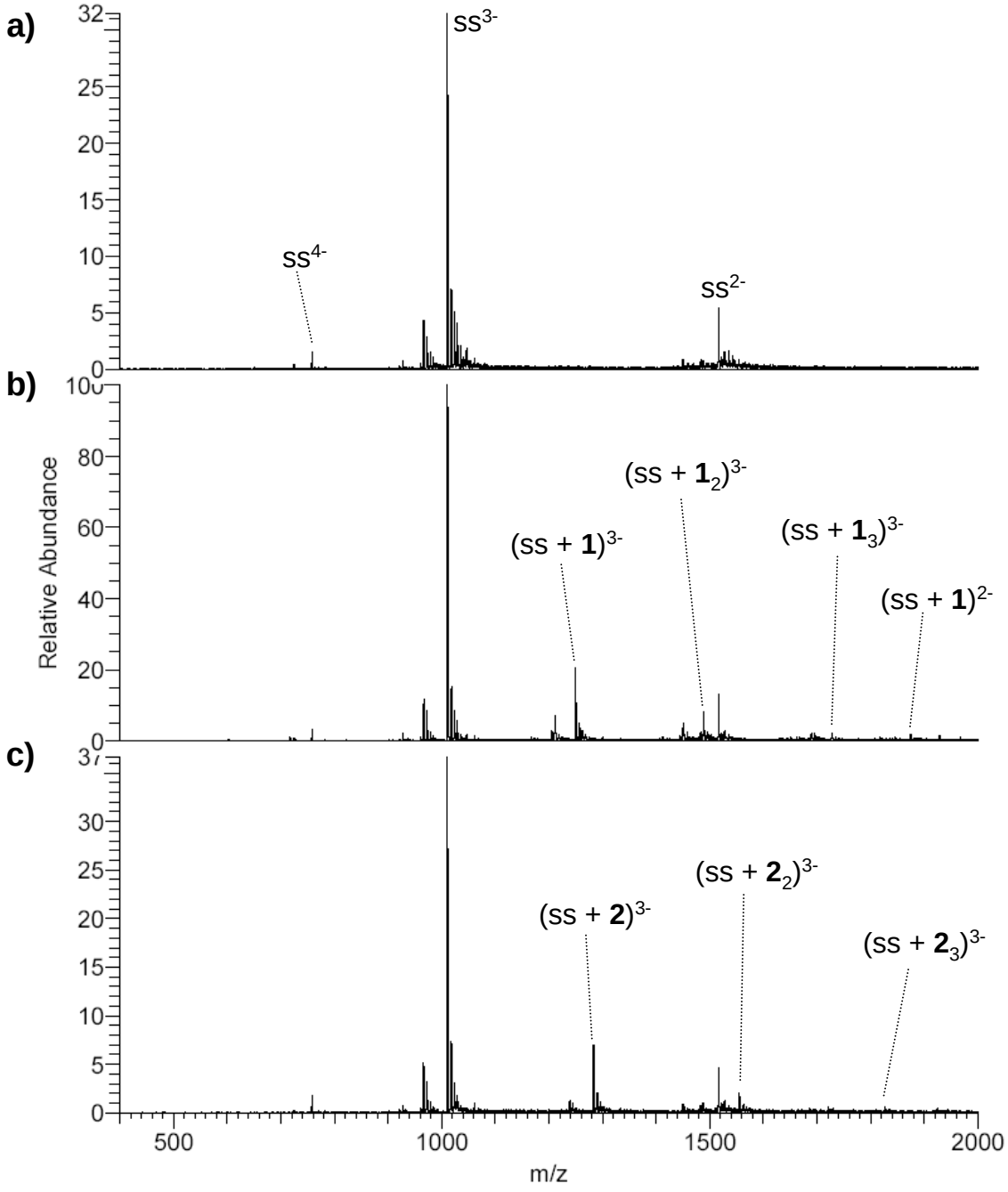

Figure 6-10. ESI-mass spectra of dGCATGC alone (a) and with either **1** (b) or **2** (c). Single stranded species are denoted by ss, and duplex structures are labeled as ds.

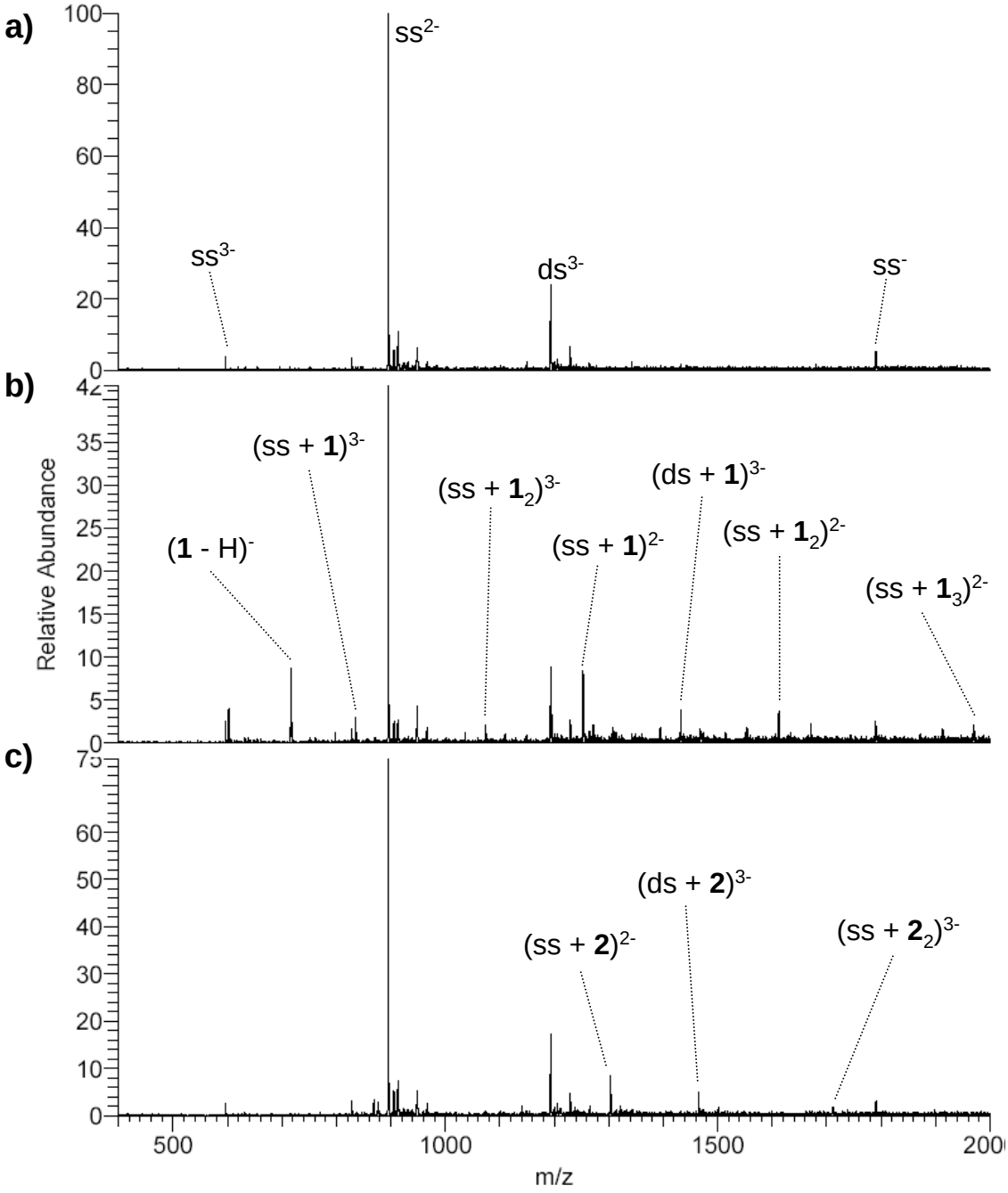

Figure 6-11. ESI-mass spectra of dCGAGCTCG alone (a) and with either **1** (b) or **2** (c). Single stranded species are denoted by ss, and duplex structures are labeled as ds.

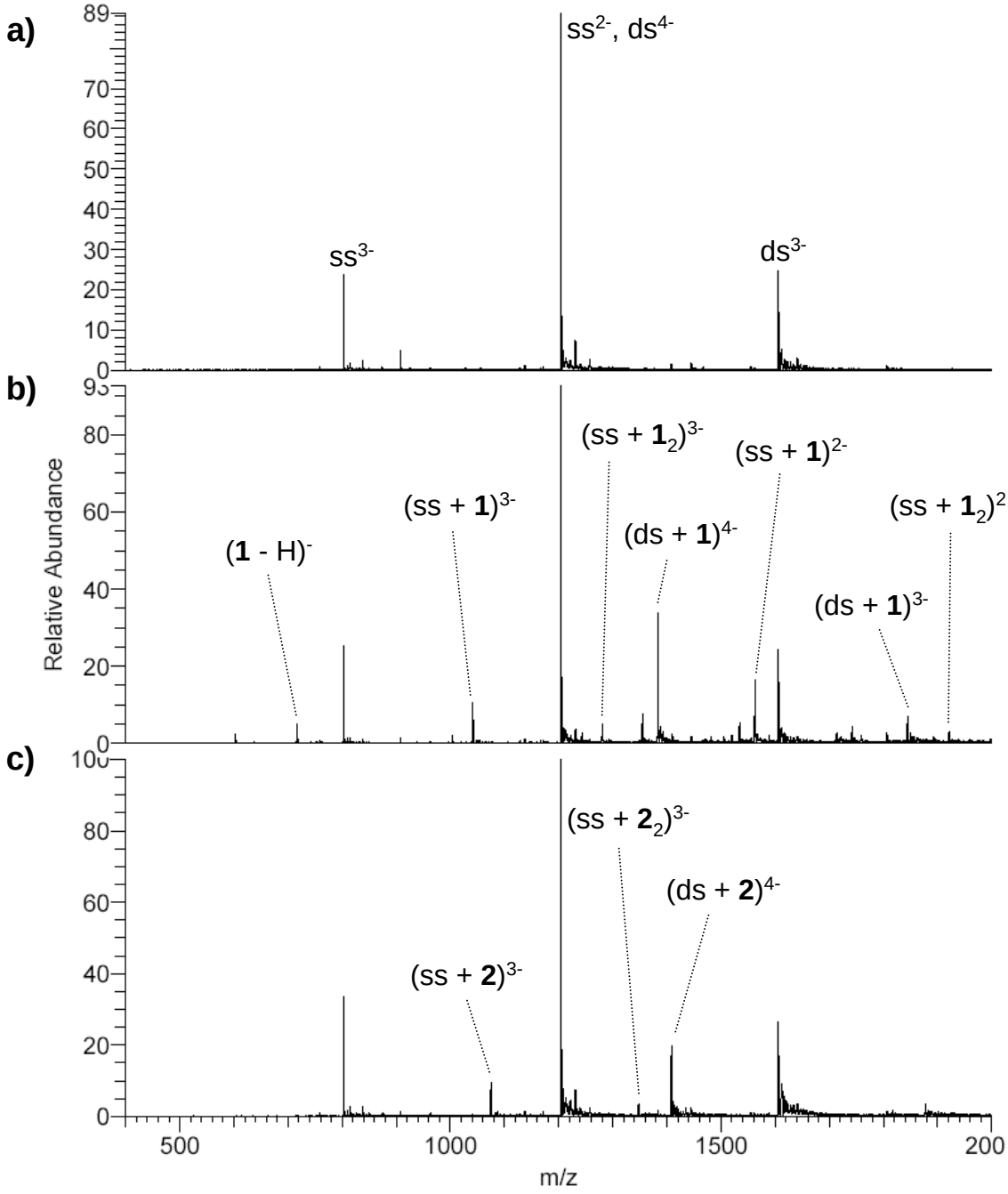

Figure 6-12. ESI-mass spectra of dGCTGCAGC alone (a) and with either **1** (b) or **2** (c). Single stranded species are denoted by ss, and duplex structures are labeled as ds.

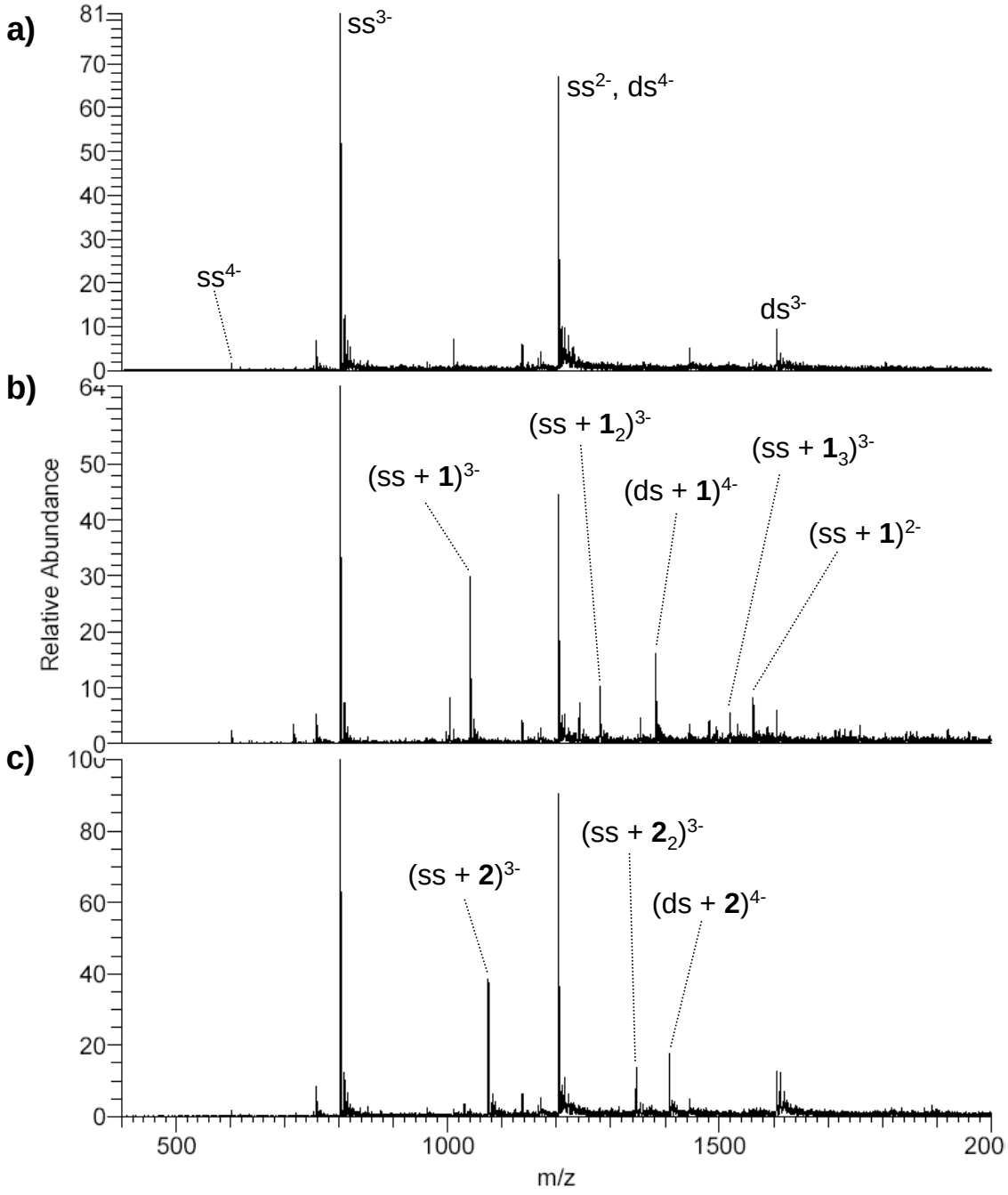

varying DNA:ligand stoichiometries were observed with low abundances for these two oligonucleotides with both **1** and **2**, respectively. Furthermore, higher numbers of both **1** and **2** adducted to the oligonucleotides, including complexes containing three or more stoichiometric equivalents of the synthetic nucleosides, were observed in most cases. This stands in sharp contrast to the behavior with quadruplex DNA where only **1** adducted appreciably, and no binding to the single strand was observed in the presence of the quadruplex structures. Aggregation of the synthetic nucleosides with single strands occurs only in the absence of a specific interaction between the nucleoside and a quadruplex as was observed for experiments with **2** where interactions with the quadruplex were precluded. This is likely due either to blocking the binding site as discussed above or the absence of any available quadruplexes as in this experiment.

Additionally, three self-complementary sequences, dGCATGC, dCGAGCTCG, and dGCTGCAGC, were annealed to allow complexation of **1** and **2** with duplex DNA to be evaluated (Figures 6-10 to 6-12). Both **1** and **2** formed moderately low abundance aggregates with all of the duplexes. Some higher order duplex:ligand binding stoichiometries were observed, and the numerous aggregates revealed no indication of any specificity.

6.4 Conclusions

In experiments with triacetyl nucleosides, the pyrrole-inosine nucleoside **1** forms specific complexes with guanosine while simultaneously decreasing the relative abundance of octameric guanosine. Steric blocking of the pyrrole NH proton precludes

this adduction while removing the pyrrole entirely reduces the degree of interaction. Such findings provide support for the conclusion that **1** forms hydrogen bonds with guanine through a three-point Hoogsteen-type interaction. Analogous experiments with other nucleosides demonstrated non-specific interactions when analyzed in the presence of either **1** or its sterically-blocked counterpart **2**.

Beyond its unique specificity towards guanosine, **1** also specifically bound quadruplex structures formed from both dT_2G_5T and $dT_2AG_3T_2AG_3$. No such complexes were observed with **2**, and experiments with various singly-stranded and duplex oligonucleotides consistently yielded only non-specific aggregation. Further investigation is required to elucidate the structure of the complex between **1** and quadruplex DNA. Nonetheless, the specificity of the interaction between **1** and quadruplex DNA is noteworthy and potentially represents a novel avenue for the development of quadruplex-targeting drugs.

6.5 References

(1) Arthanari, H.; Bolton, P. H. *Chem. Biol.* **2001**. *8*, 221-230.

(2) Li, J.-L.; Harrison, J.; Reszka, A. P.; Brosh, R. M., Jr.; Bohr, V. A.; Neidle, S.; Hickson, I. D. *Biochemistry* **2001**, *40*, 15194-15202.

(3) Collins, K. *Curr. Opin. Cell Biol.* **2000**. *12*, 378-383.

(4) Kerwin, S. M. *Curr. Pharm. Des.* **2000**, *6*, 441-471.

(5) Lavelle, F.; Riou, J.-F.; Laoui, A.; Mailliet, P. *Crit. Rev. Oncol. Hematol*. **2000**, *34*, 111-126.

(6) Neidle, S.; Harrison, R. J.; Reszka, A. P.; Read, M. A. *Pharmacol. Ther.* **2000**, *85*, 133-139.

(7) Siddiqui-Jain, A.; Grand, C. L.; Bearss, D. J.; Hurley, L. H. *Proc. Nat. Acad. Sci. USA* **2002**, *99*, 11593-11598.

(8) Lin, Y.-C.; Shih, J.-W.; Hsu, C.-L.; Lin, J.-J. *J. Biol. Chem.* **2001**, *276*, 47671-47674.

(9) Zahler, A. M.; Williamson, J. R.; Cech, T. R.; Prescott, D. M. *Nature.* **1991**, *350*, 718-720.

(10) Nakatani, K.; Hagihara, S.; Sando, S.; Sakamoto, S.; Yamaguchi, K.; Maesawa, C.; Saito, I. *J. Am. Chem. Soc.* **2003**, *125*, 662-666.

(11) Guittat, L.; Alberti, P.; Rosu, F.; Van Miert, S.; Thetiot, E.; Pieters, L.; Gabelica, V.; De Pauw, E.; Ottaviani, A.; Riou, J.-F.; Mergny, J.-L. *Biochimie*. **2003**, *85*, 535-547.

(12) Redon, S.; Bombard, S.; Elizondo-Riojas, M.-A.; Chottard, J.-C. *Nucleic Acids Res.* **2003**, *31*, 1605-1613.

(13) Rosu, F.; De Pauw, E.; Guittat, L.; Alberti, P.; Lacroix, L.; Mailliet, P.; Riou, J.-F.; Mergny, J.-L. *Biochemistry* **2003**, *42*, 10361-10371.

(14) Rosu, F.; Gabelica, V.; Shin-ya, K.; De Pauw, E. *Chem. Commun.* **2003**, 2702-2703.

(15) Carrasco, C.; Rosu, F.; Gabelica, V.; Houssier, C.; De Pauw, E.; Garbay-Jaureguiberry, C.; Roques, B.; Wilson, W. D.; Chaires, J. B.; Waring, M. J.; Bailly, C. *ChemBioChem*. **2002**, *3*, 1235-1241.

(16) Kerwin, S. M.; Sun, D.; Kern, J. T.; Rangan, A.; Thomas, P. W. *Bioorg. Med. Chem. Lett.* **2001**, *11*, 2411-2414.

(17) Han, H.; Bennett, R. J.; Hurley, L. H. *Biochemistry* **2000**, *39*, 9311-9316.

(18) Fedoroff, O. Y.; Salazar, M.; Han, H.; Chemeris, V. V.; Kerwin, S. M.; Hurley, L. H. *Biochem*istry **1998**, *37*, 12367-12374.

(19) David, W. M.; Brodbelt, J.; Kerwin, S. M.; Thomas, P. W. *Anal. Chem.* **2002**, *74*, 2029-2033.

(20) Rosu, F.; Gabelica, V.; Houssier, C.; Colson, P.; De Pauw, E. *Rapid Commun. Mass Spectrom.* **2002**, *16*, 1729-1736.

(21) Randazzo, A.; Galeone, A.; Mayol, L. *Chem. Commun.* **2001**, 1030-1031.

(22) Hoogsteen, K. *Acta Crystallogr.* **1963**, *16*, 907-916.

(23) Hoogsteen, K. *Acta Crystallogr.* **1959**, *12*, 822-823.

(24) Davis, J. T. *Angew. Chem. Int. Ed.* **2004**, *43*, 668-698.

(25) Sakamoto, S.; Yamaguchi, K. *Angew. Chem. Int. Ed.* **2003**, *42*, 905-908.

(26) Haider, S.; Parkinson, G. N.; Neidle, S. *J. Mol. Biol.* **2002**, *320*, 189-200.

(27) Phan, A. T.; Modi, Y. S.; Patel, D. J. *J. Am. Chem. Soc.* **2004**, *126*, 8710-8716.

(28) Seenisamy, J.; Rezler, E. M.; Powell, T. J.; Tye, D.; Gokhale, V.; Joshi, C. S.; Siddiqui-Jain, A.; Hurley, L. H. *J. Am. Chem. Soc.* **2004**, *126*, 8702-8709.

(29) Lyonnais, S.; Hounsou, C.; Teulade-Fichou, M.-P.; Jeusset, J.; Le Cam, E.; Mirambeau, G. *Nucleic Acids Res.* **2002**, *30*, 5276-5283.

(30) Krishnan-Ghosh, Y.; Liu, D.; Balasubramanian, S. *J. Am. Chem. Soc.* **2004**, *126*, 11009-11016.

(31) Kerwin, S. M.; Chen, G.; Kern, J. T.; Thomas, P. W. *Bioorg. Med. Chem. Lett.* **2002**, *12*, 447-450.

(32) Schultze, P.; Hud, N. V.; Smith, F. W.; Feigon, J. *Nucleic Acids Res.* **1999**, *27*, 3016-3028.

(33) Phillips, K.; Dauter, Z.; Murchie, A. I. H.; Lilley, D. M. J.; Luisi, B. *J. Mol. Biol.* **1997**, *273*, 171-182.

(34) Poon, K.; Macgregor, R. B., Jr. *Biopolymers*. **1998**, *45*, 427-434.

(35) Marsh, T. C.; Henderson, E. *Biochemistry* **1994**, *33*, 10718-10724.

(36) Sen, D.; Gilbert, W. *Biochemistry* **1992**, *31*, 65-70.

(37) Wang, Y.; Patel, D. J. *Biochemistry* **1992**, *31*, 8112-8119.

(38) Rovnyak, D.; Baldus, M.; Wu, Gang; Hud, N. V.; Feignon, J.; Griffin, R. G. *J. Am. Chem. Soc.* **2000**, *122*, 11423-11429.

(39) Gilbert, D. E.; Feigon, J. *Curr. Opin. Struct. Biol.* **1999**, *9*, 305-314.

(40) Parkinson, G. N.; Lee, M. P. H.; Neidle, S. *Nature.* **2002**, *417*, 876-880.

(41) Read, M. A.; Neidle, S. *Biochemistry* **2000**, *39*, 13422-13432.

(42) Simonsson, T. *Biol. Chem.* **2001**, *382*, 621-628.

(43) Vairamani, M.; Gross, M. L. *J. Am. Chem. Soc.* **2003**, *125*, 42-43.

(44) Oehlers, L.; Mazzitelli, C. L.; Brodbelt, J. S.; Rodriguez, M.; Kerwin, S. *J. Am. Soc. Mass Spectrom.* **2004**, *15*, 1593-1603.

(45) Sessler, J. L.; Jayawickramarajah, J.; Sherman, C. L.; Brodbelt, J. S. *J. Am. Chem. Soc.* **2004**, *126*, 11460-11461.

(46) Manet, I.; Francini, L.; Masiero, S.; Pieraccini, S.; Spada, G. P.; Gottarelli, G. *Helv. Chim. Acta.* **2001**, *84*, 2096-2107.

(47) Sakamoto, S.; Nakatani, K.; Saito, I.; Yamaguchi, K. *Chem. Commun.* **2003**, 788-789.

(48) Koch, K. J.; Aggerholm, T.; Nanita, S. C.; Cooks, R. G. *J. Mass Spectrom.* **2002**, *37*, 676-686.

(49) Shi, X.; Mullaugh, K. M.; Fettinger, J. C.; Jiang, Y.; Hofstadler, S. A.; Davis, J. T. *J. Am. Chem. Soc.*, **2003**, *125*, 10830-10841.

(50) Marlow, A. L.; Mezzina, E.; Spada, G. P.; Masiero, S.; Davis, J. T.; Gottarelli, G. *J. Org. Chem.* **1999**, *64*, 5116-5123.

(51) Goodlett, D. R.; Camp, D. G., II; Hardin, C. C.; Corregan, M.; Smith, R. D. *Biol. Mass Spectrom.* **1993**, *22*, 181-183.

CHAPTER 7

Structural Evaluation of the Adduct Between a 4-Aza-3-ene-1,6-diyne and DNA Using Electrospray Ionization Mass Spectrometry

7.1 Introduction

Following the initial elucidation of the structure of the neocarzinostatin chromophore (1), much effort has been directed towards identifying additional natural enediynes and evaluating their activities (2-5). Currently, nearly twenty of these natural enediynes have been identified including calichemicin γ_1^I (6-7), dynemicin (8), and the esperamicins (9-10). While these enediynes offer extremely high cytotoxic activities, their clinical use as anti-tumor agents has been limited due to their delayed activities and general toxicity (2-5).

To overcome the shortcomings of these natural enediynes, a range of synthetic analogues have been explored (3, 11), each with the goal of improved properties for clinical use. While still capable of cleaving DNA like the natural products through cycloaromatization reactions and subsequent hydride abstraction by the diradical intermediate (2-4, 11-12), these analogues offer potential advantages such as more controlled activation of the compound *in vivo* (13-23) or increased selectivity for tumor cells (24-30).

To better evaluate the activities and properties of the many enediyne drug candidates as well as various other classes of drugs being developed, a technique for analyzing the interactions between these compounds and DNA using a flow injection analysis (FIA) coupled to an electrospray ionization mass spectrometer (ESI-MS) is presented. This analysis offers several key advantages over the traditional gel-based electrophoretic techniques. First, the dramatically better resolution of mass spectrometry versus polyacrylamide gel electrophoresis allows differentiation of similarly sized species, enabling the detection of very small molecules adducted to DNA. Second, while gel electrophoresis typically requires micrograms of sample, with this FIA method, a mass spectrum can easily be collected with nanograms, a sensitivity advantage of up to three orders of magnitude. Lastly, FIA-ESI-MS is easily adaptable to high-throughput analyses (31-33).

In recent years, applications of ESI-MS for DNA analysis have begun to mature (34-35). A critical component of many of these experiments is the application of tandem mass spectrometry to probe the fragments produced when DNA ions or DNA-drug complexes are energized in the gas phase (36-42). Collisionally-activated dissociation (CAD) (34-35, 43), infrared multiphoton dissociation (IRMPD) (44-45), and electron capture dissociation (ECD) (46) have all been demonstrated to yield useful information about oligonucleotides. Sequence determination has been a primary focus of many of these prior reports, but numerous studies of non-covalent drug attachment have also been presented (37-42). Studies of this type have been used to map the binding stoichiometries of DNA/drug complexes (38, 42, 47-52) as well as to determine both the

Chart 7-1.

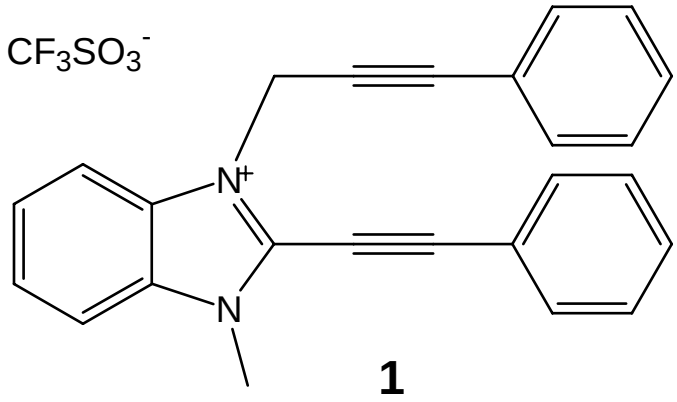

1

position and mode of attachment of a drug to an oligonucleotide sequence (38, 42, 47-49, 51-53). Despite the potential advantages in applying ESI-MS to the study of enediyne-DNA interactions, we have found no reports exploring this method.

Previous studies have shown that **1** (Chart 7-1) interacts with DNA in at least three ways: via frank strand scission and the formation of at least two different adducts (29). One of these adducts subsequently effects specific cleavage of the oligonucleotide sequence at cytidine residues (29), likely through a mode of action very different from the radical-induced cleavages commonly observed with enediyne drugs (2-5). It has been proposed that the adduct results from a nucleophilic attack of one of the alkynes on the enediyne by the DNA (28). The gel electrophoresis experiments used in the discovery of this behavior lacked both the mass resolution to accurately characterize the adducts and the ability to further probe the structures of the adducts. In this study is presented an examination of these adducts by ESI-MS. In addition to confirming the information previously obtained by gel electrophoresis, the mass spectrometric analysis reveals the identity and stoichiometry of the adducts. Furthermore, through tandem MS experiments,

a series of clues obtained about the structure of the adduct has helped to identify both the location and mechanism of attachment to the oligonucleotide structure.

7.2 Experimental

7.2.1 Reagents.

The oligonucleotides and primers were synthesized on a PerSeptive Biosystems Expedite 8909 DNA synthesizer (Framingham, MA) and purified by reversed-phase chromatography. Concentrations were determined by UV absorption at 260 nm. The enediyne, **1**, was prepared according to previously published procedures (27).

7.2.2 Preparation of Samples for Analysis.

Mixtures of the different oligonucleotides at 360 μM with 3.6 mM of **1** were prepared in a 10 μM sodium phosphate buffer at either pH 6 or 8 also containing 8% DMSO (Sigma Chemical Company, St. Louis, MO). These mixtures were then incubated at 37°C for 20 hours (dCC) or 24 hours (other oligonucleotides). Following incubation, the samples were desalted either by reversed-phase HPLC (dCC) or with C_{18} Waters Sep-Pak cartridges (other oligonucleotides). Samples were further purified using C_{18} ZipTips (Millipore, Bedford, MA) immediately prior to analysis.

7.2.3 Methods and Instrumentation.

Prepared samples were analyzed on a ThermoFinnigan LCQ Duo quadrupole ion trap mass spectrometer equipped with the standard ESI source (San Jose, CA). Injections of 1-5 μL for the FIA were made with a Waters Alliance 2690 Separations Module (Midford, MA) with a carrier flow of A.C.S. Grade Spectranalyzed methanol (Fisher

Figure 7-1. Mass spectrum of dC_8 incubated with **1**.

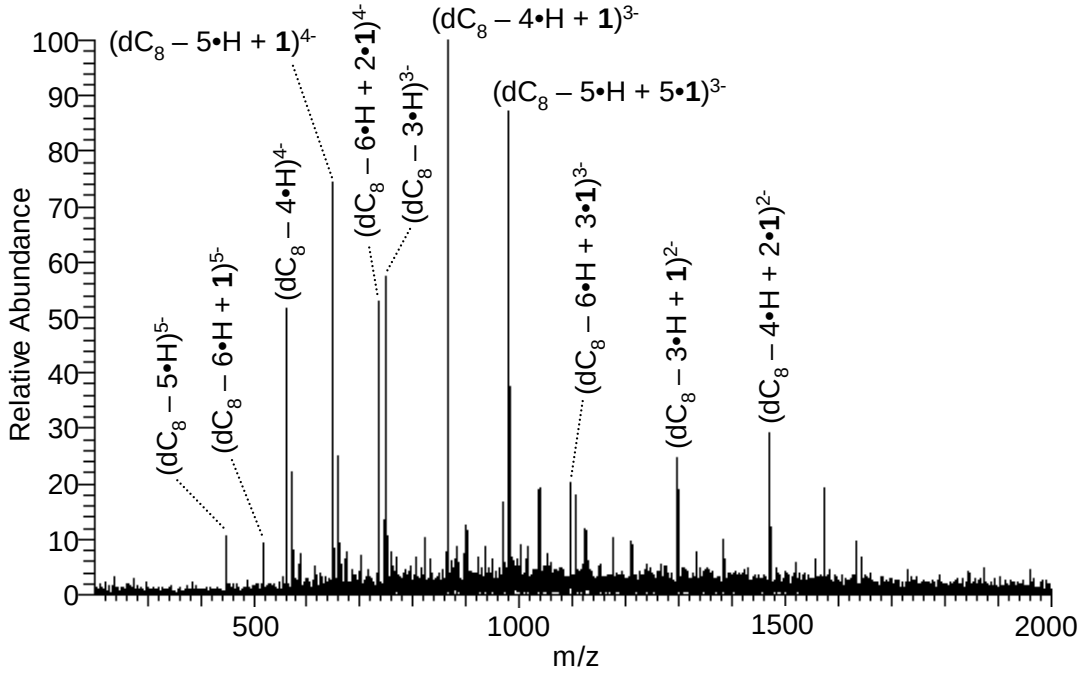

Scientific, Fair Lawn, NJ) at 10 μL/min. Mass spectra were obtained by integrating the signal across the FIA peak. Nomenclature for identifying oligonucleotide fragments followed the conventions set forth by McLuckey, et al. (36).

7.3 Results and Discussion

7.3.1 Interactions between 1 and dC_8.

Armed with the previous results indicating that cytidine-specific cleavage of the oligonucleotide-**1** adduct was observed on heat treatment with piperidine (28-29), interactions between the enediyne and an all cytidine oligonucleotide, dC_8, were examined to determine whether or not the adducts could be isolated and studied. The mass spectrum obtained by FIA-ESI-MS analysis of a mixture incubated at pH 8 revealed

Figure 7-2. Mass spectrum of dCT_5 incubated with **1** at pH 8 (a) and pH 6 (b).

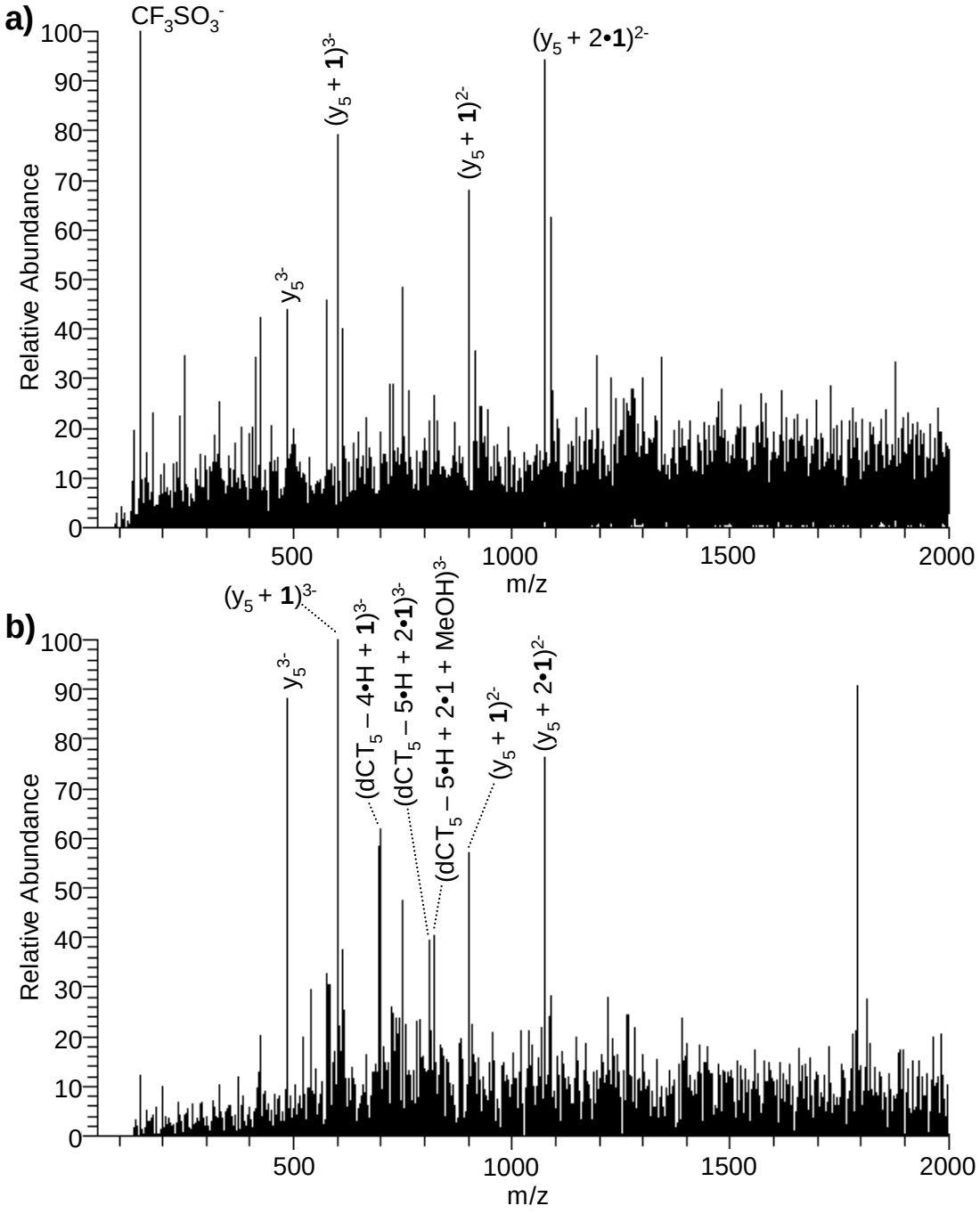

many ions containing dC_8, most of which also contained up to three molecules of **1** per oligonucleotide (Figure 7-1). Although the wide range of adducts formed indicated that **1** readily bound the cytidine-rich oligonucleotide under these conditions and provided ready confirmation that ESI-MS could be used to detect the incubation products, the resulting ions revealed little about the mode of binding. Clearly, the sequence homogeneity precluded formation of one specific adduct structure, and thus oligonucleotides containing a single cytidine were used for more detailed structural studies, as described below.

7.3.2 Interactions between 1 and either dCT_5 or dT_2CT_3.

Having established that **1** readily adducts to cytidine-containing oligonucleotides, its interactions with two different sequences containing a single cytidine base were analyzed. Previous studies indicated that DNA cleavage was observed on heat treatment with piperidine following incubation at higher pH values (28). The ESI mass spectra of oligonucleotide-**1** mixtures incubated at pH 8 and pH 6 yielded similar product ions. For instance, ESI-MS of the dCT_5-**1** mixture incubated at pH 8 (Figure 7-2a) primarily yielded several y_5 fragments with various charges and incorporating **1**. The only ion from this spectrum absent in the ESI mass spectrum obtained for analogous mixture incubated at pH 6 (Figure 7-2b) corresponded to the $CF_3SO_3^-$ counter-ion. Since the S/N in both of these mass spectra was modest due to the low concentrations and the minimal volumes of sample used for the FIA, this analysis focuses on the results for the samples incubated at pH 6 because of the larger ion abundances and the greater numbers of ions observed. Whenever possible CAD spectra were collected for the various adducts

observed at both pH values, and the fragmentation patterns revealed no significant discrepancies.

FIA-ESI-MS analysis of the mixture of dCT_5 and **1** incubated at pH 6 yielded an assortment of product ions containing **1** (Figure 7-2b), and many of these products correspond to cleaved fragments of the oligonucleotide. In particular, several y_5 products both alone and with one or two molecules of **1** were observed. The array of y_5 products results from cleavage on the 3' side of the cytidine of the dCT_5 oligonucleotide and provides striking evidence for the expected heat-induced cleavage observed previously for this compound (28-29). The selectivity for cleavage specific to the cytidine position is remarkable. In addition to the y_5 products in Figure 7-2b, two adducts of the intact dCT_5 oligonucleotide, $(dCT_5 - 4\bullet H + \mathbf{1})^{3-}$ and $(dCT_5 - 5\bullet H + 2\bullet\mathbf{1} + MeOH)^{3-}$ at 822 Th, were observed along with two ions, at 749 and 1791 Th, for which formulas could not be assigned, but dissociated to yield fragments indicating the presence of both dCT_5 and **1** (see below).

The product ions from Figure 7-2b with sufficient abundance, y_5^{3-} at 485 Th, $(y_5 + \mathbf{1})^{3-}$ at 600 Th, $(dCT_5 - 4\bullet H + \mathbf{1})^{3-}$ at 697 Th, 749 Th, $(dCT_5 - 5\bullet H + 2\bullet\mathbf{1} + MeOH)^{3-}$ at 822 Th, $(y_5 + \mathbf{1})^{2-}$ at 901 Th, $(y_5 + 2\bullet\mathbf{1})^{2-}$ at 1074 Th, and 1791 Th, were isolated and subjected to CAD. The resulting CAD mass spectra (Figures 7-3 through 7-5) reveal a combination of fragments resulting from ejection of **1** and backbone cleavages typical of CAD of oligonucleotides (36). For the related y_5 parent ions (Figures 7-3a, 7-3b, 7-4c, and 7-5a), whenever the parent also contained **1**, one dominant fragmentation pathway was ejection of **1**, suggesting the molecule of **1** was only weakly attached to these

Figure 7-3. CAD of ions isolated from the mass spectrum of dCT_5 incubated with **1** at pH 6. Parent ions were (a) y_5^{3-} at 485 Th, (b) $(y_5 + \mathbf{1})^{3-}$ at 600 Th, and (c) $(dCT_5 - 4\bullet H + \mathbf{1})^{3-}$ at 697 Th.

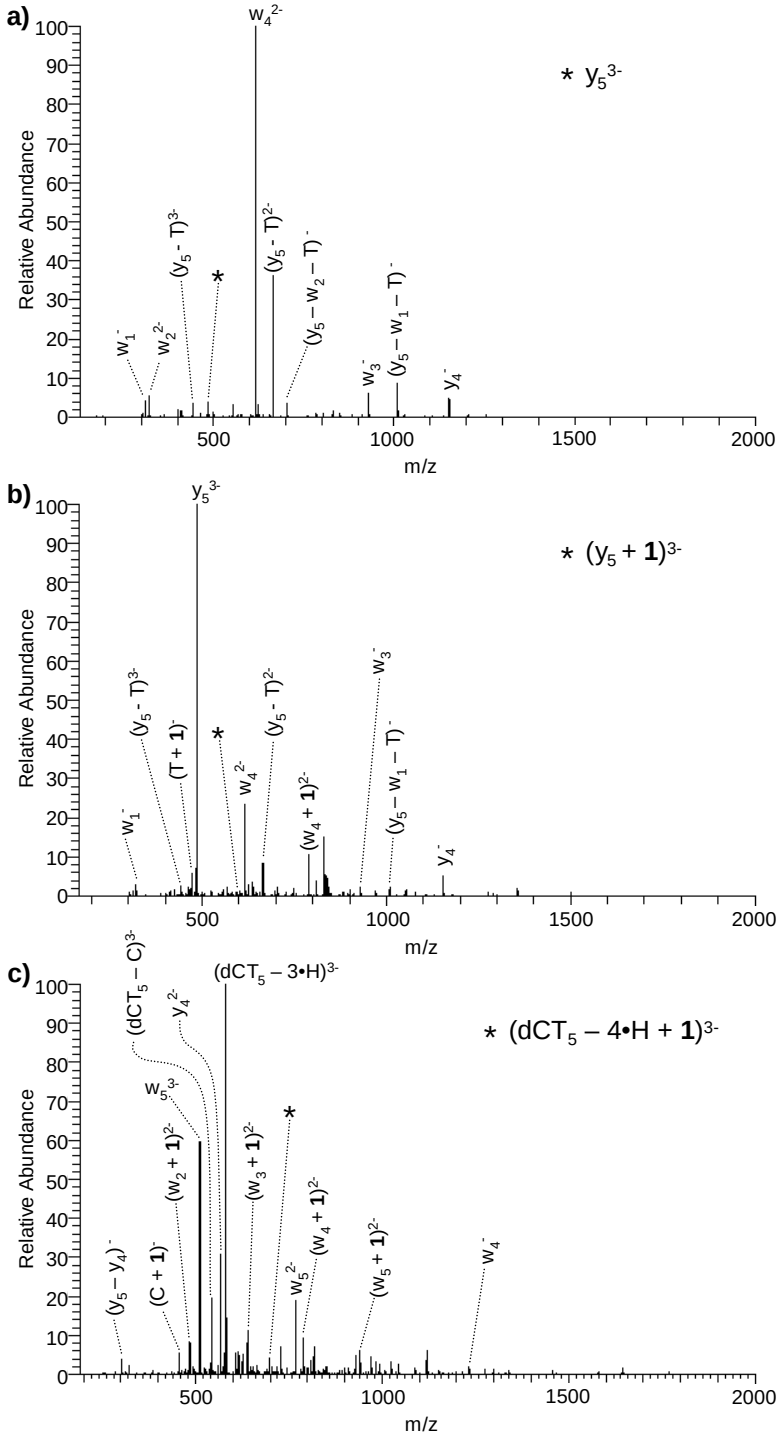

Figure 7-4. CAD of ions isolated from the mass spectrum of dCT_5 incubated with **1** at pH 6. Parent ions were (a) 749 Th, (b) $(dCT_5 - 5\bullet H + 2\bullet\mathbf{1} + MeOH)^{3-}$ at 822 Th, and (c) $(y_5 + \mathbf{1})^{2-}$ at 901 Th.

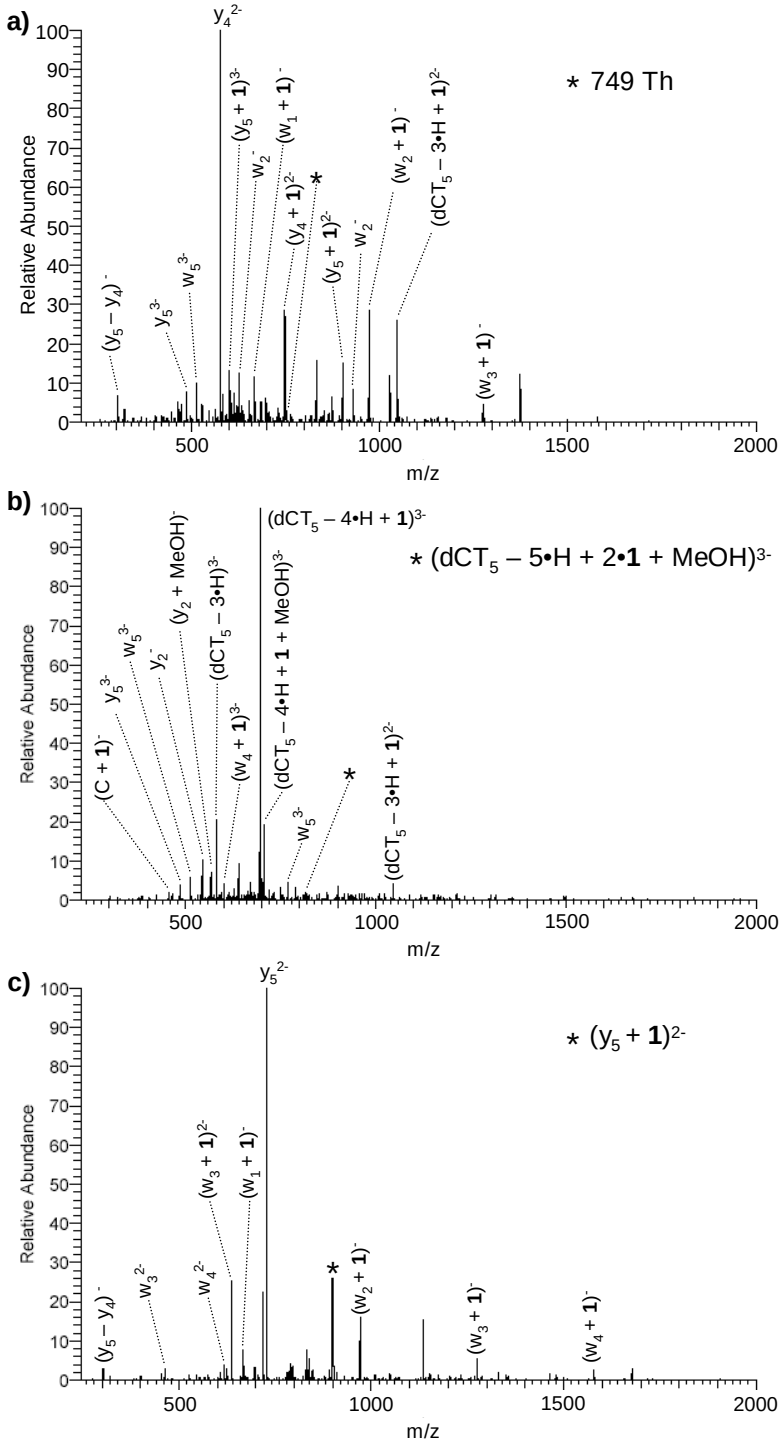

Figure 7-5. CAD of ions isolated from the mass spectrum of dCT_5 incubated with **1** at pH 6. Parent ions were (a) $(y_5 + 2\bullet\mathbf{1})^{2-}$ at 1074 Th and (b) 1791 Th.

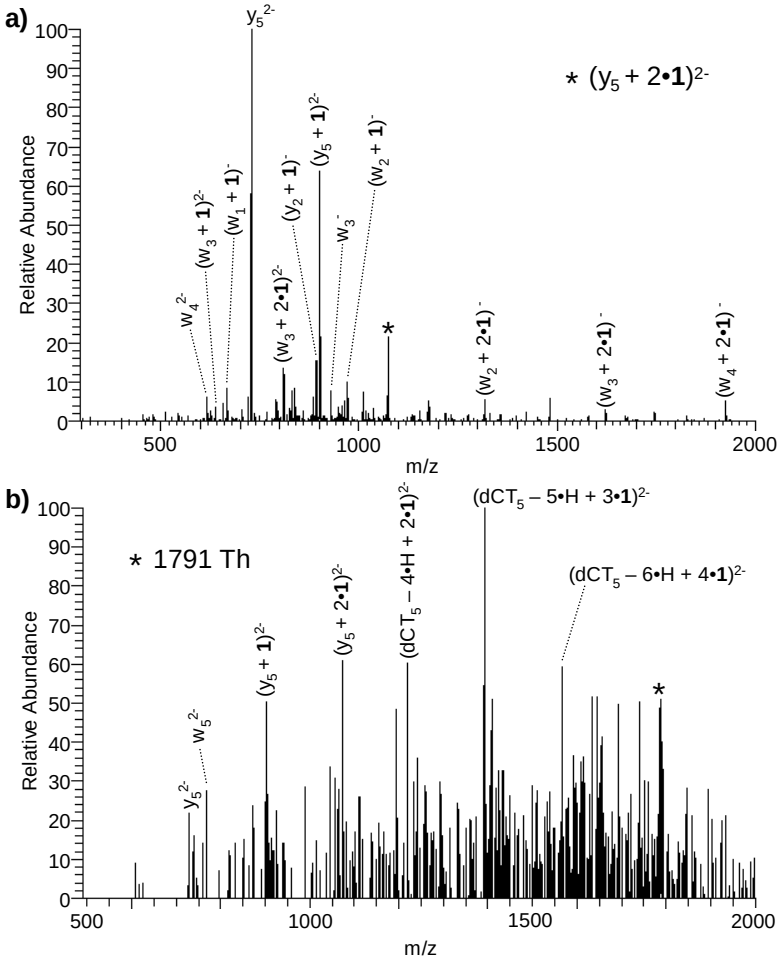

oligonucleotide fragments containing only thymine residues. Of the backbone fragments observed, both w ions and (y_5 – w – base) ions, analogs to the (a – base) fragment ions typically produced upon activation of intact oligonucleotide ions, were observed. The fragmentation patterns of the $(y_5 + \mathbf{1})^{-2}$ (Figure 7-4c) and $(y_5 + 2\bullet\mathbf{1})^{-2}$ ions (Figure 7-5aare especially interesting because a variety of w_n and (w_n + **1**) fragment ions are observed, indicating that **1** likely can attach to any of the thymine residues.

Figure 7-6. Mass spectrum of dT_2CT_3 incubated with **1** at pH 6.

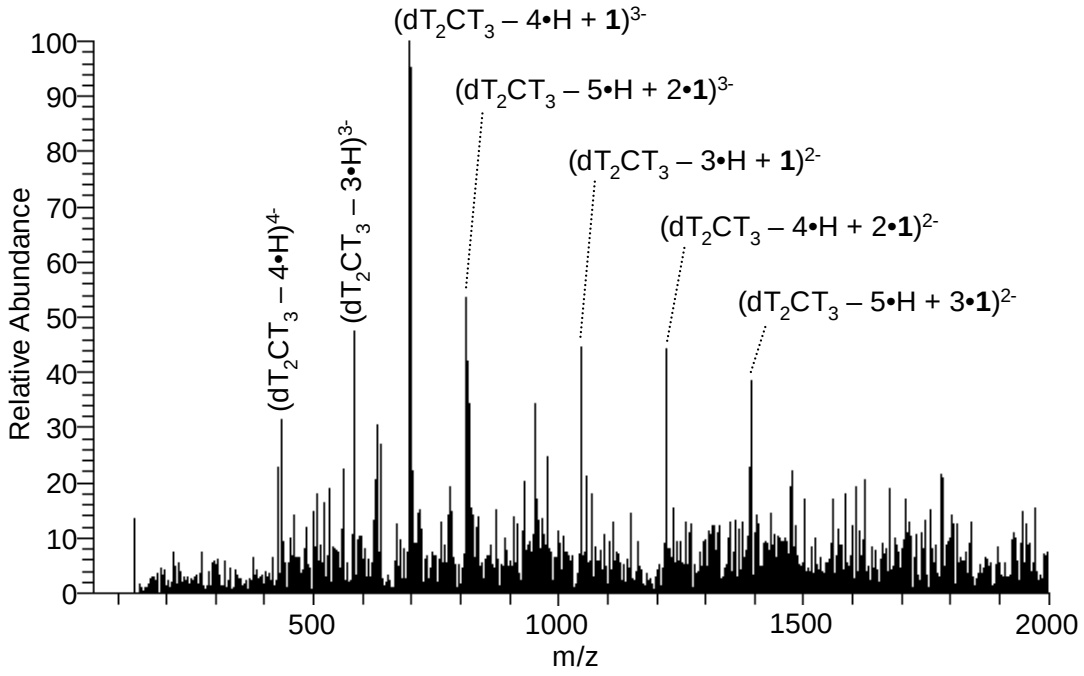

The striking prevalence of 3' fragments in the CAD spectra of intact, (dCT_5 + **1**) and (dCT_5 + 2•**1** + CH_3OH) ions is also noteworthy (Figures 7-3c and 7-4b). Although complementary fragments are typically observed, in these experiments w ions dominated the array of fragments while corresponding (a – base) fragments were not observed. This may indicate localization of the positively-charged **1** on the 5' cytidine, precluding the formation of negatively-charged (a – base) fragments. Lastly, CAD of the products at 749 and 1791 Th with unassigned molecular formulas (Figures 7-4a and 7-5b) yielded fragments similar to those observed with the other parent ions, suggestive that these parents contained the intact dCT_5 oligonucleotide, some number of **1**, and some other unidentified species (such as counter-ions or solvent molecules).

Similar ESI-MS/MS analysis of the products obtained upon incubation of **1** with dT_2CT_3 yielded somewhat different results. In this case, except for a weakly abundant w_2 adduct observed in the pH 8 spectrum (data not shown), all of the products observed contained the intact oligonucleotide (Figure 7-6). The fragments corresponding to cleavage at the cytidine observed for the experiments with dCT_5 described above were completely absent with dT_2CT_3. Also, a larger number of adducts of the intact oligonucleotide were formed, including: $(dT_2CT_3 - 4\bullet H + \mathbf{1})^{3-}$, $(dT_2CT_3 - 5\bullet H + 2\bullet\mathbf{1})^{3-}$, $(dT_2CT_3 - 3\bullet H + \mathbf{1})^{2-}$, $(dT_2CT_3 - 4\bullet H + 2\bullet\mathbf{1})^{2-}$, and $(dT_2CT_3 - 5\bullet H + 3\bullet\mathbf{1})^{2-}$.

As before, the more abundant ions in Figure 7-6, $(dT_2CT_3 - 4\bullet H)^{4-}$ at 436 Th, $(dT_2CT_3 - 3\bullet H)^{3-}$ at 582 Th, $(dT_2CT_3 - 4\bullet H + \mathbf{1})^{3-}$ at 697 Th, $(dT_2CT_3 - 5\bullet H + 2\bullet\mathbf{1})^{3-}$ at 813 Th, 951 Th, $(dT_2CT_3 - 3\bullet H + \mathbf{1})^{2-}$ at 1046 Th, $(dT_2CT_3 - 4\bullet H + 2\bullet\mathbf{1})^{2-}$ at 1220 Th, and $(dT_2CT_3 - 5\bullet H + 2\bullet\mathbf{1})^{2-}$ at 1392 Th, were isolated and subjected to CAD for structural characterization (Figures 7-7 through 7-9). In this case, although 3' fragments of the intact oligonucleotides were again most common, a fair number of the complementary (a – base) ions were observed among fragments resulting from both adducted (Figures 7-7c, 7-8a, 7-8c, 7-9a, and 7-9b) and non-adducted (Figures 7-7a and 7-7b) oligonucleotides. The position of these backbone cleavages seemed to have no relation to the position of cytidine in the oligonucleotide. Also, upon dissociation of the **1**—dT_2CT_3 adducts, both adducted fragment ions (i.e. ones that contain **1**) and non-adducted fragments (i.e. ones without **1**) were generated in similar abundances. That this was consistently true regardless of the oligonucleotide sequence (dT_2CT_3 versus dCT_5) offers further evidence that the linkage between **1** and the oligonucleotide is at least of

Figure 7-7. CAD of ions isolated from the mass spectrum of dT_2CT_3 incubated with **1** at pH 6. Parent ions were (a) $(dT_2CT_3 - 4\bullet H)^{4-}$ at 436 Th, (b) $(dT_2CT_3 - 3\bullet H)^{3-}$ at 582 Th, and (c) $(dT_2CT_3 - 4\bullet H + \mathbf{1})^{3-}$ at 697 Th.

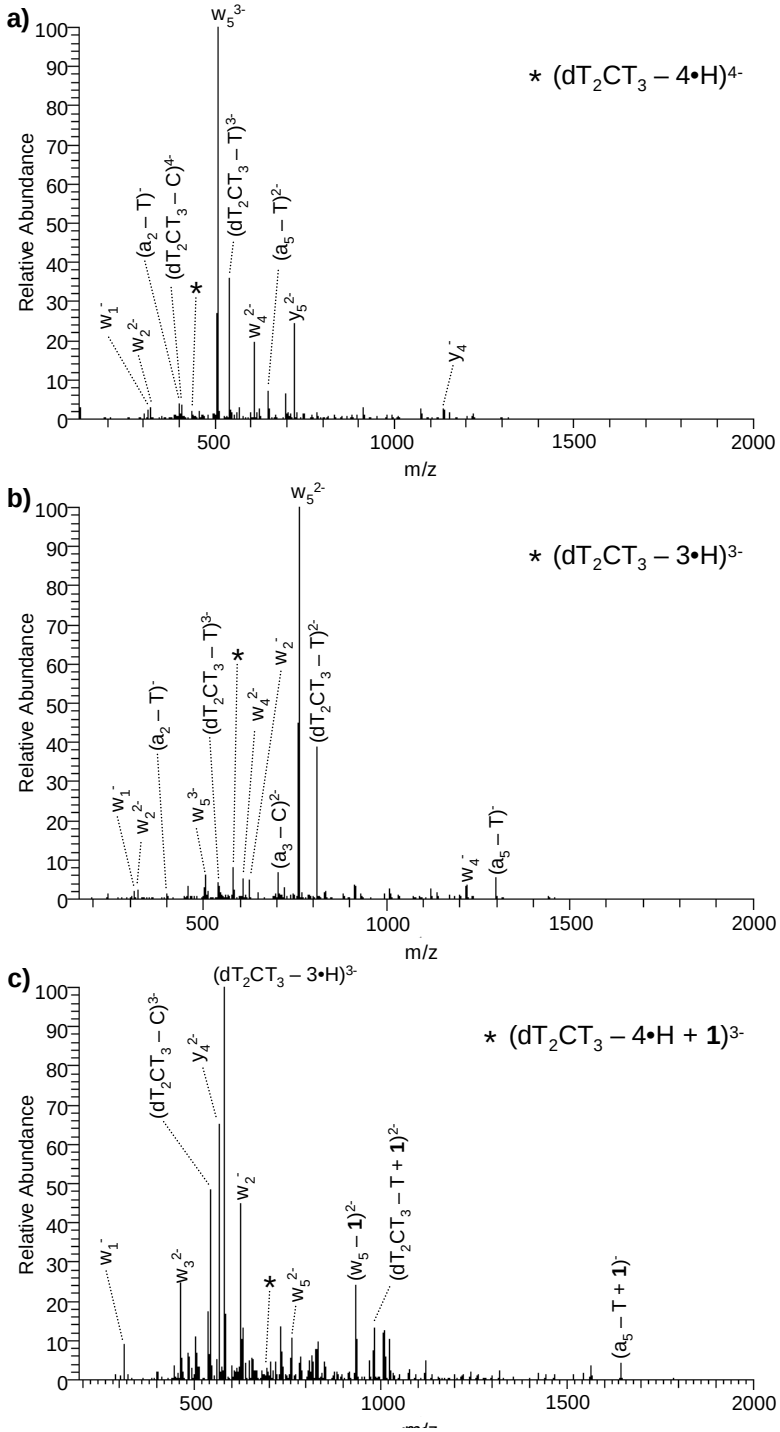

Figure 7-8. CAD of ions isolated from the mass spectrum of dT_2CT_3 incubated with **1** at pH 6. Parent ions were (a) $(dT_2CT_3 - 5\bullet H + 2\bullet\mathbf{1})^{3-}$ at 813 Th, (b) 951 Th, and (c) $(dT_2CT_3 - 3\bullet H + \mathbf{1})^{2-}$ at 1046 Th.

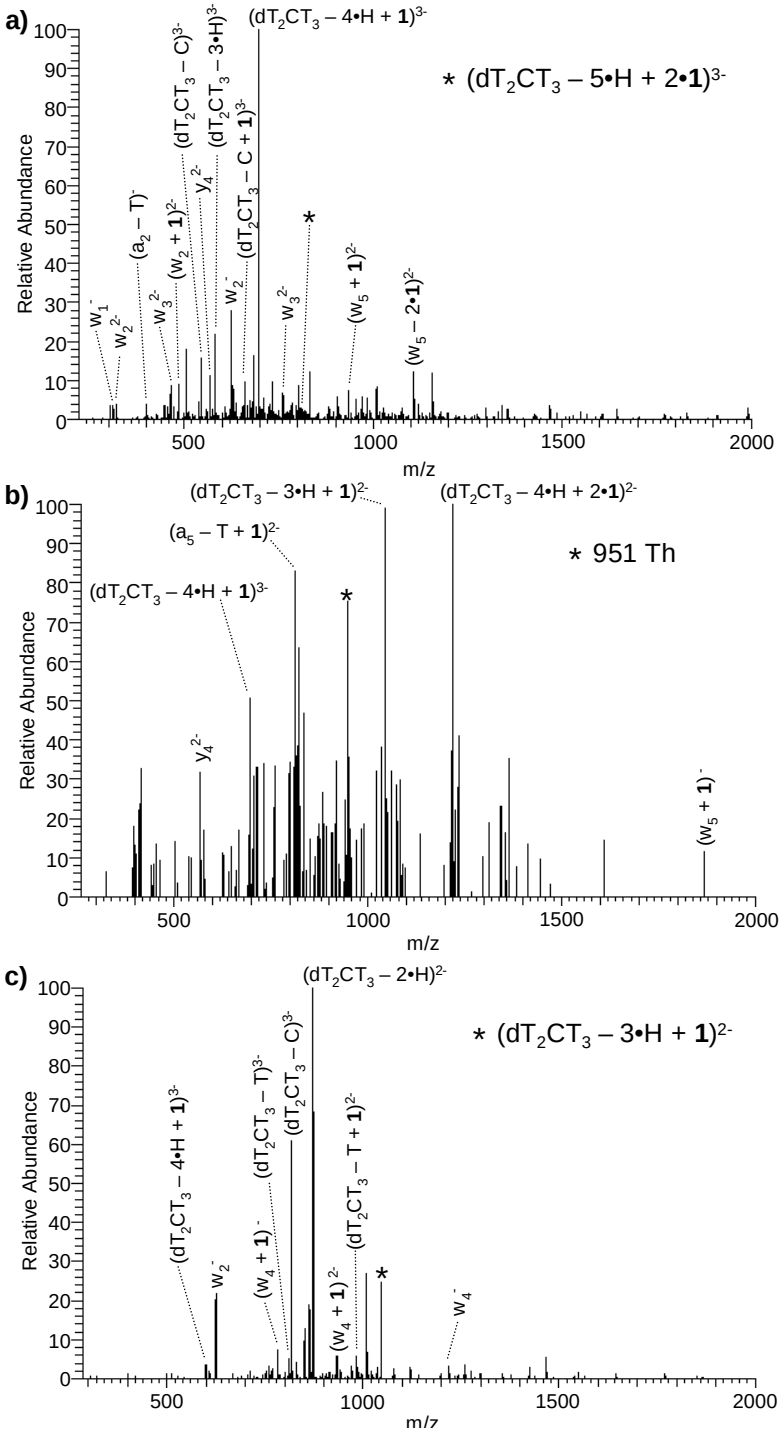

Figure 7-9. CAD of ions isolated from the mass spectrum of dT_2CT_3 incubated with **1** at pH 6. Parent ions were (a) $(dT_2CT_3 - 4\bullet H + 2\bullet\mathbf{1})^{2-}$ at 1220 Th and (b) $(dT_2CT_3 - 5\bullet H + 2\bullet\mathbf{1})^{2-}$ at 1392 Th.

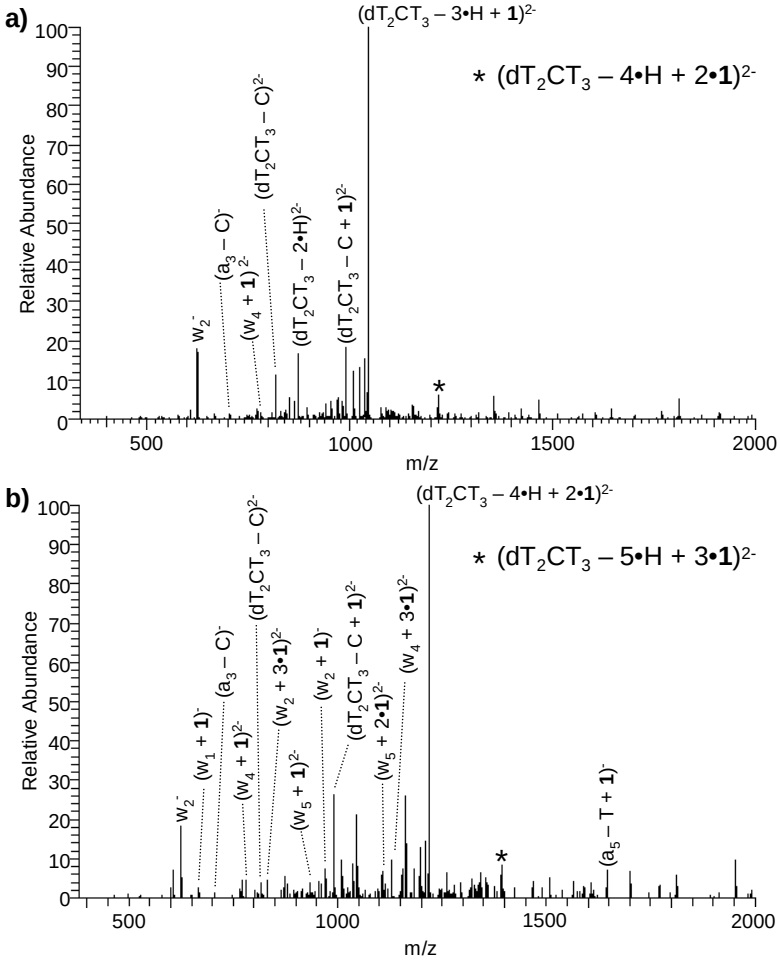

comparable strength to the internal covalent bonds in the oligonucleotide. CAD of the unassigned ion at 951 Th revealed that this ion contained both intact dT_2CT_3 and **1**.

With both dCT_5 and dT_2CT_3, more than a single molecule of **1** was observed bound to the oligonucleotide which implies that despite the preference for reaction with cytidine previously observed (29), interactions with other sites on the oligonucleotide also occur. These multiply adducted species clearly cannot yield much information about

the location of the enediyne, but an examination of the singly-adducted intact oligonucleotides reveals some clues. From the experiments with dCT_5, the only suitable parent containing a single molecule of **1** was $(dCT_5 - 4H + \mathbf{1})^{3-}$. On fragmentation (Figure 7-3c), it yielded two different w fragments, w_2 and w_4, as well as an (a_5 – base) fragment that each contained a molecule of **1**. Two possible scenarios can rationalize this behavior. First, **1** could be localized on the thymine in the fifth position because it is the only residue contained in all three of the fragments. An alternative conclusion is that **1** did not localize at a specific site on the oligonucleotide sequence, but rather, the parent ion was a mixture of different adducted structures. Additionally, the cleaved ions in the parent spectrum, y_5^{3-}, $(y_5 + \mathbf{1})^{3-}$, $(y_5 + \mathbf{1})^{2-}$, and $(y_5 + 2\bullet\mathbf{1})^{2-}$, also suggest that when **1** interacted with the cytidine it lead to subsequent cleavage either before or during the MS analysis.

An analogous intact adduct, $(dT_2CT_3 - 4\bullet H + \mathbf{1})^{3-}$, along with several other adducts between **1** and dT_2CT_3 were also examined. In these CAD mass spectra (Figures 7-7c, 7-8a, 7-8c, 7-9a, and 7-9b), nearly all the observed ions containing **1** also contained the cytidine residue. Although it cannot be confirmed whether this results from localized or random attachment, in this case there is no apparent reason to discount the possibility of localization at the cytidine. Also, the lack of cleaved ions in the parent spectrum observed for the incubation of dT_2CT_3 with **1** (Figure 7-6) is consistent with localization of **1** is localized on the cytidine. The data support that the **1**-induced cleavage at cytidine proceeds more readily with 3' as opposed to internal cytidine residues.

Figure 7-10. Mass spectrum of dCC incubated with **1** at pH 6 collected for 100-1000 Th (a) and 400-1000 Th to exclude the large $\mathbf{1}^{+}$ ion (b).

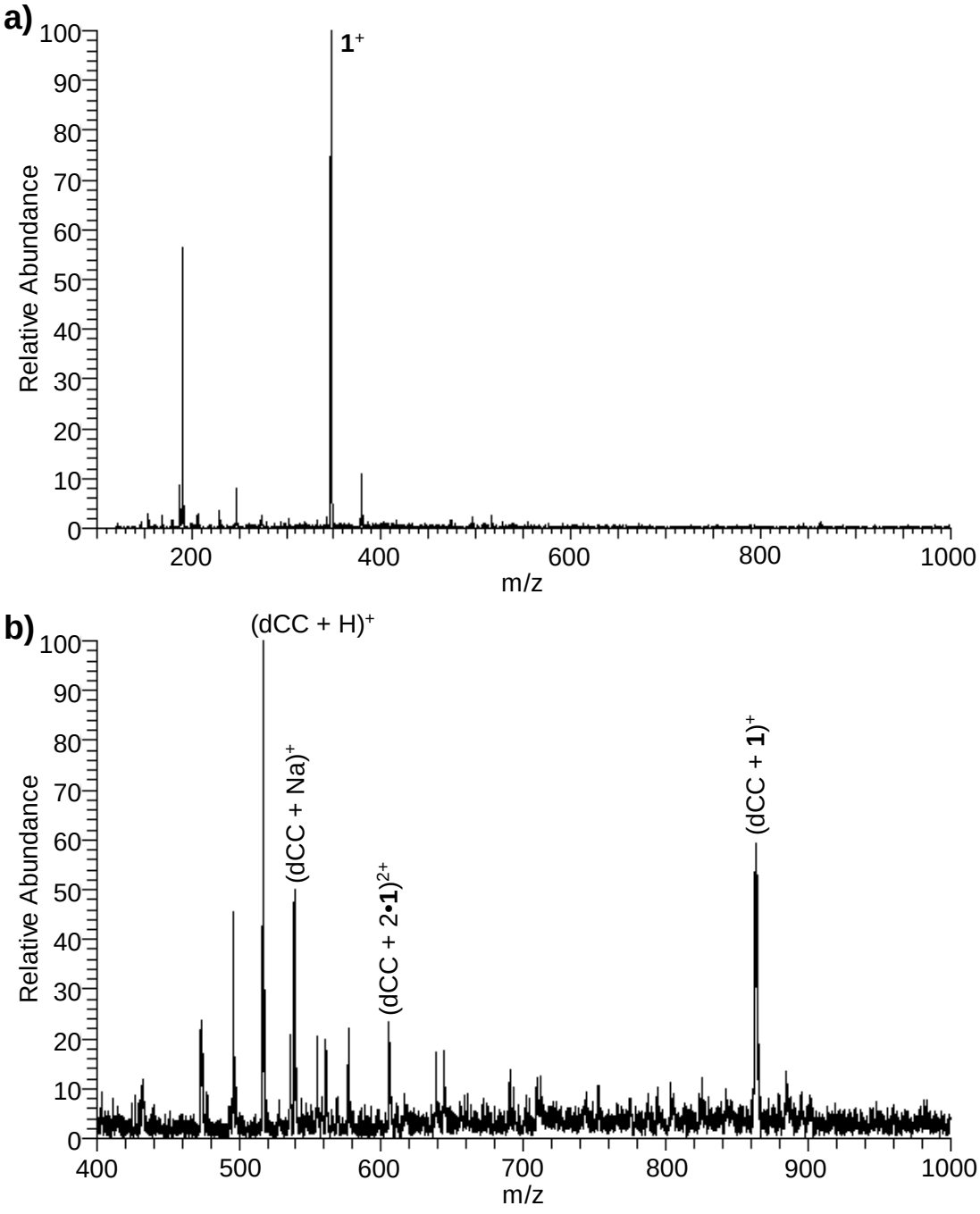

7.3.3 Interactions between 1 and dCC.

Experiments with the dinucleotide dCC incubated with **1** at pH 6 yielded results indicative of the binding between the oligonucleotide and **1**. In the negative mode typically used for DNA analysis due to the acidic phosphate backbone, the only detectable ion was the $CF_3SO_3^-$ counter-ion to **1**. With such a small oligonucleotide, however, the electrostatics are not necessarily dominated by the phosphate groups, and positive mode analysis becomes feasible (Figure 7-10a). Although the dominant ion in the positive mode spectrum was free $\mathbf{1}^+$, by excluding this ion from those stored in the ion trap, both the protonated dinucleotide and a $(dCC + \mathbf{1})^+$ ion were detected along with lower abundance ions corresponding to a $(dCC + 2\bullet\mathbf{1})^{2+}$ adduct (Figure 7-10b).

On isolation of the $(dCC + \mathbf{1})^+$ ion and subsequent fragmentation by CAD, two species related to ejection of **1** from the oligonucleotide, $(dCC + H)^+$ and $\mathbf{1}^+$, were observed. These species, however, were dwarfed by a product corresponding to an adduct between **1** and the cytidine nucleobase (Figure 7-11a) formed via detachment of the cytidine nucleobase from the deoxyribose of the dCC backbone. Likely the product of a base-loss mechanism similar to the fragmentation commonly observed for CAD of oligonucleotides (36), the presence of this ion offers strong evidence for attachment of **1** directly to the nucleobase.

To further probe the structure of this adduct, the $(C + \mathbf{1})^+$ fragment was then isolated and subjected to a second stage of CAD (Figure 7-11b). An assortment of fragments resulted for which proposed structures are shown in Scheme 7-1. The structures in Scheme 7-1 are consistent both with the observed m/z values and the

Figure 7-11. Tandem mass spectra from incubated with **1**. (a) CAD of (dCC + **1**)$^+$ at 863 Th. (b) CAD (MS^3).of (C + **1**)$^+$ at 458 Th from the spectra in (a).

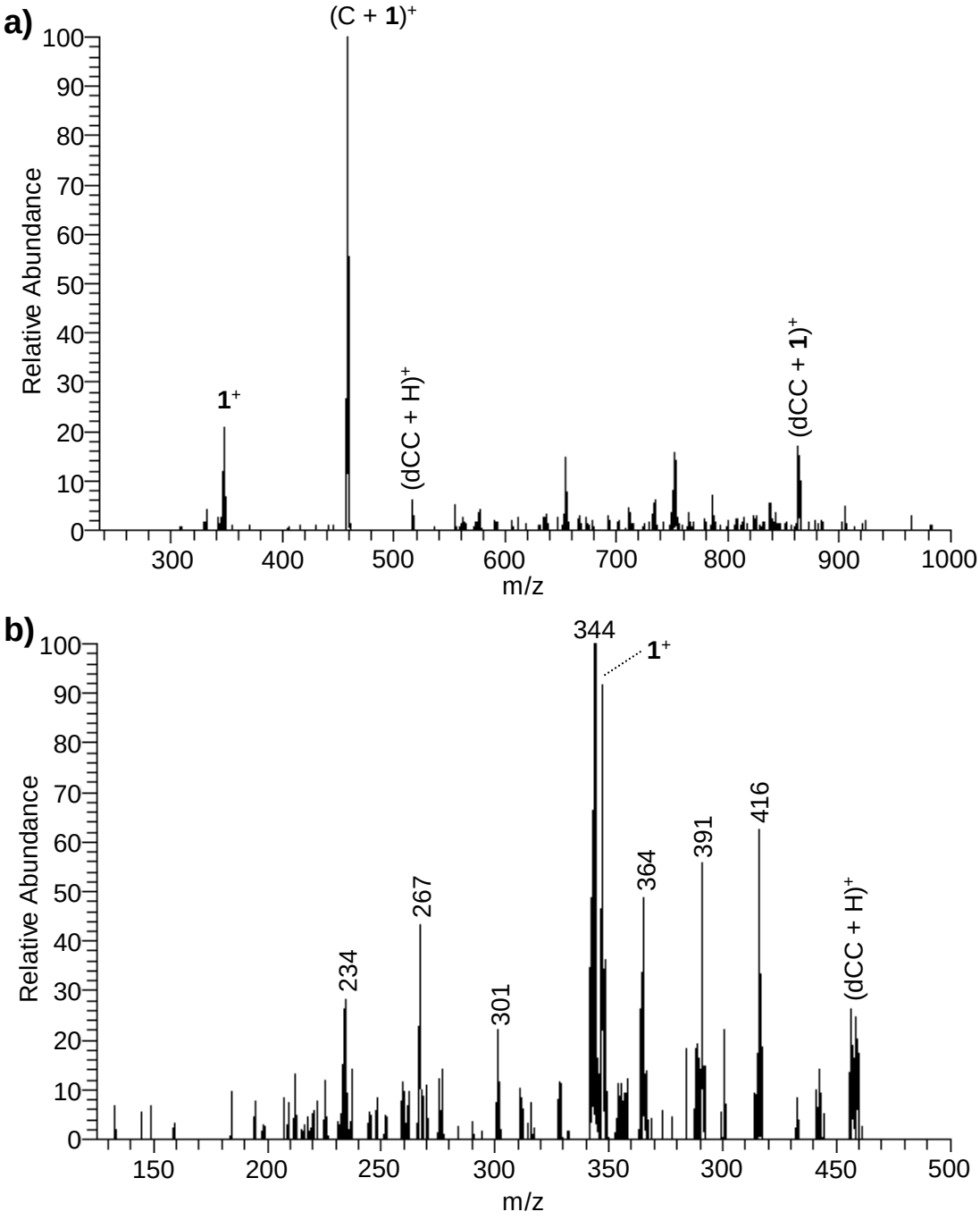

Scheme 7-1.

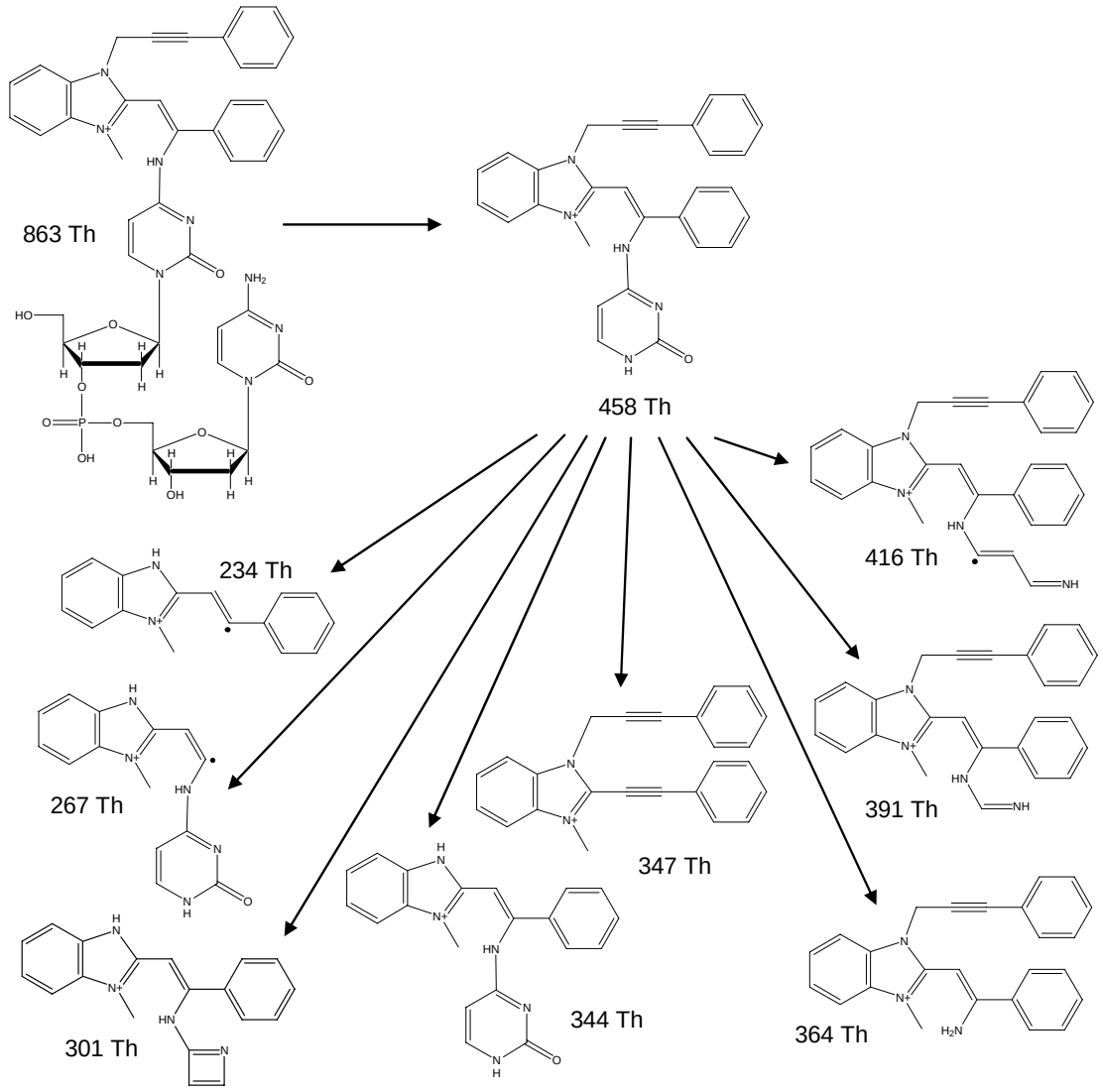

precursor structures, but others are feasible. The most abundant fragments resulted from detachment of the nucleobase leaving an intact $\mathbf{1}^+$ ion at m/z 347 or the loss of a propynyl benzene yielding the ion at 344 Th. This 344 Th fragment along with the ones at 234 and 267 Th resulting from both the loss of a propynyl benzene and either the cytidine nucleobase or a benzene radical, respectively, indicate that the enediyne binds to cytidine

through the ethynyl benzene because attachment to the propynyl benzene fails to yield reasonable fragment structures for these masses. Other fragments observed correspond to losses of various parts of the cytidine nucleobase. One of these, the fragment at 364 Th, would be difficult to justify were the cytidine bound through the pyrimidine nitrogen rather than through the amine.

7.4 Conclusions

Electrospray ionization mass spectrometric analysis of carefully selected oligonucleotides incubated with the novel enediyne drug **1** revealed several types of information about the interactions between **1** and DNA. First, **1** readily formed adducts of various stoichiometries with dC_8 consistent with previous observations (29), and the mass analysis confirmed a direct interaction not mediated by metals or other compounds. Collisionally activated dissociation of these adducts revealed that, in many cases, both ejection of the drug and DNA backbone cleavages occurred to similar extents, indicating that the interaction between **1** and DNA is of comparable strength to the bonds in the oligonucleotide suggesting that the DNA-drug adduct forms through a covalent linkage.

From a comparison of the interactions of **1** with dCT_5 and dT_2CT_3 it became apparent that the extent of cytidine-specific backbone cleavage induced by **1** varied significantly with the DNA sequence. When reacted under identical conditions, extensive cleavage of dCT_5 adjacent to the cytidine was observed in the mass spectrum while only the intact oligonucleotide was observed for dT_2CT_3. Also, for both sequences extensive adduction of **1** was observed.

Lastly, evaluation of adducts formed between **1** and the dinucleotide dCC provided strong evidence for attachment of the enediyne directly to the cytidine nucleobase. Additional CAD studies of the cytidine-**1** adduct provided an array of fragment ions consistent with the adduct forming through nucleophilic attack of the ethynyl benzene of **1** by the cytidine amino group.

7.5 References

(1) Edo, K.; Mizugaki, M.; Koide, Y.; Seto, H.; Furihata, K.; Otake, N.; Ishida, N. *Tetrahedron Lett.* **1985**, *26*, 331-334.

(2) Nicolaou, K. C.; Dai, W.-M. *Angew. Chem. Int. Ed. Eng.* **1991**, *30*, 1387-1416.

(3) Nicolaou, K. C.; Smith, A. L.; Yue, E. W. *Proc. Natl. Acad. Sci. USA* **1993**, *90*, 5881-5888.

(4) Smith, A. L.; Nicolaou, K. C. *J. Med. Chem.* **1996**, *39*, 2103-2117.

(5) Galm, U.; Hager, M. H.; Van Lanen, S. G.; Ju, J.; Thorson, J. S.; Shen, B. *Chem. Rev.* **2005**, *105*, 739-758.

(6) Lee, M. D.; Dunne, T. S.; Siegel, M. M.; Chang, C. C.; Morton, G. O.; Borders, D. B. *J. Am. Chem. Soc.* **1987**, *109*, 3464-3466.

(7) Lee, M. D.; Dunne, T. S.; Chang, C. C.; Ellestad, G. A.; Siegel, M. M.; Morton, G. O.; McGahren, W. J.; Borders, D. B. *J. Am. Chem. Soc.* **1987**, *109*, 3466-3468.

(8) Konishi, M.; Ohkuma, H.; Matsumoto, K.; Tsuno, T.; Kamei, H.; Miyaki, T.; Oki, T.; Kawaguchi, H.; VanDuyne, G. D.; Clardy, J. Dynemicin A, *J. Antibiot.* **1989**, *42*, 1449-1452.

(9) Golik, J.; Clardy, J.; Dubay, G.; Groenewold, G.; Kawaguchi, H.; Konishi, M.; Krishnan, B.; Ohkuma, H.; Saitoh, K.; Doyle, T. W. *J. Am. Chem. Soc.* **1987**, *109*, 3461-3462.

(10) Golik, J.; Dubay, G.; Groenewold, G.; Kawaguchi, H.; Konishi, M.; Krishnan, B.; Ohkuma, H.; Saitoh, K.; Doyle, T. W. *J. Am. Chem. Soc.* **1987**, *109*, 3462-3464.

(11) Jones, G. B.; Fouad, F. S. *Curr. Pharm. Des.* **2002**, *8*, 2415-2440.

(12) Klein, M.; Walenzyk, T.; König, B. *Collect. Czech. Chem. Commun.* **2004**, *69*, 945-965.

(13) McPhee, M. M.; Kerwin, S. M. *J. Org. Chem.* **1996**, *61*, 9385-9393.

(14) Jones, G. B.; Wright, J. M.; Rush, T. M.; Plourde, G. W., II; Kelton, T. F.; Mathews, J. E.; Huber, R. S.; Davidson, J. P. *J. Org. Chem.* **1997**, *62*, 9379-9381.

(15) Dai, W.-M.; Lai, K. W.; Wu, A.; Hamaguchi, W.; Lee, M. Y. H.; Zhou, L.; Ishii, A.; Nishimoto, S. *J. Med. Chem.* **2002**, *45*, 758-761.

(16) Banfi, L.; Guanti, G. *Eur. J. Org. Chem.* **2002**, 3745-3755.

(17) Schmittel, M.; Viola, G.; Dall'Acqua, F.; Morbach, G. *Chem. Comm.* **2003**, 646-647.

(18) Guanti, G.; Riva, R. *Org. Biomol. Chem.* **2003**, *1*, 3967-3976.

(19) Suzuki, I.; Shigenaga, A.; Nemoto, H.; Shibuya, M. *Tetrahedron Lett.* **2004**, *45*, 1955-1959.

(20) Usuki, T.; Inoue, M.; Hirama, M.; Tanaka, T. *J. Am. Chem. Soc.* **2004**, *126*, 3022-3023.

(21) Suzuki, I.; Uno, S.; Tsuchiya, Y.; Shigenaga, A.; Hisao, N.; Shibuya, M. *Bioorg. Med. Chem. Lett.* **2004**, *14*, 2959-2962.

(22) Fouad, F. S.; Crasto, C. F.; Lin, Y.; Jones, G. B. *Tetrahedron Lett.* **2004**, *45*, 7753-7756.

(23) Basak, A.; Roy, S. K.; Mandal, S. *Angew. Chem. Int. Ed.* **2005**, *44*, 132-135.

(24) Boger, D. L.; Zhou, J. *J. Org. Chem.* **1993**, *58*, 3018-3024.

(25) Toshima, K.; Ohta, K.; Ohashi, A.; Nakamura, T.; Nakata, M.; Matsumura, S. *J. Chem. Soc. Chem. Commun.* **1993**, 1525-1527.

(26) Tokuda, M.; Fujiwara, K.; Gomibuchi, T.; Hirama, M.; Uesugi, M.; Sugiura, Y. *Tetrahedron Lett.* **1993**, *34*, 669-672.

(27) David, W. M.; Kumar, D.; Kerwin, S. M. *Bioorg. Med. Chem. Lett.* **2000**, *10*, 2509-2512.

(28) Kumar, D.; David, W. M.; Kerwin, S. M. *Bioorg. Med. Chem. Lett.* **2001**, *11*, 2971-2974.

(29) Tuntiwechapikul, W.; David, W. M.; Kumar, D.; Salazar, M.; Kerwin, S. M. *Biochemistry* **2002**, *41*, 5283-5290.

(30) Sinha, S. C.; Li, L.-S.; Miller, G. P.; Dutta, S.; Rader, C.; Lerner, R. A. *Proc. Natl. Acad. Sci. USA* **2004**, *101*, 3095-3099.

(31) Liebisch, G.; Drobnik, W.; Lieser, B.; Schmitz, G. *Clin. Chem.* **2002**, *48*, 2217-2224.

(32) Gooding, K. B.; Higgs, R.; Hodge, B.; Stauffer, E.; Heinz, B.; McKnight, K.; Philpps, K.; Shapiro, M.; Winkler, M.; Ng, W.-L.; Julian, R. K. *J. Am. Soc. Mass Spectrom.* **2004**, *15*, 884-892.

(33) Qian, J.; Voorbach, M. J.; Huth, J. R.; Coen, M. L.; Zhang, H.; Ng, S.-C.; Comess, K. M.; Petros, A. M.; Rosenberg, S. H.; Warrior, U.; Burns, D. J. *Anal. Biochem.* 2**004**, *328*, 131-138.

(34) Limbach, P. A. *Mass Spec. Rev.* **1996**, *15*, 297-336.

(35) Nordhoff, E.; Kirpekar, F.; Roepstorff, P. *Mass Spec. Rev*. **1996**, *15*, 67-138.

(36) McLuckey, S. A.; Van Berkel, G. J.; Glish, G. L. *J. Am. Soc. Mass Spectrom.* **1992**, 3, 60-70.

(37) Smith, R. D.; Bruce, J. E.; Wu, Q.; Lei, Q. P. *Chem. Soc. Rev.* **1997**, *26*, 191-202.

(38) Gabelica, V.; De Pauw, E.; Rosu, F. *J. Mass Spectrom.* 1999, *34*, 1328-1337.

(39) Beck, J. L.; Colgrave, M. L.; Ralph, S. F.; Sheil, M. M. *Mass Spec. Rev.* **2001**, *20*, 61 – 87.

(40) Hofstadler, S. A.; Griffey, R. H. *Chem. Rev*. **2001**, *101*, 377-390.

(41) Gabelica, V.; De Pauw, E. *J. Am. Soc. Mass Spectrom.* **2001**, *13*, 91-98.

(42) Rosu, F.; Gabelica, V.; Houssier, C.; Colson, P.; De Pauw, E. *Rapid. Commun. Mass Spectrom.* **2002**, *16*, 1729-1736.

(43) Little, D. P.; Chorush, R. A.; Speir, J. P.; Senko, M. W.; Kelleher, N. L.; McLafferty, F. W. *J. Am. Chem. Soc.* **1994**, *116*, 4893-4897.

(44) Little, D. P.; Speir, J. P.; Senko, M. W.; O'Connor, P. B.; McLafferty, F. W. *Anal. Chem.* **1994**, *66*, 2809-2815.

(45) Keller, K. M.; Brodbelt, J. S. *Anal. Biochem*. **2004**, *326*, 200-210.

(46) Schultz, K. N.; Håkansson, K. *Int. J. Mass Spectrom.* **2004**, *234*, 123-130.

(47) Wan, K. X.; Shibue, T.; Gross, M. L. *J. Am. Chem. Soc.* **2000**, *122*, 300-307.

(48) David, W. M.; Brodbelt, J.; Kerwin, S. M.; Thomas, P. W. *Anal. Chem.* **2002**, *74*, 2029-2033.

(49) Rosu, F.; Gabelica, V.; Houssier, C.; De Pauw, E. *Nucleic Acids Res.* **2002**, *30*, e82.

(50) Gupta, R.; Beck, J. L.; Ralph, S. F.; Sheil, M. M.; Aldrich-Wright, J. R. *J. Am. Soc. Mass Spectrom.* **2004**, *15*, 1382-1391.

(51) Oehlers, L.; Mazzitelli, C. L.; Brodbelt, J. S.; Rodriguez, M.; Kerwin, S. *J. Am. Soc. Mass Spectrom.* **2004**, *15*, 1593-1603.

(52) Pothukuchy, A.; Mazzitelli, C. L.; Rodriguez, M. L.; Tuesuwan, B.; Salazar, M.; Brodbelt, J. S.; Kerwin, S. M. *Biochemistry* **2005**, *44*, 2163-2172.

(53) Wan, K. X.; Gross, M. L.; Shibue, T. *J. Am. Soc. Mass Spectrom.* **2000**, *11*, 450-457.

CHAPTER 8

Conclusions

Electrospray ionization mass spectrometry has great potential for the analysis of molecular recognition processes in solution. The work presented in this dissertation pushed the boundaries of the types of molecular recognition systems that can be studied with ESI-MS and increased the quality of the results that can be obtained. Mathematical modeling of the ESI source and its ability to transfer non-covalent complexes to the gas phase has explained many of the previously unexplained factors that can introduce significant errors into the measurements of the binding of these complexes, and applications of ESI-MS to the analysis of novel crown ether-metal sandwich complexes and different types of DNA-drug complexes demonstrated the ability of ESI-MS analyses to make significant contributions to widely varying areas of molecular recognition and supramolecular chemistry.

Mathematical modeling of the electrospray ionization source when used to transfer non-covalent complexes from solution to the gas phase yielded several key conclusions about the factors influencing the distribution of complex ions observed in the mass spectrometer. By treating the electrospray droplets as systems at equilibrium where the species can partition between a bulk solution-like interior and the air interface on the droplet surface, the surface concentrations of the host-guest complexes calculated by solving the coupled solution and partitioning equilibria correlate well with abundances of

ions observed experimentally for both isolated 1:1 binding and competitive binding systems. In general, in the polar solvents typically used for ESI-MS, the ability of a particular host-guest complex to exist preferentially on the droplet surface and thus be more efficiently ionized depends on its hydrophobic character; more hydrophobic species tend to have a greater affinity for the surface while more hydrophilic species tend to be well solvated in the interiors of the droplets.

In addition to factors such as the ESI current and background salt concentrations which impact all analytes, it was found that differences in the surface affinities of different host-guest complexes can significantly alter the distribution of ions in a mass spectrum. Of particular interest is the fact that the ionization efficiencies determined by these surface affinities can often outweigh the solution binding interactions in their impact on observed mass spectra. As a result, care must be taken to ensure that ESI-MS measurements of molecular recognition processes solution accurately reflect the solution through appropriate corrections or adequate verification that corrections are unnecessary for a particular chemical system.

Through applying ESI-MS to the molecular recognition of novel chemical systems, formation of ligand-metal-ligand sandwich complexes was found to be greatly enhanced through the incorporation of aromatic side groups on the crown ether ligands studied, presumably due to the added stabilization resulting from pi-stacking interactions between the two ligands in the complex. Furthermore, the incorporation of an electron-poor quinoxaline in the novel crown ether studied caused the preferential formation of mixed-ligand sandwich complexes with crowns containing an electron-rich benzene. The

donor-acceptor interactions between the electron-poor and electron-rich pi systems contributed up to 17 kJ/mol of added stabilization when compared to the corresponding homo-ligand complexes.

ESI-MS techniques have been applied equally successfully to the study of molecular recognition involving biological molecules. In particular, the recognition of different DNA and DNA-related structures by two different types of novel drug compounds was probed. In experiments with a pyrrole-inosine nucleoside designed to specifically interact with guanine preferentially over the other natural nucleobases, this specificity was confirmed and the ability of the pyrrole-inosine to disrupt the naturally-forming guanine tetrads was established. Sterically blocking the Hoogsteen hydrogen-bonding face of the pyrrole-inosine nucleoside largely eliminated these interactions, establishing that the interactions with guanine likely occur through this hydrogen-bonding face. Further experiments demonstrated a specific affinity of this synthetic nucleoside for quadruplex DNA structures. Analogous experiments with the pyrrole-inosine and either singly-stranded oligonucleotides or duplex DNA structures revealed only non-specific aggregation.

Analysis of the interactions between an acyclic analog to the natural enediyne anti-tumor drugs highlighted a different aspect of the ability of ESI-MS to shed light on molecular recognition. In contrast to the non-covalent interactions studied in the previous experiments, the enediyne drug was found to bind covalently to cytidine nucleobases. Beyond confirming the presence of adducts, more detailed information was obtained through the use of collisionally-activated dissociation to conduct a tandem MS

analysis of the DNA-drug adduct. Evaluation of the resulting fragment ions allowed a potential assignment of the cytidine amine as the binding site of the enediyne and has provided evidence of the structure of the adduct between DNA and the enediyne drug.

The pursuit of better and more widely applicable ESI-MS analyses of molecular recognition through experiments like those presented here offers the potential to increase both the accuracy and efficiency of measurements of many types of chemical interactions. In this work, the application of electrospray ionization mass spectrometry has enhanced the understanding of the crown ether-metal and DNA-drug complexes studied. While important in their own right, the techniques developed in these experiments and the insights gained through mathematical modeling of the electrospray source further strengthen ESI-MS as a tool for studying many sorts of molecular recognition interactions in solution, helping to ensure that it will continue to assist in the development and characterization of molecular recognition agents across the chemical disciplines.

As research continues in these areas, ESI-MS will continue to strengthen. More fundamental studies of the behavior of the electrospray source and the mechanisms of ion formation should allow ESI-MS to quantitatively measure solution binding more accurately and conveniently than many of the traditional techniques. Beyond the relatively small molecular systems that have long been the purview of mass spectrometry, further development of the unique ability of ESI-MS to deeply probe the interactions between large biological molecules in both carefully controlled conditions and in the

native matrices will ensure its continually increasing importance in the rapidly expanding field of biochemical research.

Vita

Courtney Lawrence Sherman was born in Beaumont, Texas on December 9, 1977, the son of William Lawrence Sherman and Jerraye Jo Sherman. In 1996 he received a diploma from Monsignor Kelly High School in Beaumont. He subsequently entered Texas A&M University in College Station, Texas, where he earned the degree of Bachelor of Science in Chemistry in 2000. Following his graduation from Texas A&M, he wed Karen Cormier in May of 2000. Courtney entered graduate school at the University of Texas in Austin, Texas, in September 2000.

Permanent Address: 12316 Orkney Lane, Manor, TX, 78653

This dissertation was typed by the author.